UC San Diego

UC San Diego Electronic Theses and Dissertations

Title

Cross-layer design of wideband CDMA systems and cooperative diversity for wireless ad hoc networks :

Permalink

https://escholarship.org/uc/item/6xb1v2zg

Author

Annavajjala, Ramesh

Publication Date

2006

Peer reviewed|Thesis/dissertation

eScholarship.org Powered by the California Digital Library
University of California

UNIVERSITY OF CALIFORNIA, SAN DIEGO

Cross-Layer Design of Wideband CDMA Systems and Cooperative Diversity for Wireless Ad Hoc Networks

A dissertation submitted in partial satisfaction
of the requirements for the degree
Doctor of Philosophy

in

Electrical Engineering
(Communication Theory and Systems)

by

Ramesh Annavajjala

Committee in charge:

Pamela C. Cosman, Chair
Laurence B. Milstein, Co-Chair
Patrick J. Fitzsimmons
William S. Hodgkiss
Jack K. Wolf

2006

© Copyright
Ramesh Annavajjala, 2006
All rights reserved

The dissertation of Ramesh Annavajjala is approved, and is acceptable in quality and form for publication on microfilm:

Co-Chair

Chair

University of California, San Diego

2006

To my mother

TABLE OF CONTENTS

LIST OF FIGURES

LIST OF TABLES

ACKNOWLEDGMENTS

I would like to express my deepest gratitude to my advisers Profs. Pamela Cosman and Laurence Milstein for their encouragement, invaluable advise, and most importantly, for giving me the theoretically infinite freedom to pursue my research interests in my own way. This freedom gave me immense opportunities to collaborate with various professors, researchers, and students, both within and outside UCSD. Prof. Cosman's constructive criticism, both technical and non-technical, significantly helped me to better understand and improve myself. Prof. Milstein, for his disciplined life and dedication to the profession, in both teaching and research, was always a great source of inspiration to me.

I am very grateful to Profs. Patrick Fitzsimmons, William Hodgkiss, and Jack Wolf, for serving on my committee. I should also thank Prof. Fitzsimmons for his lucid presentation of the course Probability Theory (Math 280-A/B/C), Prof. Hodgkiss for his teaching of the course Detection Theory (ECE 254), and Prof. Wolf for his enlightening treatment of the course Information Theory (ECE 255A). I thank the Purkayastha/TimeLine Ventures for awarding me a graduate student fellowship for the year 2002–2003. I would also like to acknowledge the generous support, in the form of a research assistantship, from the Office of Naval Research to accomplish this research work.

There are many researchers from whom, with active collaboration, I have learned a great deal. Notable among them are Dr. Marvin Simon at the Jet Propulsion Laboratory, CA, Prof. Bhaskar Rao at UCSD, and Prof. A. Chockalingam at the Indian Institute of Science (IISc), Bangalore, India. Dr. Simon, for his dedication to the field, and for his leadership role, was always a true hero to me. I sincerely thank Prof. Rao for encouraging me to participate in his weekly MIMO group meetings, and for the valuable collaboration we started recently. I gratefully acknowledge the active, and long term collaboration that I have had with Prof. Chockalingam, my ex-adviser at the IISc.

A number of people made my stay at UCSD memorable. I express my thanks to

Sandeep, Thanos and Yushi of the Code Lab, Eric, Matteo, Mishal, Patrick, Preeti, Sumit, and Yoav of the CWC Lab, and Aditya, Chandra, Jun and Yoga of the DSP Lab. A special thanks must go to Nandu for friendship, computer support, and for the ongoing research collaboration. Finally, I would like express my sincere gratitude to my brother and sister-in-law, and my love to my niece, who provided joyful moments with their presence in La Jolla. Outside UCSD, I should thank the folks, Manohar, Suren and Vibhor, in Bangalore for the ongoing collaborative research.

Chapter 2 of this thesis, in full, is a reprint of the material as it appears in R. Annavajjala, P. C. Cosman, and L. B. Milstein, "On Source Coding, Channel Coding and Spreading Tradeoffs in a DS-CDMA System Operating over Frequency Selective Fading Channels with Narrowband Interference," *IEEE Journal on Selected Areas in Communications*, vol. 23, no. 5, May 2005, pp. 1034-1044. Chapter 3 of this thesis, in full, is a reprint of the material as it appears in R. Annavajjala, P. C. Cosman, and L. B. Milstein, "Tradeoff Between Source Coding and Spreading in a Multicarrier DS-CDMA System Operating over Multipath Fading Channels with Narrow-Band Interference," in *Proc. IEEE Military Communications Conference (MILCOM)*, November 2004. Chapter 4 of this thesis, in full, is a reprint of the material as it appears in R. Annavajjala, P. C. Cosman, and L. B. Milstein, "On Optimum Noncoherent Amplify-and-Forward Reception for Cooperative Diversity," submitted to the *IEEE Transactions on Communications*, August 2005. Chapter 5 of this thesis, in full, is a reprint of the material as it appears in R. Annavajjala, P. C. Cosman, and L. B. Milstein, "On Statistical Channel Knowledge-Based Optimum Power Allocation for Relaying Protocols," submitted to the *IEEE Journal on Selected Areas in Communications*, February 2006. I was the primary author and the co-authors Prof. Cosman and Prof. Milstein directed and supervised the research which forms the basis for Chapters 2-5.

VITA

1977	Born, Warangal, India
1998	B. Tech, Electronics and Communications Engineering, National Institute of Technology, Warangal, India
2001	M. Eng., Telecommunications, Indian Institute of Science, Bangalore, India
2006	Ph. D., Electrical Engineering (Communication Theory and Systems), University of California, San Diego
1999-2001	Graduate Student, Electrical Communication Engineering, Indian Institute of Science, Bangalore, India
2002-2003	Purkayastha/TimeLine ventures graduate fellowship, University of California, San Diego
2003-2006	Research Assistant, University of California, San Diego
1998-1999	Engineer R&D, C. M. C R&D Center, Hyderabad, India
2001-2002	Systems Design Engineer, Synopsys Inc., Bangalore Center, India

PUBLICATIONS

♦ User Cooperation Diversity

J1. Ramesh Annavajjala, P. C. Cosman, and L. B. Milstein, "Statistical Channel Knowledge based Optimum Power Allocation for Relaying Protocols," submitted to *IEEE Jl. Selected Areas in Communications,* February 2006. (**Revised version in review**).

J2. Ramesh Annavajjala, P. C. Cosman, and L. B. Milstein, "On Optimum Noncoherent Amplify-and-Forward Reception for Cooperative Diversity," submitted to *IEEE Trans. Commun.,* August 2005. (**In revision**).

C1. Ramesh Annavajjala, P. C. Cosman, and L. B. Milstein, "On Optimum Power Control with Mean Channel Gains for Relaying Protocols," presented at the *WICAT* workshop on Cooperative Communications, Polytechnic University, Brooklyn, NY, October 2005.

C2. Ramesh Annavajjala, P. C. Cosman, and L. B. Milstein, "On the Performance of Optimum Noncoherent Amplify-and-Forward Reception for Cooperative Diversity," in *Proc. IEEE MILCOM'05,* October 2005, Atlantic City, New Jersey, USA.

♦ Cross-Layer Design for Wideband CDMA Systems

J1. Ramesh Annavajjala, P. C. Cosman, and L. B. Milstein, "Source Coding, Channel Coding and Spreading Tradeoffs in a DS-CDMA System Operating over Frequency Selective Fading Channels with Narrow-Band Interference," in *IEEE Jl. of Select. Communications,* May 2005.

C1. Ramesh Annavajjala, P. C. Cosman, and L. B. Milstein, "Tradeoff Between Source Coding and Spreading in a Multicarrier DS-CDMA System Operating over Multipath Fading Channels with Narrow-Band Interference," in *IEEE MILCOM'2004,* Monterey, CA, November 2004.

♦ Interference Cancellation in CDMA Systems

J1. S. Manohar, V. Tikiya, Ramesh Annavajjala, A. Chockalingam, "BER-Optimal Linear Parallel Interference Cancellation for Multicarrier DS-CDMA in Rayleigh Fading," accepted in the *IEEE Trans. Commun.,* July 2006.

C1. S. Manohar, V. Tikiya, Ramesh Annavajjala, A. Chockalingam, "BER Analysis of Weighted Interference Cancellation in Multicarrier DS-CDMA Systems," in the *IEEE WCNC'2006,* Las Vegas, Nevada, April 2006.

C2. S. Manohar, V. Tikiya, Ramesh Annavajjala, A. Chockalingam, "BER-Optimized Linear Parallel Interference Cancellers for Multicarrier DS-CDMA Systems," in *Proc. IEEE GLOBECOM'2005,* St. Louis, November-December 2005.

C3. V. Tikiya, Ramesh Annavajjala, and A. Chockalingam, "Performance Analysis of a Parallel Interference Canceller on Rayleigh Fading Channels," in *Proc. IEEE VTC'2004 (Spring),* Milan, Italy, May 2004.

♦ Space-Time Codes and Transmit Beamforming

J1. M. S. Raju, Ramesh Annavajjala and A. Chockalingam, "BER Analysis of QAM on Fading Channels with Transmit Diversity," in *IEEE Trans. Wireless Commun.,* March 2006.

J2. Y. Isukapalli, Ramesh Annavajjala, and B. D. Rao, "Performance Analysis of Transmit Beamforming for MISO Systems with Imperfect Feedback," submitted to the *IEEE Transactions on Communications,* June 2006.

C1. M. S. Raju, Ramesh Annavajjala and A. Chockalingam, "LLR based BER Analysis of Orthogonal STBCs using QAM on Rayleigh Fading Channels," in *IEEE PIMRC'2004,* Barcelona, September 2004.

C2. M. S. Raju, Ramesh Annavajjala and A. Chockalingam, "BER Analysis of QAM with Transmit Diversity in Rayleigh Fading Channels," in *IEEE GLOBECOM'2003,* San Francisco, USA, December 2003.

♦ Coded Performance on Fading Channels

J1. Ramesh Annavajjala, A. Chockalingam, and L. B. Milstein, "Performance Analysis of Coded Communication Systems on Nakagami Fading Channels with Selection Combining," in *IEEE Trans. Commun.,* July, 2004.

J2. Ramesh Annavajjala, A. Chockalingam, and L. B. Milstein, "Performance Analysis of TCM with Generalized Selection Combining on Rayleigh Fading Channels," in *IEEE Communication Letters,* July 2003.

J3. Ramesh Annavajjala, A. Chockalingam, and L. B. Milstein, "SNR Estimation in Generalized Fading Channels and its Application to Turbo Decoding," in *IEEE Trans. Commun.,* November 2002.

C1. Ramesh Annavajjala and L. B. Milstein, "Capacity and Cutoff Rate for M-ary NCFSK Signals on Rayleigh Fading Channels with GSC Reception," in *IEEE ISIT'2003,* Yokohama, Japan, June 2003.

C2. Ramesh Annavajjala, A. Chockalingam, and L. B. Milstein, "Performance Analysis of TCM with Generalized Selection Combining on Rayleigh Fading Channels," in *Proc. IEEE GLOBECOM'2002,* Taipei, Taiwan, November 2002.

C3. Ramesh Annavajjala, A. Chockalingam, and L. B. Milstein, "Performance of Noncoherent Turbo Detection on Rayleigh Fading Channels," *Proc. IEEE GLOBECOM'2001,* San Antonio, USA, November 2001.

C4. Ramesh Annavajjala, A. Chockalingam, and L. B. Milstein, "Bounds on the Performance of Turbo Codes on Nakagami Fading Channels with Diversity Combining," in *Proc. IEEE GLOBECOM'2001,* San Antonio, USA, November 2001.

C5. Ramesh Annavajjala, "Noncoherent Turbo Detection on Rayleigh Fading Channels without Channel State Information," in *IEEE ISCTA'2001*, Ambleside, U.K, July 2001.

C6. Ramesh Annavajjala, A. Chockalingam, and L. B. Milstein, "SNR Estimation in Nakagami Fading with Diversity for Turbo Decoding," in *Proc. IEEE MILCOM'2001,* McLean, USA, October 2001.

C7. Ramesh Annavajjala, A. Chockalingam, and L. B. Milstein, "SNR Estimation in Generalized Fading Channels and its Application to Turbo Decoding," in *Proc. IEEE ICC'2001,* Helsinki, Finland, June 2001.

♦ Effects of Imperfect Channel Knowledge

J1. Ramesh Annavajjala, P. C. Cosman, and L. B. Milstein, "Performance Analysis of Linear Modulation Schemes with Generalized Diversity Combining on Rayleigh Fading Channels with Noisy Channel Estimates," submitted to *IEEE Trans. Info. Theory,* June 2005. (**In Review**).

J2. Ramesh Annavajjala and L. B. Milstein, "Performance Analysis of Optimum and Suboptimum Selection Diversity Schemes on Rayleigh Fading Channels with Imperfect Channel Estimates," accepted in the *IEEE Trans. Vehicular Technol.,* July 2006.

J3. Ramesh Annavajjala "Comments on 'Exact Error-Rate Analysis of Diversity 16-QAM with Channel Estimation Errors," in *IEEE Trans. Commun.,* March 2006.

J4. Ramesh Annavajjala and L. B. Milstein, "Performance Analysis of Linear Diversity Combining Schemes on Rayleigh Fading Channels with Binary Signaling and Gaussian Weighting Errors," in *IEEE Trans. Wireless Commun.,* September 2005.

J5. Ramesh Annavajjala, "A Simple Approach to Error Probability with Binary Signaling over Generalized Fading Channels with Maximal Ratio Combining and Noisy Channel Estimates," in *IEEE Trans. Wireless Commun.,* March 2005.

C1. Ramesh Annavajjala and L. B. Milstein, "Analysis of Selection Combining Schemes on Rayleigh Fading Channels with Noisy Channel Estimates," in *IEEE WCNC'2004,* Atlanta, USA, March 2004.

C2. Ramesh Annavajjala and L. B. Milstein, "On the Performance of Diversity Combining Schemes on Rayleigh Fading Channels with Noisy Channel Estimates," in *IEEE MILCOM'2003,* Boston, USA, October 2003.

♦ Optimum Selection and Generalized Selection Combining

J1. Ramesh Annavajjala, A. Chockalingam, and L. B. Milstein, "Further Results on Selection Combining of Binary NCFSK Signals in Rayleigh Fading Channels," in *IEEE Trans. Commun.,* June, 2004.

J2. Ramesh Annavajjala, A. Chockalingam, and L. B. Milstein, "Performance Analysis of Generalized Selection Combining of M-ary NCFSK Signals in Rayleigh Fading Channels," submitted to *IEEE Trans. Commun.,* May 2002.

C1. M. S. Raju, Ramesh Annavajjala, and A. Chockalingam. "Optimum Selection Combining for M-QAM on Fading Channels," in *IEEE WCNC'2005,* New Orleans, LA, USA, March 2005.

C2. Ramesh Annavajjala, A. Chockalingam, and L. B. Milstein, "Generalized Selection Combining of M-ary NCFSK Signals in Rayleigh Fading Channels," in *IEEE ICC'2003,* Alaska, USA, May 2003.

C3. Ramesh Annavajjala, A. Chockalingam, and L. B. Milstein, "Optimum Selection Combining of Binary NCFSK Signals in Independent Fading Channels," in *Proc. IEEE GLOBECOM'2002,* Taipei, Taiwan, November 2002.

C4. Ramesh Annavajjala, A. Chockalingam, and L. B. Milstein, "Performance Analysis of a (3, L) Selection Combining Scheme for Binary NCFSK Signals in Rayleigh Fading Channels," in *Proc. IEEE GLOBECOM'2002,* Taipei, Taiwan, November 2002.

♦ Digital Modulations, Channel Modelling, and Adaptation in Cellular Systems

J1. M. K. Simon and Ramesh Annavajjala, "On the Optimality of Bit Detection of Certain Digital Modulations," in *IEEE Trans. Commun.,* February 2005.

C1. Ramesh Annavajjala, A. Chockalingam, P. C. Cosman, and L. B. Milstein, "First-order Markov Models for Packet Transmission on Rayleigh Fading Channels with DPSK/NCFSK Modulation," to appear in *IEEE ISIT'06*, Seattle, Washington, July 2006.

C2. Ramesh Annavajjala and L. B. Milstein, "On the Capacity of Dual Diversity Combining Schemes on Correlated Rayleigh Fading Channels with Unequal Branch Gains," in *IEEE WCNC'2004,* Atlanta, USA, March 2004.

C3. Ramesh Annavajjala, A. Chockalingam, and L. B. Milstein, "A First Order Markov Model for Correlated Nakagami-m Fading Channels," in *Proc. IEEE ICC'2002,* New York, USA, September 2001.

C4. Ramesh Annavajjala and A. Chockalingam, "Performance Analysis of Adaptive Modulation with Optimum Power Control in Cellular Systems," in *Proc. IEEE ICPWC'2000,* Hyderabad, India, December 2000.

ABSTRACT OF THE DISSERTATION

Cross-Layer Design of Wideband CDMA Systems and Cooperative Diversity for Wireless Ad Hoc Networks

by

Ramesh Annavajjala

Doctor of Philosophy in Electrical Engineering
(Communication Theory and Systems)

University of California, San Diego, 2006

Professor Pamela C. Cosman, Chair

Professor Laurence B. Milstein, Co-Chair

Some of the challenges in the design of next generation wireless systems are providing high data rate multimedia services, increasing user capacity, improving reliability and range, terminal mobility, robustness to interference, limited spectrum availability, and transmission power constraints. The approaches that we take in this dissertation to address some of the aforementioned issues are cross-layer design and user cooperation.

In the first part of the dissertation, on a wideband CDMA channel with a finite transmission bandwidth constraint, we consider the problem of optimal bandwidth allocation for source coding, channel coding and spread-spectrum modulation. For analytical tractability, we assume a memoryless Gaussian source with an optimum quantizer, a con-

volutional encoder with a soft-decision decoder, and a spread-spectrum modulator with random spreading codes and a RAKE receiver. In the presence of both multiple access interference (MAI) and narrowband interference (NBI), for frequency-selective Nakagami fading channels, we derive upper and lower bounds on the end-to-end average source distortion. Since an exact expression for the average distortion is difficult to derive, we seek to obtain the three-tuple (i.e., source coding rate, channel coding rate, and spreading factor) that optimizes the upper and lower bounds on the average distortion. Under various channel conditions and interference levels, we numerically computed the optimum three-tuple, and verify the accuracy with system-level simulations. For small values of spreading factor, we show that the system performance is hurt by the self-interference of the user-of-interest, thus cautioning against aggressive channel coding. Since a multi-carrier DS-CDMA (or, simply MC-CDMA) system is more robust to NBI, we propose to employ an MC-CDMA system to improve the distortion performance on channels with severe NBI. For a fixed channel code rate, we then quantify the tradeoff between source coding and spreading for an MC-CDMA system.

In the second part of the dissertation, we consider a parallel relay channel wherein the relay nodes help the source transmissions to provide improved reliability at the destination. With multiple relay nodes, we design and analyze robust noncoherent amplify-and-forward receivers for use on rapidly-varying Rayleigh fading channels with unknown instantaneous channel knowledge. Next, with a sum power constraint, we consider the problem of optimal transmit power allocation when only statistical knowledge, in terms of the average fading power, of the channel is available at the transmitting nodes. We quantify the improvements in both outage probability performance and asymptotic cooperation gain of various relaying protocols with optimal power allocation.

CHAPTER 1

Introduction

Next generation, also referred to as fourth generation (4G), wireless systems are expected to provide increased spectral efficiency, and high quality multimedia content with improved reliability [1]. Some of the challenges in realizing this goal are battery power concerns of mobile handsets, limited spectrum availability, robustness to channel quality and interference conditions, ubiquitous coverage, and terminal mobility.

Since the transmissions over a wireless channel are broadcast in nature, and the effects of physical layer imperfections, such as packet errors, will be propagated throughout the communication protocol stack, it is rather a challenging task to design efficient communication protocols. In this context, the validity of the traditional approach of layered communication protocol architecture is being reexamined by the research community. A perspective, termed *cross-layer design*, has emerged that allows us to design a protocol stack by actively exploiting the dependencies among protocol layers to maximize the performance gains [2]-[5].

As an instructive example of cross-layer design, consider a typical communication protocol stack as shown in Fig. 1.1. Instead of a traditional OSI (open systems interconnections) approach of seven layers [6], for simplicity, only five layers are shown in Fig. 1.3. Some possible functionalities are also listed below each layer's title. To motivate the cross-layer design perspective, consider a fixed transmission bandwidth of W Hz. The transmission rate supported with this bandwidth can be allocated among the different layers in a number of ways. For example, the entire rate can be allocated to source

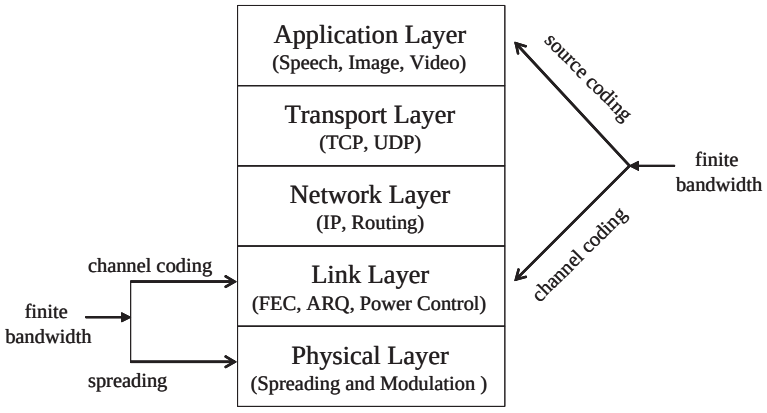

Figure 1.1 *A cross-layer design example: Here, for a finite bandwidth, either the source code rate and channel cod rate are jointly optimized, or the spreading factor and the channel code rate are jointly optimized.*

coding (i.e., the application layer), leaving no rate to channel coding (i.e., the link layer) or modulation (i.e., the physical layer), thus seriously compromising the communication reliability. On the other hand, the total rate can be apportioned between the link layer and the application layer. More rate for source coding leads to less rate for channel protection, and hence more channel errors, whereas allocating more rate for channel coding (i.e., better protection against channel errors) potentially leads to an increase in source distortion (i.e., fewer bits are available to represent a source sample). Thus, there exists a tradeoff between source and channel coding, which is characterized in [7], [8], and [9]. In an analogous manner, using a spread-spectrum modulation approach, the total chip rate can also be shared between the physical layer and the link layer. In this scenario, we observe that more rate for channel coding leads to less robustness against interference and multipath. On the other hand, more spreading bandwidth (i.e., higher chip rate) might lead to too weak channel coding. This tradeoff in the literature is termed *coding-spreading tradeoff*, and is addressed in [10] by Hui, [11] by Li and Milstein, [12] by Massey, [13] by Bickel *et al*, [14] by Mandayam and Holtzman, [15] by Motani and Veeravalli, [16] by Veeravalli and Mantravadi, and [17] by Lian *et al*.

In fact, as shown in Fig. 1.2, one can generalize the above framework by allocating the

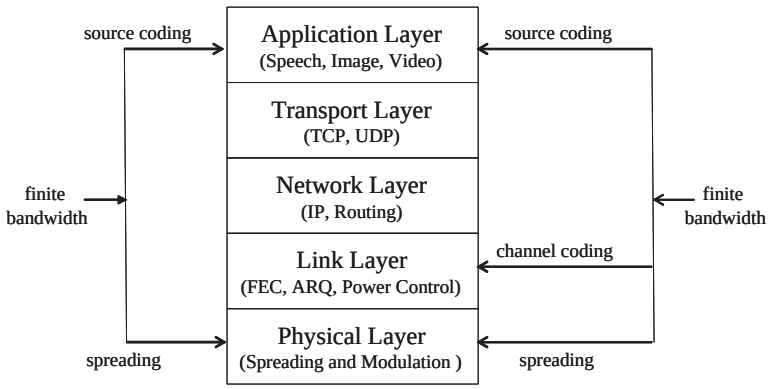

Figure 1.2 *Cross-layer approaches considered in this dissertation: Here, for a finite bandwidth, a three-way optimization of source code rate, channel code rate and spreading factor is considered in Chapter. 2. A simple case, in which the channel code rate is fixed, of jointly optimizing spreading factor and the source code rate is also investigated in Chapter. 3.*

available bandwidth, in an optimal manner, to source coding, channel coding and spreading. Initial results in this direction are obtained in [18] for a frequency-flat Rayleigh fading DS-CDMA (direct-sequence code-division multiple access) channel. In this dissertation, we extend the results of [18] to channels with frequency-selective generalized fading, and narrowband interference (NBI). This thesis also considers a simplified scenario in which we fix the channel coding rate, also shown in Fig. 1.2, and investigate the tradeoff between source coding and spreading for a multi-carrier DS-CDMA (or, simply MC-CDMA) system.

The huge success of wireless local area networks (WLANs) led the 4G wireless research community to consider the possibility of integrating WLAN and cellular systems to provide improvements in mobility and range extensions for high data rate users [19] (see Fig. 1.3). In this context, relay-based deployment concepts have recently become popular [20], which are also finding interesting applications in infrastructure-based wireless systems as well as in wireless mesh networks [21]. The relay channel, shown in Fig. 1.4, has a rich history. In [22], Van Der Meulen introduced the relay channel in the context of his study on three-terminal communication channels. Later Meulen [23] and

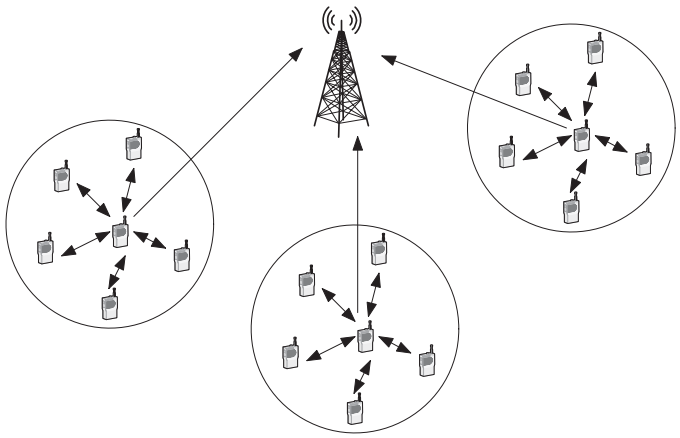

Figure 1.3 *A wireless system consisting of both cellular and ad-hoc networks as component subsystems.*

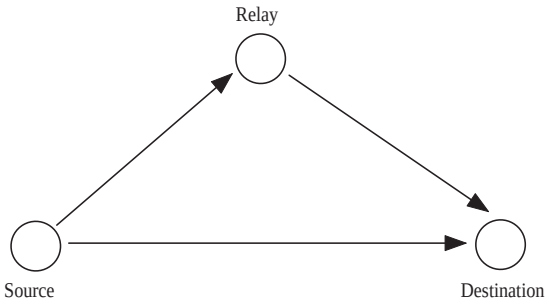

Figure 1.4 *The relay channel.*

Sato [24] presented upper bounds to the relay channel capacity. Although the exact capacity of a general relay channel is not yet fully characterized, Cover and El Gamal in [25] derived upper bounds on the capacity of a general relay channel and the exact capacity of a Gaussian degraded relay channel.

A recent study [26] by a European research organization has predicted that the future growth in wireless might be fueled by mobile terminals cooperating with each other. In a cooperating wireless network, a more general framework than the previously discussed relay-assisted communication scenario, the user terminals share their available resources, such as transmission time, antennas, battery power and channel bandwidth, in such a

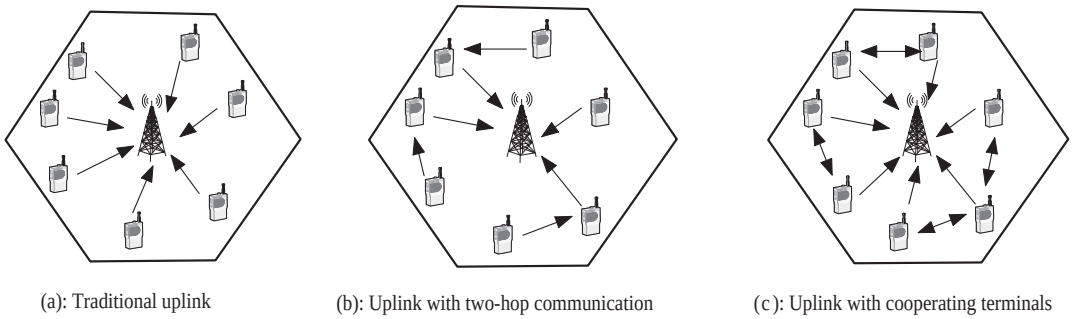

(a): Traditional uplink (b): Uplink with two-hop communication (c): Uplink with cooperating terminals

Figure 1.5 *In this figure, (a) shows a conventional uplink of a single cell. A two-hop uplink approach of (b) might be more efficient for terminals at the cell boundary. Generalization of the two-hop idea of (b) leads to the concept of* cooperating terminals*, shown in (c), wherein each terminal can simultaneously act as a source as well as a relay.*

way that a significant improvement in the overall network utility (such as improvements in system throughput, or reduction in network operating cost) can be realized. As an example, a distinction among a conventional cellular uplink, a two-hop relay-assisted uplink, and an uplink based on cooperating terminals, is illustrated in Fig. 1.5. For a tutorial on user cooperation, we refer the reader to [27].

In this dissertation, we consider a scenario in which multiple relay nodes help the source transmissions by forming a parallel relay network (see Fig. 1.6). We first address the key issue of the end-to-end reliability (as measured by the average probability of error at the destination) when instantaneous channel state information (CSI) is not available to the nodes in the network. In a later part of this thesis, we quantify the benefits of optimum power allocation with various relaying protocols when the total network transmit power is kept constant. Here, we assume that the receivers have perfect CSI, whereas only statistical knowledge of the channel (i.e., average channel fading power) is available to the transmitters.

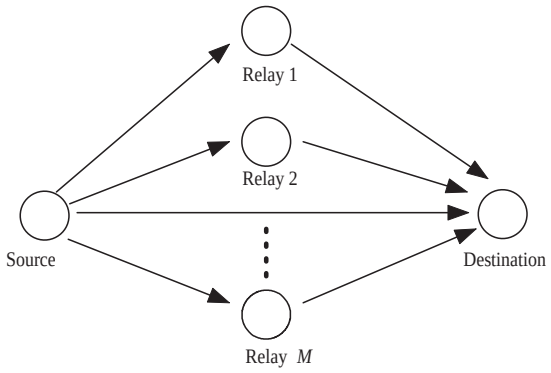

Figure 1.6 *A parallel relay network formed with multiple relay nodes.*

1.1 Thesis Organization

The main contributions of this dissertation are contained in Chapters 2-5. The chapters are organized in such a way that Chapters 2 and 3 can be read together, whereas Chapters 4 and 5 can be pursued independently.

In Chapter 2, with a constraint on the transmission bandwidth, we study the three way tradeoff among source coding, channel coding and spreading for a wideband DS-CDMA system. Assuming a Gaussian source with optimum quantizer, a convolutional code with soft-decision decoder, and a randomly spread DS-CDMA system with RAKE reception, we present upper and lower bounds on the end-to-end average source distortion. Our numerical results in Chapter 2 demonstrate that the optimal three-tuple (i.e., source coding rate, channel coding rate, and spreading factor), that is, the one that minimizes the distortion upper bound, is quite close to the one based on the lower bound on the average distortion. Interestingly, for small values of spreading factor, our simulations show that the distortion performance can be compromised by the self-interference of the user-of-interest, thus cautioning against aggressive channel coding.

In Chapter 3, we are concerned with improving the distortion performance on channels with severe NBI. Since an MC-CDMA system is more robust to NBI than a DS-CDMA system, in Chapter 3 we propose to use an MC-CDMA system in place of the

conventional DS-CDMA system to improve the distortion performance. Our results with MC-CDMA show an improvement in not only the average distortion performance, but also the three-way tradeoff performance. That is, under various channel conditions, for the same bandwidth constraint with approximately identical receiver complexities for both DS- and MC-CDMA systems, our results show that an MC-CDMA system supports a larger source coding rate than does a DS-CDMA system. Our results in both Chapters 2 and 3 show that the optimal bandwidth allocation, in general, depends on the system and the channel conditions, such as the total number of active users, the average jammer-to-signal power ratio (JSR), and the number of resolved multipath components together with their power delay profile.

In Chapters 4 and 5, we study the parallel relay channel model of Fig. 1.6 in detail. On rapidly-varying Rayleigh fading channels with no CSI at the receiving nodes, in Chapter 4 we present optimum noncoherent amplify-and-forward (AF) detectors for both OOK and BFSK modulations. We derive upper and lower bounds on the average probability of error, and prove that the asymptotic diversity order of a noncoherent AF receiver is twice that of a noncoherent DF (decode-and-forward) receiver. To minimize the implementation complexity, we also propose suboptimum receivers along with their performance evaluations.

With a constraint on the average sum power of the source and all the relay nodes, Chapter 5 considers the problem of optimal transmit power allocation. In this chapter, we assume that the receivers have perfect knowledge of the CSI, whereas only statistical knowledge of the channel is available at the transmitting nodes. We quantify the improvements in outage probability performance, as well as the asymptotic cooperation gain of various relaying protocols with optimal power allocation.

CHAPTER 2

Source Coding, Channel Coding and Spreading Tradeoffs in a DS-CDMA System

2.1 Introduction

It is well known that efficient channel coding together with the processing gain inherent in the use of spread-spectrum enables a direct-sequence CDMA system to successfully combat the effects of multipath distortion, multiple access interference (MAI), and intentional/unintentional narrow-band interference [28]-[30]. However, for a fixed spread bandwidth, transmission of high quality source information competes for the available bandwidth with channel coding and spreading. This motivates us to study the tradeoffs involved among source coding, channel coding and spreading in a DS-CDMA system.

We first briefly review the related previous work. In [7] and [8], an information theoretic approach is taken to investigate the tradeoffs between source and channel coding. In [11] and [16], the tradeoff between coding and spreading is investigated for a spread-spectrum system. Using system level simulations, in [31], Zhao *et al.* studied the problem of optimal bandwidth allocation among source coder, channel coder, and spread-spectrum modulator for progressive transmission of images over frequency-selective fading channels with MAI. Recently, in [18], an analysis was presented for the optimal bandwidth allocation on additive white Gaussian noise (AWGN) and flat Rayleigh fading CDMA channels with both block coding with hard-decision decoding and convolutional coding with soft-decision decoding.

In this chapter, we extend the analysis of [18] to the case of a frequency-selective fading channel with NBI. We assume a Gaussian source with the optimum scalar quantizer and a binary convolutional code with soft-decision decoding. For the sake of generality, we model the individual multipath components as independent, Nakagami-m distributed with arbitrary fading parameters, and assume that the NBI is a Gaussian distributed partial-band interferer (PBI). Using a standard Gaussian approximation for the MAI, we obtain an upper and a lower bound on the pairwise error probability (PEP) with soft-decision decoding, using which we bound the end-to-end average source distortion. In our analysis, we assume that the self-interference is negligible. As a consequence, our analytical results apply to scenarios such as where the dominant source of interference is due to MAI and/or jamming. We first note that the joint three-way constrained optimization of the source code rate, the channel code rate, and the spreading factor can be simplified into an unconstrained optimization problem over two variables. Upon fixing the channel code rate, we show that both upper and lower bound-based distortion functions are convex functions of the source code rate. An explicit solution for the optimum source code rate, that minimizes the average distortion, is difficult to obtain and requires computer-based search techniques. We note that the analysis of [18], which is valid for both an AWGN channel and a flat Rayleigh fading channel, can be viewed as a special case of the analysis presented in this chapter. Numerical results are given for the optimum source code rate and spreading factor, parameterized by the channel code rate and code constraint length. Results indicate that the optimal bandwidth allocation, in general, depends on the system and the channel conditions, such as the total number of active users, the average jammer-to-signal power ratio, and the number of resolved multipath components together with their power delay profile.

The rest of this chapter is organized as follows. In Section 2.2, we introduce our system and the channel model and derive upper and lower bounds on the pairwise error probability with soft-decision decoding. Analysis of the end-to-end average distortion with soft-decision channel decoding is presented in Section 2.3, and the optimum band-

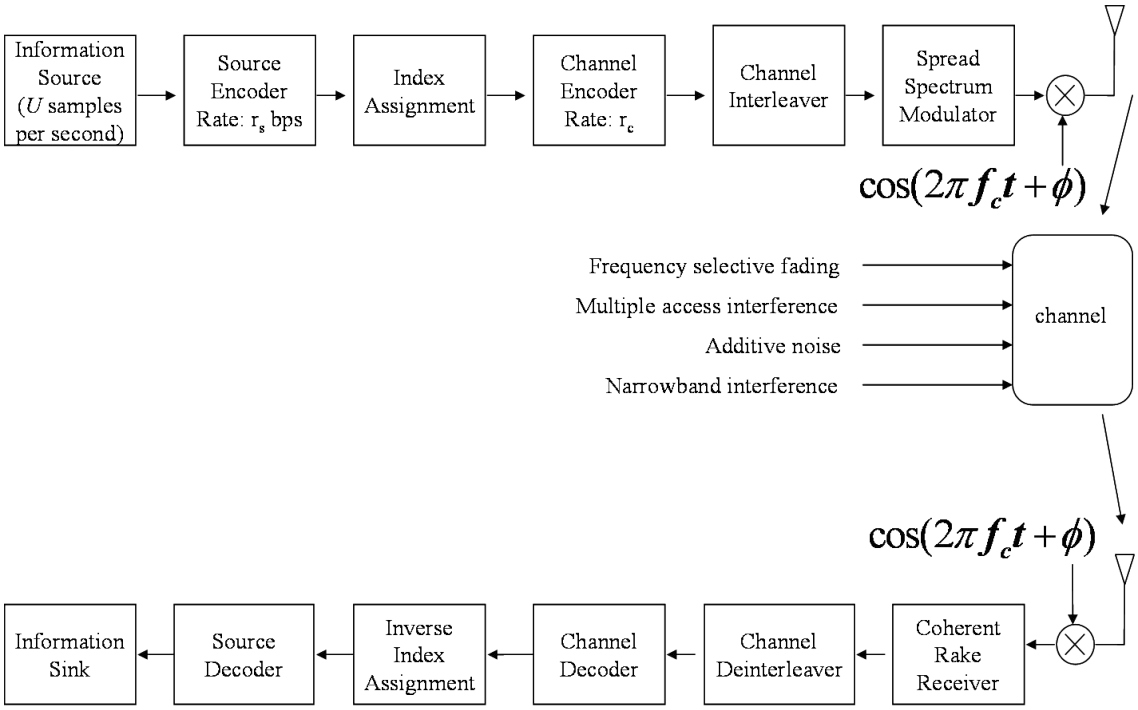

Figure 2.1 *Block diagram of the transmitter–receiver pair for the desired user.*

width allocation problem is detailed in Section 2.4. Numerical results and discussion are provided in Section 2.5. Finally, we conclude our work in Section 2.6.

2.2 System Model

The transmitter-receiver pair for the user of interest is shown in Fig. 2.1. The information source is quantized by the source encoder with a rate of r_s bits per source sample, which are then mapped onto a new bit index of the same length r_s using an index assignment block. While ordinarily the purpose of an index assignment is to permute indices so that small Hamming distance corresponds to close quantization levels, for ease of analysis, as in [32], [18], we assume a random index assignment with a one-to-one mapping of indices from 0 through $2^{r_s} - 1$.

The bit stream at the output of the index assignment block is encoded with a convo-

lutional code of rate r_c, whose output is interleaved, assumed to be ideal, before passing through the spread-spectrum modulator. We now present the mathematical model for the transmitter, the channel and the receiver.

2.2.1 Transmit Signal Model

With K_u simultaneous users in the system, the transmitted signal for the kth user is denoted by $S^{(k)}(t)$, and is expressed in the form

$$S^{(k)}(t) = \sqrt{2P}a^{(k)}(t)d^{(k)}(t)\cos(2\pi f_c t + \phi^{(k)}), \tag{2.1}$$

where P is the transmit power, assumed to be common to all the users, f_c is the carrier frequency in Hertz, $\phi^{(k)}$ is the initial phase angle and $a^{(k)}(t)$ is the spreading code sequence of the kth user, which can be expressed as $a^{(k)}(t) = \sum_{j=-\infty}^{\infty} a_k[j]h_{T_c}(t - jT_c)$, where $a_k[j] \in \{-1, +1\}$, and $h_{\mathcal{T}}(t)$ is a rectangular pulse shape filter with $h_{\mathcal{T}}(t) = 1$ for $0 \leq t < \mathcal{T}$, and is zero elsewhere. The data signal of the kth user, $d^{(k)}(t)$, is given by $d^{(k)}(t) = \sum_{j=-\infty}^{\infty} d_k[j]h_{T_s}(t-jT_s)$, where $d_k[j] \in \{-1, 1\}$ denote the coded data stream, and T_s is the symbol duration, which is related to the bit duration, T_b, by $T_s = T_b r_c$ so that the energy-per-bit, E_b, can be expressed as $E_b = PT_b = PT_s/r_c$. We assume that the spreading sequence $\{a_k[j]\}$ is long enough to be considered as a random binary sequence with period much longer than the symbol duration. The spread factor, $\mathcal{S}_F$, of this coded system is defined as $\mathcal{S}_F = T_s/T_c = T_b r_c/T_c$.

2.2.2 Channel Model

The channel is assumed to be frequency-selective and is slowly fading over the duration of T_s. The low-pass equivalent impulse response for the kth user is given by

$$h^{(k)}(t) = \sum_{l=0}^{L-1} \alpha_l^{(k)} e^{j\theta_l^{(k)}} \delta(t - \tau_l^{(k)}), \tag{2.2}$$

where L is the number of resolved multipaths, which is related to the multipath delay spread T_m and the chip duration T_c by $L = \lfloor T_m/T_c \rfloor + 1$, where $\lfloor x \rfloor$ denotes the largest integer that is less than or equal to x. $\alpha_l^{(k)}$ is the random amplitude fade on the lth path, which is assumed to be Nakagami-m distributed with the probability density function (pdf) [33]

$$f_{\alpha_l^{(k)}}(x) = \frac{2m_l^{m_l}}{\Omega_l^{m_l}\Gamma(m_l)} \exp\left(-\frac{m_l x^2}{\Omega_l}\right) x^{2m_l-1}, \;\; x \geq 0, \tag{2.3}$$

where $m_l \geq 0.5$ is the Nakagami parameter, also known as the fading severity index, and $\Omega_l = E[(\alpha_l^{(k)})^2]$ is the average fading power on the lth path, which is assumed to be independent of the user index k. We note that the pdf expression of (2.3) allows us to investigate the bandwidth tradeoff problem on generalized wideband fading channels with variable severity of individual resolvable multipaths. For simplicity, similar to [34]-[35], we assume that the random phase $\theta_l^{(k)}$ is independent of $\alpha_l^{(k)}$, and is uniformly distributed over $[0, 2\pi)$. The random variable (r.v) $\tau_l^{(k)}$ denotes propagation delay on the lth path, and is assumed to be uniformly distributed in $[0, T_c)$.

In addition to the above described multipath, the transmitted signal is also affected by a narrow-band jammer, which, in this chapter, is modelled as a Gaussian-distributed PBI, $J(t)$, with a power spectral density (PSD)

$$S_J(f) = \begin{cases} \frac{\eta_J}{2} & \text{for } f_c - \frac{W_J}{2} \leq |f| \leq f_c + \frac{W_J}{2} \\ 0 & \text{otherwise,} \end{cases} \tag{2.4}$$

where η_J and W_J are the one-sided power spectral density and the bandwidth of the PBI, respectively. Finally, the average power of the jammer is denoted by $\mathcal{N}_J$, and is given by $\mathcal{N}_J = \eta_J W_J$.

2.2.3 Receiver Model

Without loss of generality, we assume that the first user (i.e., $k = 1$) is the user-of-interest. With this, the received signal after passing through the frequency-selective

fading channel with a PBI can be expressed as

$$r(t) = \sum_{k=1}^{K_u} \sqrt{2P} \sum_{l=0}^{L-1} \alpha_l^{(k)} a^{(k)}(t-\tau_l^{(k)}) d^{(k)}(t-\tau_l^{(k)}) \cos(2\pi f_c t + \psi_l^{(k)}) + n(t) + J(t), \quad (2.5)$$

where $\psi_l^{(k)} = -2\pi f_c \tau_l^{(k)} + \theta_l^{(k)} + \phi^{(k)}$ is the effective phase on the lth path of the kth user, and $n(t)$ is zero-mean AWGN with two-sided power spectral density of $N_0/2$.

We assume that the code acquisition for the desired user is successful, so that the matched filter on the first finger of the RAKE receiver is synchronized to the last path of the desired user. We also assume perfect knowledge of the desired user's fade coefficients, $\{\alpha_l^{(1)}\}$. With this, the output of the RAKE receiver during the nth code symbol is given by [34]

$$\begin{aligned} Z_n &= \sum_{l=0}^{L-1} \int_{lT_c}^{lT_c+T_s} r(t)\alpha_l^{(1)}[n] a^{(1)}(t - lT_c) \cos(w_c t + \psi_l^{(1)}[n]) dt \\ &= \sum_{l=0}^{L-1} \left(D_l[n] + I_l^{SI}[n] + I_l^{MAI}[n] + N_l[n] + J_l[n] \right), \end{aligned} \quad (2.6)$$

where the subscript l and the index n denote, respectively, the path index and the symbol index, and the other terms of (2.6) are defined as follows: $a) D_l[n]$ is the component of the test statistic due to the desired user, $b) I_l^{SI}$ is the self interference of user 1, due to the non-impulsive nature of the autocorrelation function of the spreading code, $c) I_l^{MAI}[n]$ is the MAI due to the other $K_u - 1$ users, $d) N_l[n]$ is the contribution due to the AWGN, and $e) J_l[n]$ is the contribution made by the jammer. Following the analysis of [34], one can show that the terms $D_l[n]$, $I_l^{MAI}[n]$, $I_l^{SI}[n]$, $N_l[n]$ and $J_l[n]$ are, respectively, given by

$$D_l[n] = \sqrt{\frac{P}{2}} d_1[n] T_s \left(\alpha_l^{(1)}[n] \right)^2 \quad (2.7)$$

$$I_l^{MAI}[n] = \sqrt{\frac{P}{2}} \sum_{k=2}^{K_u} \sum_{j=0}^{L-1} \alpha_l^{(1)}[n]\alpha_j^{(k)}[n] \times \Big(d_k[n-1]R_{k,1}(\tau_{l,j}^{(k)}[n]) + d_k[n]\widehat{R}_{k,1}(\tau_{l,j}^{(k)}[n]) \Big) \cos(\psi_{l,j}^{(k)}[n]) \quad (2.8)$$

$$I_l^{SI}[n] = \sqrt{\frac{P}{2}} \sum_{i=0, i\neq l}^{L-1} \alpha_l^{(1)}[n]\alpha_i^{(1)}[n] \times \Big(d_1[n-1]R_{1,1}(\tau_{l,i}^{(1)}[n]) + d_1[n]\widehat{R}_{1,1}(\tau_{l,i}^{(1)}[n]) \Big) \cos(\psi_{l,i}^{(1)}[n]) \quad (2.9)$$

$$N_l[n] = \int_{lT_c}^{lT_c+T_s} n(t)\alpha_l^{(1)}[n]a^{(1)}(t-lT_c)\cos(w_c t + \psi_l^{(1)}[n])dt \quad (2.10)$$

$$\text{and } J_l[n] = \int_{lT_c}^{lT_c+T_s} J(t)\alpha_l^{(1)}[n]a^{(1)}(t-lT_c)\cos(w_c t + \psi_l^{(1)}[n])dt, \quad (2.11)$$

where, for $k = 2, \ldots, K_u$, $\tau_{l,j}^{(k)}[n] = \tau_j^{(k)}[n] - \tau_l^{(1)}[n]$, $\psi_{l,j}^{(k)}[n] = \psi_j^{(k)}[n] - \psi_l^{(1)}[n]$, and the partial correlation coefficients $R_{k,1}(\cdot)$ and $\widehat{R}_{k,1}(\cdot)$ are defined as $R_{k,1}(\tau) = \int_0^{\tau} a^{(k)}(t-\tau)a^{(1)}(t)dt$ and $\widehat{R}_{k,1}(\tau) = \int_{\tau}^{T_s} a^{(k)}(t-\tau)a^{(1)}(t)dt$.

We are interested in obtaining the statistics of Z_n at the output of the RAKE receiver. For analytical tractability, conditioned on $\{\alpha_l^{(1)}[n]\}$ and $a^{(1)}(t)$, for a large number of users, we model the interference terms of (2.8)-(2.11) as Gaussian processes and obtain the following conditional variance [34],[35]:

$$(\sigma_l^{MAI}[n])^2 = \frac{PT_sT_c}{6}(\alpha_l^{(1)}[n])^2(K_u - 1)\Omega_T \quad (2.12)$$

with Ω_T is defined as

$$\Omega_T = \sum_{l=0}^{L-1} \Omega_l. \quad (2.13)$$

For a large number of users, the contribution of self-interference is negligible compared

with the MAI, allowing us to ignore the contribution due to $I_l^{SI}[n]$. The variance of AWGN can be computed as [34],[35]

$$(\sigma_l^N[n])^2 = E[(N_l[n])^2] = \frac{T_s\eta_0}{4}(\alpha_l^{(1)}[n])^2, \tag{2.14}$$

whereas the variance of the jammer's contribution, after some algebra, can be shown to be

$$\begin{aligned}(\sigma_l^J[n])^2 &= E[(J_l[n])^2] = (\alpha_l^{(1)}[n])^2 T_s \frac{1}{4}\int_{-\infty}^{\infty} |H(f)|^2 \left(S_J(f-f_c)+S_J(f+f_c)\right)\frac{df}{T_c} \\ &= (\alpha_l^{(1)}[n])^2 T_s \frac{\eta_J}{4}\int_{-W_J/2}^{W_J/2} |H(f)|^2 \frac{df}{T_c},\end{aligned} \tag{2.15}$$

where $H(f)$ is the Fourier transform of $h_{T_c}(t)$. Let us define by $\rho_J = W_J/W$ the fraction of the total bandwidth occupied by the jammer, where $W = 1/T_c$ is the CDMA system bandwidth. Let $\mathrm{JSR} = \eta_J W_J/P = \mathcal{N}_J/P$ denote the jammer-to-signal power ratio, and $\gamma_b = PT_b/N_0 = E_b/N_0$ denote the signal-to-noise ratio (SNR) per information bit. We also define $\zeta_J = \int_{-W_J/2}^{W_J/2} |H(f)|^2 df/T_c = \int_{-\rho_J/2}^{\rho_J/2} \frac{\sin^2 \pi u}{\pi^2 u^2} du$. Using integration by parts, ζ_J can be simplified as $\zeta_J = 2(\cos(\pi\rho_J)-1)/(\pi^2\rho_J) + (2/\pi)\mathrm{Si}[\pi\rho_J]$, where $\mathrm{Si}[u] = \int_0^u \frac{dt}{t}\sin t$ [36], so that (2.15) can be simplified to

$$(\sigma_l^J[n])^2 = (\alpha_l^{(1)}[n])^2 \frac{\eta_0}{4}\frac{T_s \mathrm{JSR}\gamma_b r_c}{\mathcal{S}_F \rho_J}\zeta_J. \tag{2.16}$$

Using the results of (2.12)-(2.15), the decision statistic, Z_n, at the output of the RAKE receiver for the nth symbol is given by

$$Z_n = d_1[n]T_s\sqrt{\frac{P}{2}}\sum_{l=0}^{L-1}(\alpha_l^{(1)}[n])^2 + \eta_e[n] \tag{2.17}$$

where $\eta_e[n]$ is approximately Gaussian with zero-mean and variance

$$\sigma_e^2[n] = \sum_{l=0}^{L-1} (\alpha_l^{(1)}[n])^2 \frac{N_e}{2},$$

and

$$N_e \triangleq 2PT_s^2 \left\{ \frac{(K_u - 1)\Omega_T}{6\mathcal{S}_F} + \frac{\eta_0}{4PT_s} + \frac{\eta_0}{4PT_s} \frac{\mathrm{JSR}\gamma_b r_c \zeta_J}{\mathcal{S}_F \rho_J} \right\}. \tag{2.18}$$

2.2.4 Frame Error Rate with Convolutional Coding

The RAKE receiver outputs, $\{Z_n\}$, corresponding to a given coded frame, are passed to the deinterleaver and are then used by the Viterbi decoder for soft-decision decoding. For convenience, let us define $\beta_n = \sum_{l=0}^{L-1} (\alpha_l^{(1)}[n])^2$, and $\underline{\beta} = (\beta_1, \ldots, \beta_N)$, where N is the frame length, and for simplicity, we have dropped the index of the desired user. It is well known that at high SNR, the key performance metric with channel coding is the pairwise error probability between two codewords [37]. The PEP between two codewords $\mathbf{x} = (x_1, \ldots, x_N)$ and $\mathbf{y} = (y_1, \ldots, y_N)$ which differ in d positions is

$$\begin{aligned} P_2(d|\underline{\alpha}) &= \mathrm{Prob}\left(\sum_{n=1}^{N} (z_n - x_n)^2 > \sum_{n=1}^{N} (z_n - y_n)^2 \right) \\ &= \mathrm{Prob}\left(\sum_{n=1}^{N} z_n (x_n - y_n) < 0 \right) \\ &= \mathrm{Prob}\left(\sum_{n=1}^{N} \eta_e[n](x_n - y_n) < -\sqrt{\frac{PT_s^2}{2}} \sum_{n=1}^{N} \beta_n x_n (x_n - y_n) \right), \end{aligned} \tag{2.19}$$

where in the last step of (2.19) we have used (2.17). Without loss of generality, we assume that the codewords $\mathbf{x}$ and $\mathbf{y}$ differ in the first d positions. Then, using the Chernoff bound, $Q(x) \leq 1/2 \exp(-x^2/2)$ for $x \geq 0$, we can upper bound (2.19) as

$$P_2(d|\underline{\beta}) \leq \frac{1}{2} \exp\left(-\Gamma \sum_{n=1}^{d} \beta_n \right), \tag{2.20}$$

where Γ is the signal-to-interference-plus-noise ratio (SINR) and is given by

$$\Gamma = \frac{\frac{PT_s}{N_0}}{1 + \frac{PT_s}{N_0 \mathcal{S}_F}\left\{\frac{2}{3}(K_u - 1)\Omega_T + \frac{\mathrm{JSR}\zeta_J}{\rho_J}\right\}} = \frac{r_c\gamma_b}{1 + \frac{r_c\gamma_b}{\mathcal{S}_F}\Delta}, \tag{2.21}$$

and where we have used $T_s = r_c T_b$, $E_b = PT_b$, and $\Delta = \frac{2}{3}(K_u - 1)\Omega_T + \frac{\mathrm{JSR}\zeta_J}{\rho_J}$. Note that Δ, being a function of the multipath channel profile, the number of active users, and the JSR, is independent of r_c, $\mathcal{S}_F$, and the SNR-per-bit of the desired user, γ_b. Upon taking the expectation of (2.20) over the distribution of (2.3), we obtain

$$\begin{aligned} \overline{P}_2(d) = E\left\{P_2(d|\underline{\beta})\right\} &\leq \frac{1}{2}\prod_{l=0}^{L-1}\left(\frac{m_l}{m_l + \Gamma\Omega_l}\right)^{m_l d} < \frac{1}{2}\prod_{l=0}^{L-1}\left(\frac{m_l}{\Omega_l}\right)^{m_l d}\Gamma^{-d\sum_{l=0}^{L-1} m_l} \\ &= C(\underline{m}, \underline{\Omega}, d)\Gamma^{-md}, \end{aligned} \tag{2.22}$$

where $m = \sum_{l=0}^{L-1} m_l$, $\underline{m} = (m_0, \ldots, m_{L-1})$, $\underline{\Omega} = (\Omega_0, \ldots, \Omega_{L-1})$, and $C(\underline{m}, \underline{\Omega}, d) = \frac{1}{2}\prod_{l=0}^{L-1}\left(\frac{m_l}{\Omega_l}\right)^{m_l d}$. In this chapter, we assume that the maximum average SINR, $\overline{\Gamma}_{\max} = \Gamma \times \max(\Omega_l)$ is at least greater than unity (i.e., above 0 dB).

We note that an exact expression for the frame error rate (FER) for a convolutional code with soft-decision decoding is difficult to derive, which motivates us to employ the union bound, as it is sufficiently tight at high SNR. A tight upper bound on the FER of a convolutional code with block lengths larger than the constraint length is obtained in [18], using which we obtain the FER for our system as

$$\begin{aligned} P_B &\leq \sum_d t(d)\overline{P}_2(d) \\ &< \sum_d t(d)C(\underline{m}, \underline{\Omega}, d)\Gamma^{-md}, \end{aligned} \tag{2.23}$$

where $t(d)$ is a function of the weight spectrum [37] of the underlying convolutional code. We are also interested in a lower bound on the FER, which can be obtained by taking only the dominant term of (2.23). However, the Chernoff upper bound on PEP of (2.22) is no

longer useful. In Appendix-A, we derive a lower bound for $\overline{P}_2(d)$, using which the lower bound on the FER can be obtained as

$$P_B \geq t(d_{free})D(m, d_{free})(1 + \Gamma\omega)^{-md_{free}}, \tag{2.24}$$

where d_{free} is the free distance of the code, and $D(m, d)$ and ω are defined in Appendix-A.

2.3 End-to-End Average Distortion

For simplicity, we assume that the information source is Gaussian-distributed with independent and identically distributed source samples, each with unit variance. If r_s denotes the number of bits-per-source sample, then the average source distortion with minimum mean square error scalar quantization on a noise-free channel is approximated, for large r_s, as $D(r_s) = \epsilon 2^{-2r_s}$, where ϵ depends on the quantizer [38]. Note that each coded frame of length N contains Nr_c/r_s source samples. Then, the average distortion per source sample can be written as [39, Eqn. (10)]

$$\begin{aligned}
\mathcal{D}(r_s, r_c, \mathcal{S}_F) &= \frac{Nr_c/r_s(1 - P_B(r_c, \mathcal{S}_F))\epsilon 2^{-2r_s} + Nr_c/r_s P_B(r_c, \mathcal{S}_F)}{Nr_c/r_s} \\
&= \left((1 - P_B(r_c, \mathcal{S}_F))\epsilon 2^{-2r_s} + P_B(r_c, \mathcal{S}_F)\right) \\
&\leq \left(\epsilon 2^{-2r_s} + P_B(r_c, \mathcal{S}_F)\right) \\
&\leq \left(\epsilon 2^{-2r_s} + \sum_d t(d)C(\underline{m}, \underline{\Omega}, d)\Gamma^{-md}\right) \\
&\triangleq D_u(r_s, r_c, \mathcal{S}_F),
\end{aligned} \tag{2.25}$$

where the above upper bound is quite accurate in the high SNR region. Note that the term $t(d)$ of (2.25) depends on the number of input and output bits, and on the particular encoder used to realize the convolutional code of given rate. It also depends on the code's

constraint length[1] (i.e., the number of memory elements used). Unfortunately, in general, a functional relationship between $t(d)$ and r_c is not known.

A lower bound on the end-to-end average distortion can be obtained by first lower bounding the frame error rate, $P_B(r_c, \mathcal{S}_F)$ by the term with minimum free distance d_{free} as $P_B(r_c, \mathcal{S}_F) \geq t(d_{free})P_2(d_{free})$. With this, a lower bound on the average distortion can be obtained as

$$\begin{aligned} \mathcal{D}(r_s, r_c, \mathcal{S}_F) &\geq \epsilon 2^{-2r_s} + t(d_{free})P_2(d_{free})(1 - \epsilon 2^{-2r_s}) \\ &= \epsilon 2^{-2r_s} + t(d_{free})D(m, d_{free})(1 + \Gamma\omega)^{-md_{free}}(1 - \epsilon 2^{-2r_s}) \\ &\triangleq D_{lower}(r_s, r_c, \mathcal{S}_F), \end{aligned} \tag{2.26}$$

where in the second step of (2.26) we have used (2.24). In what follows, we consider both the upper bound and lower bound on the average distortion, (2.25) and (2.26), as our objective functions.

2.4 Optimum Bandwidth Allocation

If we denote by $\mathcal{U}$ the number of source samples per second available to the source coder, then the total rate at the output of the spread-spectrum modulator is given by $\mathcal{U}r_s\frac{1}{r_c}\mathcal{S}_F$, which should not exceed the spread-spectrum bandwidth W. That is, the variables r_s, r_c and $\mathcal{S}_F$ are related by $r_s\mathcal{S}_F/r_c \leq C_0$, where $C_0 = W/\mathcal{U}$. The distortion function is given by $D(r_s, r_c, \mathcal{S}_F)$, which can also be written as $D(r_s, r_c, C_0 r_c/r_s)$. We notice that by fixing the channel code rate, r_c, the distortion can be expressed only as a function of the source rate r_s together with the bandwidth constraint C_0. In this section, we minimize the objective functions, $D_u(r_s, r_c, \mathcal{S}_F)$ of (2.25) and $D_{lower}(r_s, r_c, \mathcal{S}_F)$ of (2.26), as a function of the source code rate r_s.

[1]Even for the same code rate, and the same constraint length, different generator polynomials result in different weight spectra, $t(d)$ [37].

2.4.1 Optimal Allocation Based on Upper Bound

With r_c fixed, we substitute $\mathcal{S}_F = C_0 r_c / r_s$ in Γ of (2.25) and simplify (2.25) in the form of a function of r_s alone as

$$D_u(r_s) = \epsilon 2^{-2r_s} + \sum_d t(d) C(\underline{m}, \underline{\Omega}, d) (r_c \gamma_b)^{-md} \left(1 + \frac{\gamma_b \Delta}{C_0} r_s\right)^{md}. \tag{2.27}$$

Differentiating (2.27) with respect to r_s we arrive at

$$\begin{aligned} \frac{d}{dr_s} D_u(r_s) &= -\epsilon 2 \ln 2 2^{-2r_s} + \\ &\quad \sum_d t(d) C(\underline{m}, \underline{\Omega}, d) (r_c \gamma_b)^{-md} md \frac{\gamma_b \Delta}{C_0} \left(1 + \frac{\gamma_b \Delta}{C_0} r_s\right)^{md-1}. \end{aligned} \tag{2.28}$$

If r_s^* is the optimum source code rate, then we have $\frac{d}{dr_s} D_u(r_s)|_{r_s = r_s^*} = 0$. Equivalently, r_s^* satisfies

$$r_s^* = \frac{1}{2} \log_2 \left(\frac{2\epsilon \ln 2}{\sum_d t(d) C(\underline{m}, \underline{\Omega}, d) (r_c \gamma_b)^{-md} md \frac{\gamma_b \Delta}{C_0} \left(1 + \frac{\gamma_b \Delta}{C_0} r_s^*\right)^{md-1}} \right). \tag{2.29}$$

The second derivative of $D_u(r_s)$ can be calculated by differentiating (2.28) with respect to r_s and results in

$$\begin{aligned} \frac{d^2}{dr_s^2} D_u(r_s) &= 4\epsilon (\ln 2)^2 2^{-2r_s} + \sum_d t(d) C(\underline{m}, \underline{\Omega}, d) (r_c \gamma_b)^{-md} \times \\ &\quad md(md-1) \left(1 + \frac{\gamma_b \Delta}{C_0} r_s\right)^{md-2} \left(\frac{\gamma_b \Delta}{C_0}\right)^2. \end{aligned} \tag{2.30}$$

Note that (2.30) is always positive, since $m = \sum_{l=0}^{L-1} m_l \geq L/2$ and $md \geq Ld/2 > 1$, showing that $D_u(r_s)$ is a convex function of r_s. The optimal 3-tuple is then given by $(r_s^*, r_c, C_0 r_c / r_s^*)$, where r_s^* can be obtained by solving (2.29).

2.4.2 Optimal Allocation Based on Lower Bound

Upon taking the first derivative of (2.26) with respect to r_s we obtain

$$\begin{aligned}\frac{d}{dr_s}D_{lower}(r_s) &= -\epsilon(2\ln 2)2^{-2r_s} + t(d_{free})D(m,d_{free})(1+\Gamma\omega)^{-md_{free}} \\ &\quad \times\epsilon(2\ln 2)2^{-2r_s} - t(d_{free})D(m,d_{free})(1-\epsilon 2^{-2r_s}) \\ &\quad \times md_{free}\omega(1+\Gamma\omega)^{-md_{free}-1}\frac{d\Gamma}{dr_s}, \end{aligned} \tag{2.31}$$

where

$$\frac{d\Gamma}{dr_s} = -\frac{r_c\gamma_b\frac{\gamma_b\Delta}{C_0}}{(1+r_s\frac{\gamma_b\Delta}{C_0})^2} = -\Gamma\frac{\frac{\gamma_b\Delta}{C_0}}{1+r_s\frac{\gamma_b\Delta}{C_0}}, \tag{2.32}$$

which is less than zero for all r_s. In Appendix-B, we prove that $D_{lower}(r_s)$ is a convex function of r_s. Upon setting $d/dr_s D_{lower}(r_s) = 0$ and solving for r_s, we arrive at the following implicit equation:

$$r_s^* = \frac{1}{2}\log_2\left(\epsilon - \frac{\epsilon 2\ln 2\left(1-t(d_{free})D(m,d_{free})(1+\Gamma^*\omega)^{-md_{free}}\right)}{t(d_{free})D(m,d_{free})(1+\Gamma^*\omega)^{-md_{free}-1}md_{free}\omega\frac{d\Gamma}{dr_s}\Big|_{r_s=r_s^*}}\right), \tag{2.33}$$

where $\Gamma^* = \Gamma$ evaluated at $r_s = r_s^*$.

2.5 Results and Discussion

In this section, we present some numerical results based on the analysis presented in Sections 2.2-2.4. Unless otherwise stated, it is assumed that the energy-per-bit (equivalently, the SNR-per-bit, γ_b) is kept constant. First, Fig. 2.2 shows the tightness of the lower and the upper bounds on the PEP for a frequency-selective i.i.d Rayleigh fading channel with $L = 4$ paths. Also shown is the true PEP from (A.2) in Appendix-A, which is numerically evaluated. We conclude from Fig. 2.2 that the bounds are sufficiently tight. In particular, for SNR-per-bit, γ_b, values less than 15 dB, the upper bound is within 2 dB

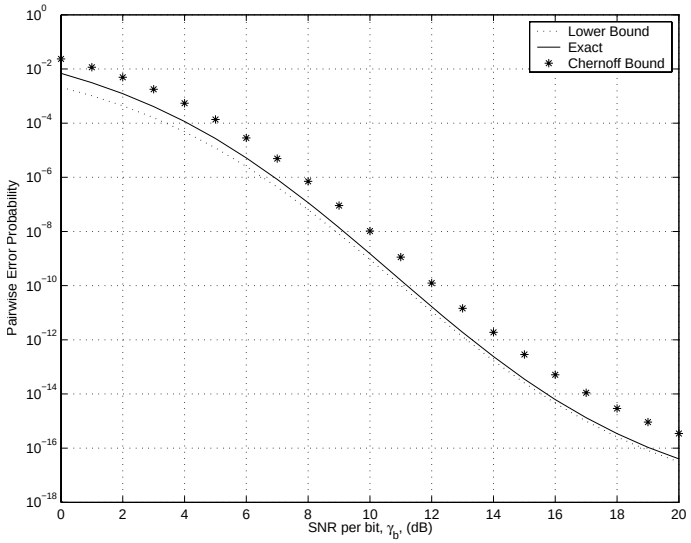

Figure 2.2 *Comparison of exact pairwise error probability with the one based on the Chernoff bound and the one based on a lower bound. Distance between two code words is set to ten. The system parameters are the following:* $K_u = 25$, *JSR = 5 dB,* $\rho_J = 0.2$, $r_c = 1/3$, $\mathcal{S}_F = 128$ *and* $L = 4$. *We assume i.i.d Rayleigh fading. That is,* $\underline{m} = (1, 1, 1, 1)$ *and* $\underline{\Omega} = (1, 1, 1, 1)$.

of the true PEP. Fig. 2.3 shows the effect of varying both JSR and K_u on the upper bound on the PEP for an exponentially decaying Nakagami multipath channel with $L = 4$ paths. From Fig. 2.3, we note that for smaller values of JSR and K_u, the bound is within 2 dB of the true PEP for γ_b less than or equal to 20 dB.

The lower and upper bounds on the average end-to-end source distortion, as derived in Section 2.3, are plotted in Fig. 2.4. For a fixed spread bandwidth and channel code rate, the average distortion is plotted as a function of the source code rate. A family of such curves is obtained for varying levels of channel code complexity, as measured by its constraint length. We notice from Fig. 2.4 that $i)$ there exists a source code rate at which the distortion is minimized, $ii)$ the minimum source code rate shifts to the right for increasing values of the channel code complexity, since a stronger channel code enables the spread-spectrum modulator to use a smaller value of the spread factor, $iii)$the lower and the upper bounds coincide at values of r_s that are near the r_s at which the distortion is minimized, after which the bounds differ by an order of magnitude. This difference in

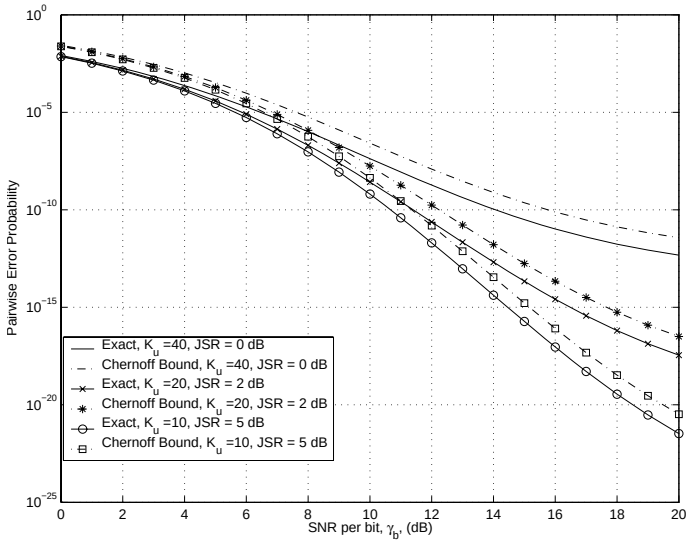

Figure 2.3 *Comparison of exact pairwise error probability with the one based on the Chernoff bound. Distance between two code words is set to ten.* $\rho_J = 0.2$*, channel code rate,* $r_c = 1/3$*, spreading factor,* $\mathcal{S}_F = 128$*. Number of multipaths,* $L = 4$ *with* $\underline{m} = (0.5, 1, 2.5, 5)$ *and* $\Omega_l = \exp(-\delta(l-1))$*,* $l = 1, \ldots, L$*, where* δ *is the decay parameter for the multipath intensity profile which is set to* 0.5*.*

the lower and the upper bounds can be explained as follows: For small values of r_s (i.e., large $\mathcal{S}_F$), the upper and lower bounds on the frame error rate are tight, resulting in a tight bound on the end-to-end distortion. This explains the behavior of the curves to the left of the minimum. However, when r_s increases, we have a smaller value for $\mathcal{S}_F$, and the Chernoff-based union bound is found to be less effective, and not comparable with the dominant term-based lower bound. This results in a large difference between the upper and lower bounds.

In Table 2.1, we present the optimum source code rate, the optimum spreading factor, and the resulting average distortion for various channel code rates. For all the channel codes, the complexity of the encoder is fixed at a constraint length of 6. Both lower and upper bounds on the distortion are considered for both i.i.d and non-i.i.d Rayleigh channels, with the constraint on the bandwidth expansion factor set to 500 (i.e., $r_s \frac{1}{r_c} \mathcal{S}_F = 500$). The number of users is fixed at $K_u = 15$. From Table 2.1, we observe that for both i.i.d and non-i.i.d fading conditions, the lower bound favors allocating more bandwidth to the

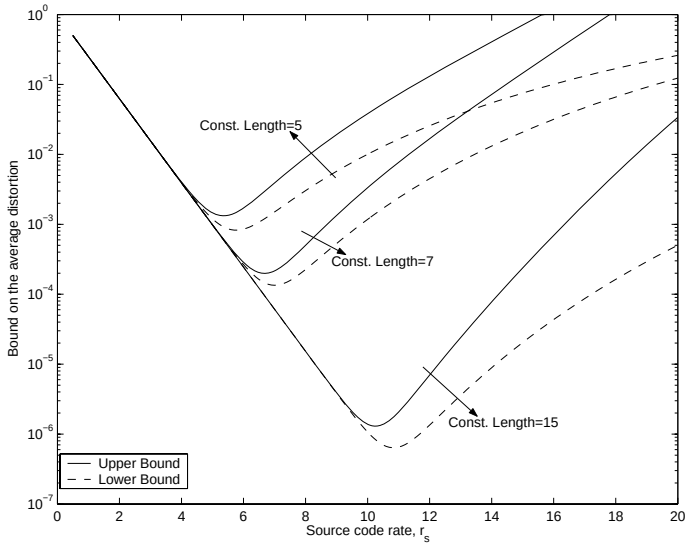

Figure 2.4 *Lower and upper bounds on the average distortion on i.i.d Rayleigh fading channels with $L = 4$ multipath components. The channel code rate is fixed to $r_c = 1/2$ and the bandwidth expansion factor is set to 500. Binary convolutional codes with various constraint lengths are used with an optimum distance spectrum, as given in [40]. The other system parameters are: JSR = 5 dB, $\rho_J = 0.25$, $K_u = 15$ and $\gamma_b = 10$ dB.*

Table 2.1 *Source code rate, spreading factor, and the minimum distortion, for a fixed channel code rate, based on both upper and lower bounds on the end-to-end average distortion. Both i.i.d and non-i.i.d Rayleigh fading channels are considered, with a multipath intensity profile (MIP) parameter $\delta = 0.5$ for the case of non-i.i.d fading.*

r_c	Channel	Lower Bound			Upper Bound		
		r_s^*	$\mathcal{S}_F = C_0 r_c / r_s^*$	$D(r_s^*)$	r_s^*	$\mathcal{S}_F = C_0 r_c / r_s^*$	$D(r_s^*)$
$\frac{1}{2}$	i.i.d	6.33	39	$3.04 \cdot 10^{-4}$	5.68	43	$6.56 \cdot 10^{-4}$
	non-i.i.d	8.81	28	1.02×10^{-5}	5.50	45	$8.44 \cdot 10^{-4}$
$\frac{1}{3}$	i.i.d	7.01	23	$1.17 \cdot 10^{-4}$	6.30	26	$2.74 \cdot 10^{-4}$
	non-i.i.d	9.78	17	$2.63 \cdot 10^{-6}$	6.17	27	$3.33 \cdot 10^{-4}$
$\frac{1}{4}$	i.i.d	6.95	17	$1.20 \cdot 10^{-4}$	6.53	19	$2.01 \cdot 10^{-4}$
	non-i.i.d	9.86	12	$2.23 \cdot 10^{-6}$	6.42	19	$2.35 \cdot 10^{-4}$

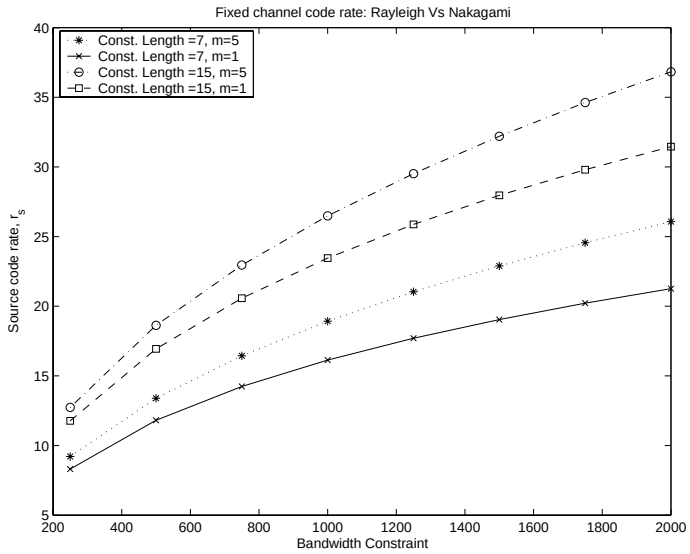

Figure 2.5 *Source code rate, for a fixed channel code, obtained using the upper bounds on the average distortion on i.i.d fading channels with $L = 4$ multipath components. Both Rayleigh fading and Nakagami fading with $m = 5$ are assumed. The channel code rate is fixed to $r_c = 1/2$ and the bandwidth expansion factor is varied. Number of information bits in the frame is set to 100. The other system parameters are: $\gamma_b = 10$ dB, $K_u = 10$, JSR = 5 dB, $\rho_J = 0.25$.*

source coder, whereas the upper bound favors increasing the spread factor. This is due to the fact that the lower bound-based end-to-end distortion is much smaller in comparison with the union upper bound-based one, and by increasing the spread factor (i.e., by reducing r_s) the upper bound-based distortion can be minimized. Table 2.1 also indicates that with decreasing channel code rates, it is beneficial to allocate more bandwidth to the source coder rather than to the spread-spectrum modulator. This can be explained as follows: For a given constraint length, a low rate channel code provides higher free distance, and hence a larger diversity order, which helps to reduce the burden on the spread-spectrum modulator.

By fixing the channel code rate at $r_c = 1/2$, and for constraint lengths of 7 and 15, r_s and $D_u(r_s)$ are plotted as a function of the bandwidth expansion factor in Figs. 2.5 and 2.6, respectively. Both Rayleigh (i.e., $m = 1$) and Nakagami fading channels are considered, with the Nakagami parameter of the latter channel set to five. From Fig. 2.5,

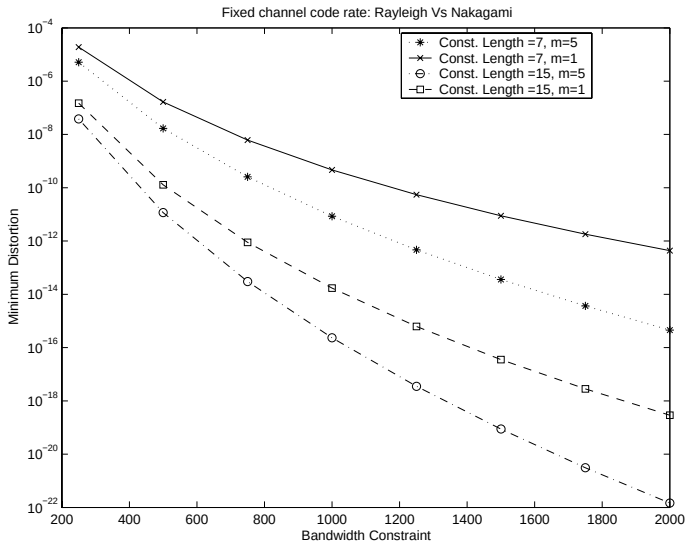

Figure 2.6 *Average distortion obtained using the source code rate of Fig. 2.5, for a fixed channel code on i.i.d fading channels with $L = 4$ multipath components. Both Rayleigh fading and Nakagami fading with $m = 5$ are assumed. The channel code rate is fixed to $r_c = 1/2$ and the bandwidth expansion factor is varied. Number of information bits in the frame is set to 100. The other system parameters are: $\gamma_b = 10$ dB, $K_u = 10$, JSR = 5 dB, $\rho_J = 0.25$.*

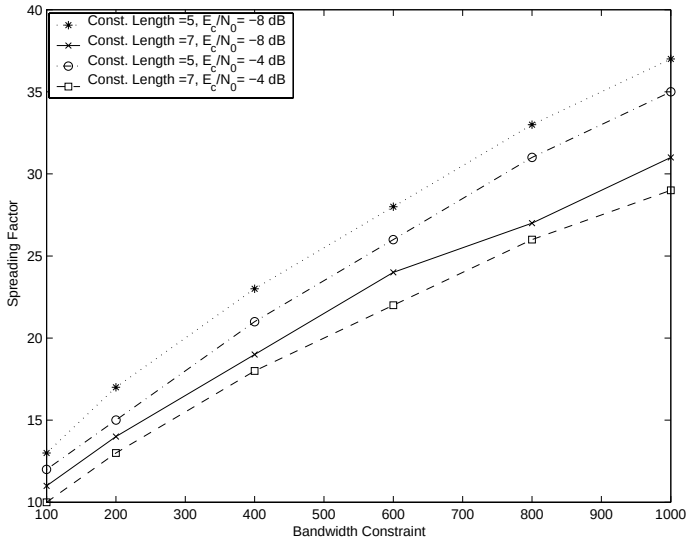

Figure 2.7 *Spreading factor, $\mathcal{S}_F$, for a fixed channel code, obtained using the upper bounds on the average distortion on i.i.d Rayleigh fading channels with $L = 4$ multipath components. The channel code rate is fixed to $r_c = 1/2$ and the bandwidth expansion factor is varied. Number of information bits in the frame is set to 100. The other system parameters are: $E_c/N_0 = PT_c/N_0$, $K_u = 10$, JSR = 5 dB, $\rho_J = 0.25$.*

we notice that as the total bandwidth increases, the source code rate increases. It is also evident that this allocation increases with the constraint length of the channel code, and with the fading severity index m of the Nakagami channel. That is, lighter fading (i.e., increasing m) and/or powerful channel code result in higher source code rate. Although not shown in Fig. 2.5, we have also found that, while the spreading factor also increases with the total bandwidth, it does not increase as rapidly as the source code rate. Fig. 2.6 shows the resulting minimum distortion based on the optimum source code rates obtained in Fig. 2.5. The average distortion decreases with the bandwidth expansion factor, the Nakagami parameter m, and the constraint length of the channel code.

In [18], some of the numerical results were obtained by fixing $E_c/N_0 = PT_c/N_0$ (i.e., the SNR per chip) instead of the SNR per bit $\gamma_b = (PT_c/N_0)\mathcal{S}_F/r_c$. Fig. 2.7 shows the tradeoff curves parameterized by E_c/N_0. Note that for a fixed E_c/N_0, the spread factor increases with the bandwidth expansion factor. This can be explained as follows: For a fixed E_c/N_0, increasing the spread factor has two effects on the system performance: a) a

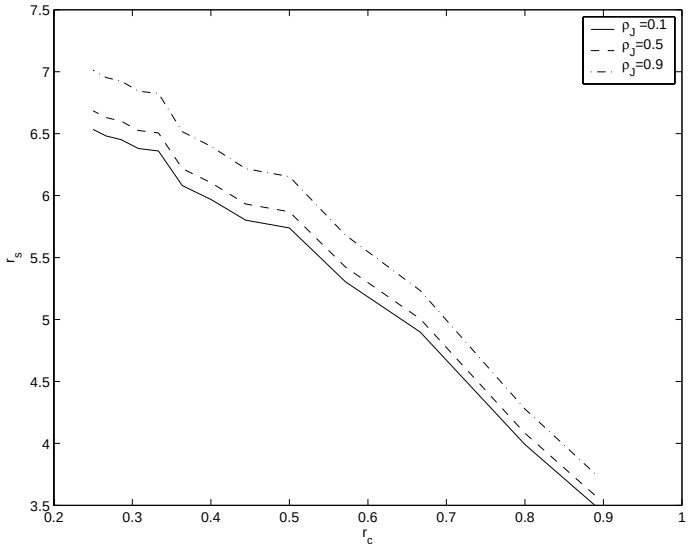

Figure 2.8 *Source code rate as a function of the channel code rate, parameterized by the fraction of the jammer's bandwidth, $\rho_J = W_J/W$. An RCPC code, with a mother code rate of $1/4$, is used with a frame length of 500 information bits. The other system parameters are: $\gamma_b = 15$ dB, $K_u = 10$, JSR=10 dB, $C_0 = 500$. Rayleigh fading channel with $L = 4$ paths with uniform multipath intensity profile is assumed.*

larger $\mathcal{S}_F$ reduces the interference from the other users; $b)$ a larger $\mathcal{S}_F$ leads to an increase in the SNR per bit, since $\gamma_b = \mathcal{S}_F(E_c/(N_0 r_c))$. However, the channel gets better with increasing E_c/N_0, and we do not need as large a γ_b, so we can reduce $\mathcal{S}_F$, and allocate more bandwidth to the source.

The effect of increasing the jammer's bandwidth on the tradeoff performance is now discussed. The source code rate and the resulting distortion are shown in Figs. 2.8 and 2.9, respectively. The fraction of the jammer's bandwidth, $\rho_J = W_J/W$, is chosen from $\{0.1, 0.5, 0.9\}$. The JSR is set to 10 dB, $\gamma_b = 15$ dB, and $K_u = 10$. We have used rate-compatible punctured convolutional (RCPC) codes with a base code rate of $1/4$ [41] and a frame length of 500 bits. The channel exhibits Rayleigh fading with a uniform MIP with $L = 4$ paths. Note that, from Fig. 2.8, when r_s is fixed, the tradeoff problem is reduced to that of a channel coding-spreading tradeoff problem. In this scenario, the expression $\Gamma = r_c\gamma_b/(1+r_c\gamma_b\Delta/\mathcal{S}_F) = r_c\gamma_b/(1+r_s\gamma_b\Delta/C_0)$ of (2.21) increases with both increasing r_c and increasing ρ_J. Hence, for a fixed r_s, the channel code rate increases with increasing

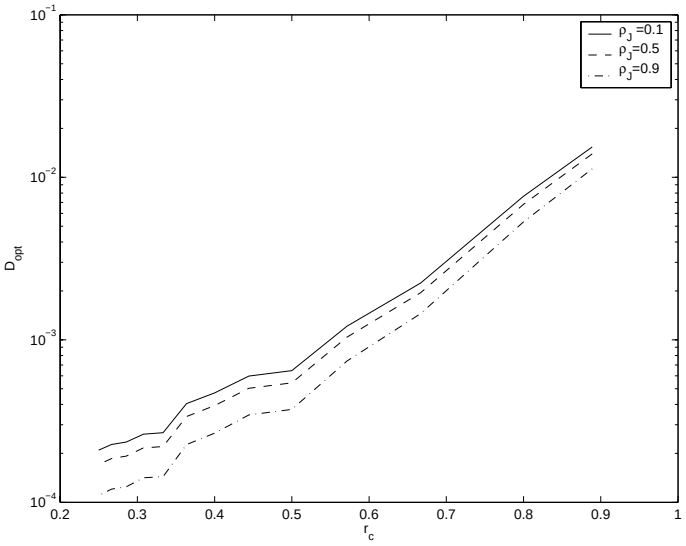

Figure 2.9 *Minimum source distortion as a function of the channel code rate, parameterized by the fraction of the jammer's bandwidth, $\rho_J = W_J/W$. An RCPC code, with a mother code rate of $1/4$, is used with a frame length of 500 information bits. The other system parameters are: $\gamma_b = 15$ dB, $K_u = 10$, JSR=10 dB, $C_0 = 500$. Rayleigh fading channel with $L = 4$ paths with uniform multipath intensity profile is assumed.*

ρ_J, and thus the spreading factor increases. However, as seen in Fig. 2.8, when r_c is fixed, the source code rate increases with increasing ρ_J, and thus the spreading factor decreases. Lastly, Fig. 2.9 shows that the average distortion decreases with increasing ρ_J.

We also investigated the effect of increasing system load (i.e., the number of users, K_u) on the bandwidth allocation. The results are summarized in Table 2.2, which correspond to constant MIP Rayleigh fading channels with $L = 4$ paths, $\gamma_b = 20$ dB and JSR = 0 dB. The bandwidth constraint is set to 500. From Table 2.2, for a given channel code rate, it is seen that the source code rate has to be decreased as the number of users increases to allow sufficient processing gain to suppress the additional MAI. Also, for a given number of users, the best performance is seen to be achieved at the lowest channel code rate. An explanation for this is given in the following paragraph.

Finally, we found the optimal 2-tuple (i.e., optimal r_s or $\mathcal{S}_F$) and the resulting minimum average distortion when RCPC codes are used. We used an RCPC code with mem-

Table 2.2 *Source code rate, spreading factor, and the minimum distortion, for a fixed channel code rate, based on both upper and lower bounds on the end-to-end average distortion. An i.i.d Rayleigh fading channel is assumed with $L = 4$ paths. The other system parameters are as follows: SNR-per-bit, $\gamma_b = 20$ dB, JSR = 0 dB, $\rho_J = 0.25$. The bandwidth constraint, C_0, is set to 500. The constraint length of the channel code is fixed to 6.*

r_c	K_u	Lower Bound			Upper Bound		
		r_s^*	$\mathcal{S}_F = C_0 r_c / r_s^*$	$D(r_s^*)$	r_s^*	$\mathcal{S}_F = C_0 r_c / r_s^*$	$D(r_s^*)$
$\frac{1}{2}$	10	11.78	21	$1.715 \cdot 10^{-7}$	11.40	21	$2.742 \cdot 10^{-7}$
	25	7.30	34	$7.683 \cdot 10^{-5}$	6.74	37	$1.495 \cdot 10^{-4}$
	50	4.95	50	$1.863 \cdot 10^{-3}$	4.29	58	$3.954 \cdot 10^{-3}$
$\frac{1}{3}$	10	13.12	12	$2.582 \cdot 10^{-8}$	12.68	13	$4.516 \cdot 10^{-8}$
	25	8.06	20	$2.671 \cdot 10^{-5}$	7.44	22	$5.651 \cdot 10^{-5}$
	50	5.45	30	$9.236 \cdot 10^{-4}$	4.74	35	$2.124 \cdot 10^{-3}$
$\frac{1}{4}$	10	13.41	9	$1.653 \cdot 10^{-8}$	13.13	9	$2.353 \cdot 10^{-8}$
	25	8.05	15	$2.557 \cdot 10^{-5}$	7.68	16	$4.014 \cdot 10^{-5}$
	50	5.84	21	$6.791 \cdot 10^{-4}$	4.91	25	$1.696 \cdot 10^{-3}$

Table 2.3 *Spreading factor, and the minimum distortion, for various punctured channel code rates from a given RCPC code, based on both the upper bound and the simulations on the end-to-end average distortion. An i.i.d Rayleigh fading channel is assumed with $L = 4$ paths. The other system parameters are as follows: SNR-per-bit, $\gamma_b = 20$ dB, JSR = 0 dB, $\rho_J = 0.25$ and $K_u = 12$. The bandwidth constraint, C_0, is set to 500. For simulations, we have used Gold codes.*

	Upper Bound			Simulation		
r_c	Distortion	r_s^*	$\mathcal{S}_F^* = C_0 r_c / r_s^*$	Distortion	r_s	$\mathcal{S}_F$
4/5	$4.491 \cdot 10^{-4}$	6.1538	65	$1.047 \cdot 10^{-4}$	6	63
4/7	$3.185 \cdot 10^{-5}$	8.6580	33	$1.893 \cdot 10^{-5}$	9	31
4/9	$1.068 \cdot 10^{-5}$	8.8889	25	$6.872 \cdot 10^{-6}$	7	31
4/11	$5.968 \cdot 10^{-6}$	9.5694	19	$1.629 \cdot 10^{-5}$	12	15
1/3	$2.926 \cdot 10^{-6}$	9.8039	17	$4.987 \cdot 10^{-3}$	11	15
2/7	$2.353 \cdot 10^{-6}$	10.204	14	$2.714 \cdot 10^{-2}$	9	15

ory four and a puncturing period of eight, as given in [41]. The code can produce thirteen punctured code rates according to a puncturing pattern. Since every possible punctured channel code rate is considered in the optimization, the two-way optimization of r_s and $\mathcal{S}_F$ is equivalent to the joint three-way optimization of r_s, r_c and $\mathcal{S}_F$. The minimum distortion and the resulting optimum r_s^* and $\mathcal{S}_F^*$ obtained by employing the upper bound are tabulated in Table 2.3 as a function of a selected subset of the available rates of the chosen RCPC code.

To carry out the simulation, we could not use the exact optimum values r_s^* and $\mathcal{S}_F^*$ obtained from the analysis. In simulation, the r_s must be restricted to be integers, and the $\mathcal{S}_F$ we restricted to be from the set of Gold codes with $\mathcal{S}_F \in \{7, 15, 31, 63\}$. For each value of r_c in Table 2.3, an (r_s, $\mathcal{S}_F$) pair for simulating the end-to-end distortion was chosen to approximately match the optimum (r_s^*, $\mathcal{S}_F^*$) pair obtained from the upper bound-based analytical results. The pair was chosen by first selecting the $\mathcal{S}_F \in \{7, 15, 31, 63\}$ which is closest to the optimum $\mathcal{S}_F^*$, and then obtaining $r_s = \lfloor C_0 r_c / \mathcal{S}_F \rfloor$. Note that, as illustrated below, picking the (r_s, $\mathcal{S}_F$) pair that best approximates the corresponding analytically derived pair does not necessarily minimize distortion, because of the differences in accounting for the self-interference.

From Table 2.3, the upper bound-based optimization shows that the minimum distortion decreases with decreasing channel code rate, indicating that the optimal system has no spreading at all. However, the simulated system in Table 2.3 shows that decreasing the channel code rate below $r_c = 4/9$ leads to an increase in the distortion. This is due to the fact that, at smaller values of $\mathcal{S}_F$ with $K_u = 12$ users, the system is affected by the self-interference of the user-of-interest, which is neglected in the upper bound-based analysis. To confirm this, we also simulated the system with $r_c = 2/7$ and other pairs of $(r_s, \mathcal{S}_F)$. With $(r_s, \mathcal{S}_F) = (2, 63)$ a distortion value of $6.197 \cdot 10^{-5}$ is observed, and with $(r_s, \mathcal{S}_F) = (4, 31)$ the distortion increases to $5.813 \cdot 10^{-4}$, but both of these are lower than the distortion of $2.714 \cdot 10^{-2}$ reported in Table 2.3 with $(r_s, \mathcal{S}_F) = (9, 15)$. For high values of r_c and $\mathcal{S}_F$, the simulated and analytic results are close. However, the simulation

shows that for small values of spreading factor, the system indeed suffers from the self-interference of the user-of-interest. The analysis, with its neglect of the self-interference term, produces unrealistically low values of distortion for these parameters, and suggests that little spreading is needed.

2.6 Conclusion

For a fixed total bandwidth expansion factor, we have studied the problem of optimal bandwidth allocation among the source coder, the channel coder, and the spread-spectrum unit for a DS-CDMA system operating over a frequency-selective Nakagami fading channel with Gaussian PBI. Assuming a Gaussian source with the optimum scalar quantizer, and a binary convolutional code with soft-decision decoding, we obtained both a lower and an upper bound on the end-to-end average source distortion. The joint three-way constrained optimization of the source code rate, the channel code rate, and the spreading factor was simplified to an unconstrained optimization problem over two variables. With a fixed channel code rate, it was shown that both upper and lower bound-based distortion functions are convex functions of the source code rate. However, an explicit solution for the optimum source code rate, that minimizes the average distortion, was difficult to obtain. Numerical results were also presented for the optimum source code rate and spreading factor, parameterized by the channel code rate, code constraint length, and various system loads. The optimal bandwidth allocation, in general, depends on the system and the channel conditions, such as the total number of active users, the average JSR power ratio, and the number of resolved multipath components together with their power delay profile.

CHAPTER 3

Tradeoff Between Source Coding and Spreading in an MC-CDMA System

3.1 Introduction

To provide wideband multimedia services with non-availability of contiguous frequency spectrum, and for the purpose of overlaying a CDMA system on existing narrowband systems, a multi-carrier version of the traditional DS-CDMA systems can be realized by employing more than one carrier [42]. Studies have shown that, with hostile NBI, MC-CDMA systems with efficient channel coding can provide improved system performance relative to their single carrier counterparts [43]-[44]. This motivates us to revisit source coding, channel coding and spreading tradeoff problem of Chapter 2 in the context of an MC-CDMA system.

In this chapter, for a fixed channel code rate, we study the bandwidth allocation problem between the source coding and spreading, when an MC-CDMA system is employed to mitigate the NBI. The source coding and channel coding components of the considered MC-CDMA system are identical to the ones presented in Chapter 2. However, as it will be made clear in this chapter, the analysis with an MC-CDMA system is significantly different from that of Chapter 2. To assess the performance improvements of MC-CDMA over DS-CDMA, we use the same PBI as that of Chapter 2. First, using a standard Gaussian approximation for the MAI, we obtain upper and lower bounds on the pairwise error probability with soft-decision decoding, and we use these results to bound the end-to-end

average source distortion. The optimal bandwidth allocation is then numerically computed by optimizing upper and lower bounds on the average distortion. Our results show an improvement in not only the average distortion performance, but also the three-way tradeoff performance. That is, under some channel conditions, for the same bandwidth constraint with approximately identical complexities for both DS- and MC-CDMA systems, we show that an MC-CDMA system supports a large source coding rate than a DS-CDMA system.

The rest of this chapter is organized as follows. In Section 3.2, we introduce the system and the channel model, and derive upper and lower bounds on the PEP with soft-decision decoding. Analysis of the end-to-end average distortion is presented in Section 3.3, whereas the optimum bandwidth allocation problem is detailed in Section 3.4. Numerical results and discussion are provided in Section 3.5. Finally, we conclude this chapter in Section 3.6.

3.2 System Model

The transmitter-receiver pair for the kth user is shown in Fig. 3.1. The information source is quantized by the source encoder with a rate of r_s bits per source sample, which are then mapped onto a new bit index of the same length r_s using an index assignment block, whose output bit stream is denoted by $\{b_n^{(k)}\}$. For ease of analysis, similar to [32], [18] and Chapter 2, we assume a random index assignment with a one-to-one mapping of indices from 0 through $2^{r_s} - 1$.

Each bit $b_n^{(k)}$ is encoded by a convolutional code of rate r_c, and the resulting code symbols are interleaved. For the purpose of analysis, we assume an ideal interleaver. Each code symbol $d_n^{(k)}$ is then spread, binary phase modulated and transmitted over the M frequency bands, each of width W_1. An optional symbol mapper can be used for coding across the carriers, as studied by [43]. If T_c and W, respectively, denote the chip duration and system bandwidth of a comparable single carrier DS-CDMA (or, simply SC-

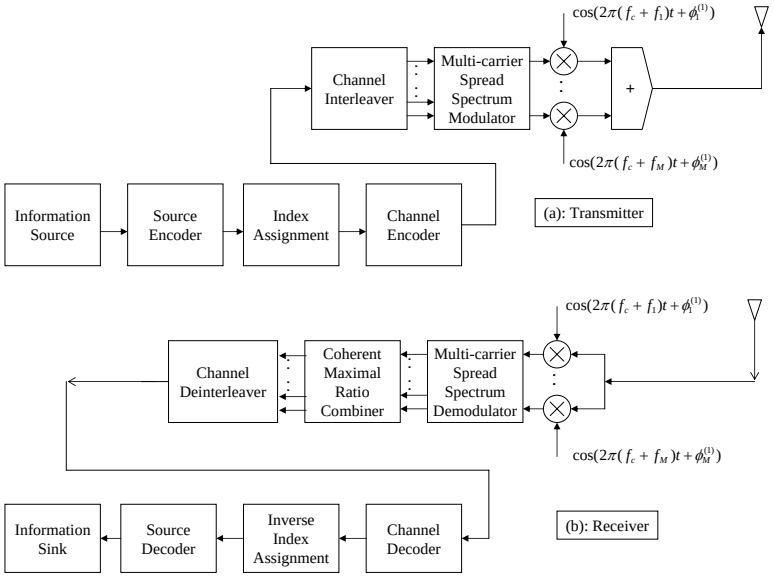

Figure 3.1 *MC-CDMA System: Transmitter–receiver pair for the desired user.*

CDMA) system, then we have $W = (1+\beta)/T_c$, where $\beta \in (0,1]$ is the roll-off factor of the chip wave-shaping filter. The bandwidth available per carrier in a MC-CDMA system is then given by $W_1 = W/M = (1+\beta)/(T_c M) = (1+\beta)/T_{c_1}$, where $T_{c_1} = MT_c$ is the corresponding chip duration in the MC-CDMA system.

Mathematically, the signal at the output of the kth user's transmitter is

$$S_k(t) = \sqrt{2E_c} \sum_{n=-\infty}^{\infty} d^{(k)}_{\lfloor n/N \rfloor} c^{(k)}_n h(t - nMT_c) \times \sum_{m=1}^{M} \cos(2\pi f_m t + \theta^{(k)}_m), \tag{3.1}$$

where $\lfloor x \rfloor$ is the largest integer that is less than or equal to x, $c^{(k)}_n$ denotes the spreading sequence, f_m is the center frequency of the mth carrier, $\theta^{(k)}_m$ denotes the initial phase angle of the kth user's mth carrier, N is the number of chips-per-code symbol-per-carrier, and E_c denotes the energy-per-chip. Also, $h(t)$ denotes the chip wave-shaping filter, and we assume that $X(f) = |H(f)|^2$ satisfies the Nyquist criterion, where $H(f)$ is the Fourier transform of $h(t)$. If we denote by $\mathcal{S}_F$ the spreading factor associated with a single carrier, then we have $\mathcal{S}_F = T_s/T_c = MT_s/T_{c_1} = MN$, where T_s is the code symbol duration.

With this, we can express N as $N = \mathcal{S}_F/M$.

We assume that the channel is frequency-selective over a bandwidth of W. However, the total bandwidth W is assumed to be partitioned into M disjoint frequency bands in such a way that each of the M bands experiences independent, frequency-flat fading. In [42], conditions were derived for satisfying this assumption. With this, the received signal of the kth user can be written as

$$\begin{aligned} r(t) &= \sum_{k=1}^{K_u} \sqrt{2E_c} \sum_{n=-\infty}^{\infty} d^{(k)}_{\lfloor n/N \rfloor} c^{(k)}_n h(t - nMT_c - \tau_k) \times \\ &\quad \sum_{m=1}^{M} \alpha^{(k)}_m \cos(2\pi f_m t + \psi_{k,m}) + n_W(t) + n_J(t), \end{aligned} \tag{3.2}$$

where τ_k is the random time delay corresponding to the kth user, assumed to be uniformly distributed in $[0, MT_c)$, K_u is the total number of active users in the system, $\alpha^{(k)}_m$ denotes the fade amplitude, $\phi^{(k)}_m$ denotes the random phase on the mth carrier of the kth user, and $\psi^{(k)}_m = \theta^{(k)}_m + \phi^{(k)}_m$ is the resultant phase on the mth carrier. The term $n_W(t)$ denotes the AWGN with a two-sided PSD of $\eta_0/2$, whereas $n_J(t)$, given in (2.4), represents the Gaussian PBI with a PSD of $S_J(f)$.

We assume that the fades are independent across the users, the carriers, and over time. We further assume that $\alpha^{(k)}_m$ is Rayleigh distributed with density function $f_{\alpha^{(k)}_m}(x) = 2xe^{-x^2}$, for $x \geq 0$, and $\phi^{(k)}_m$ is uniformly distributed over $(-\pi, \pi]$.

The receiver operation, assuming the first user is the desired user, can be briefly explained as follows. We assume that perfect carrier, code, and bit synchronization for the first user has been accomplished. The received signal of (3.2) is first chip-matched filtered, using the band-pass filters $H^*(f - f_i) + H^*(f + f_i)$, $i = 1, \ldots, M$, and then low-pass filtered with $\sqrt{2}\cos(2\pi f_i t + \phi^{(1)}_i)$, $i = 1, \ldots, M$. Each of these M outputs are correlated using the local pseudo-noise sequences. If z_i denotes the output of the

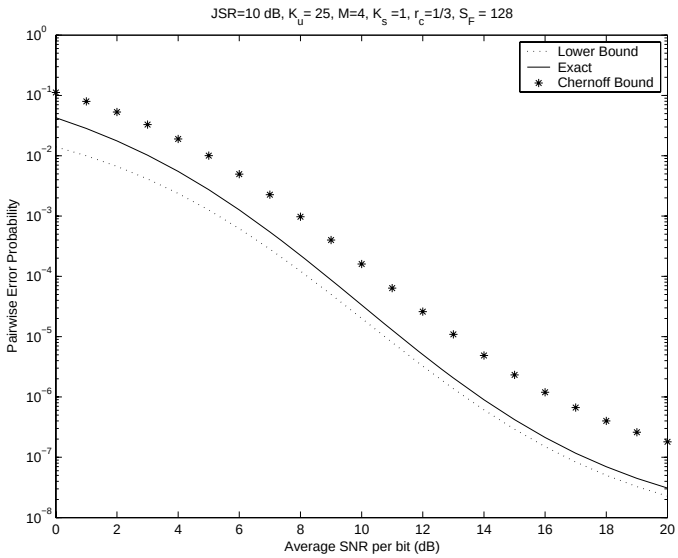

Figure 3.2 *Comparison of exact pairwise error probability with the one based on the Chernoff bound and the one based on a lower bound. The system parameters are the following:* $K_u = 25$, ***JSR = 10 dB***, $\rho_J = 0.25$, $r_c = 1/3$, $\mathcal{S}_F = 128$, *and* $M = 4$.

correlator on the ith carrier, then we have

$$z_i = S_i + I_i + J_i + N_i, \tag{3.3}$$

where S_i is the desired signal, I_i is the signal due to the other $K_u - 1$ interfering users, J_i is the contribution due to the jammer and N_i is the output due to AWGN. From [42, Eqn. (23)], the conditional mean of z_i, conditioned upon $\alpha_i^{(1)}$ and $d_{\lfloor n/N \rfloor}^{(1)}$, can be obtained as

$$E[z_i|\alpha_i^{(1)}, d_{\lfloor n/N \rfloor}^{(1)}] = d^{(1)} N \sqrt{E_c} \alpha_i^{(1)}, \tag{3.4}$$

where $d^{(1)} = \pm 1$ is the corresponding transmitted code symbol. To obtain the variance of z_i, conditioned on $\alpha_i^{(1)}$, we assume that the interference from other users, the PBI, and the AWGN are independent of each other. With this, we have

$$\begin{aligned} \text{Var}\{z_i|\alpha_i^{(1)}\} &= \sigma_i^2 = \text{Var}\{I_i|\alpha_i^{(1)}\} + \text{Var}\{J_i|\alpha_i^{(1)}\} + \text{Var}\{N_i|\alpha_i^{(1)}\} \\ &\approx NR_{I_i}(0) + NR_{J_i}(0) + N\eta_0/2, \end{aligned} \tag{3.5}$$

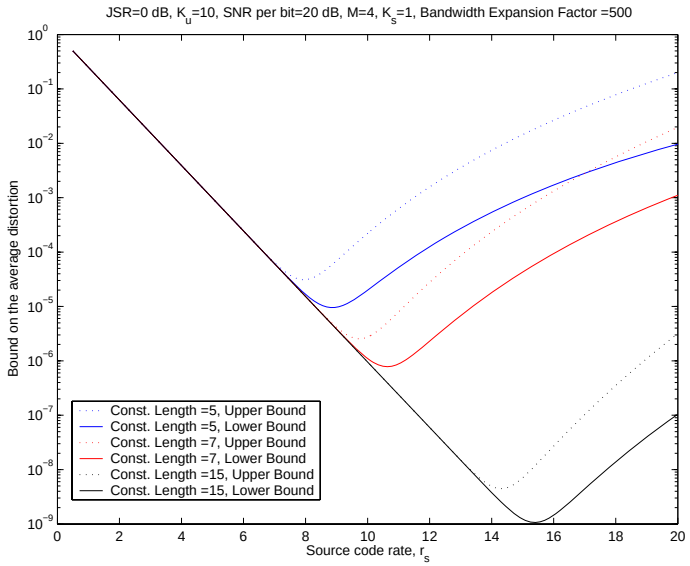

Figure 3.3 *Lower and upper bounds on the average distortion on Rayleigh fading channels with $M = 4$ carriers. The channel code rate is fixed to $r_c = 1/2$ and the bandwidth expansion factor is set to 500. Binary convolutional codes with various constraint lengths are used with an optimum distance spectrum. The other system parameters are: JSR = 0 dB, $\rho_J = 0.25$, $K_u = 10$ and $\gamma_b = 20$ dB.*

where $R_{I_i}(\tau)$ and $R_{J_i}(\tau)$ are the autocorrelation functions of the interference and jammer, respectively. In (3.5), the approximation in the last line is due to ignoring the contribution of $R_{I_i}(\tau)$ and $R_{J_i}(\tau)$ when $\tau \neq 0$ (see [42, Eqns. (25), (26) and (27)]). For simplicity, we assume that the Gaussian PBI overlaps K_s carriers, where $1 \leq K_s \leq M$. Without loss of generality, now assume that the first K_s bands are affected by the jammer. Then, with the help of [42]

$$\begin{aligned} \sigma_i^2 &= \frac{N}{2}E_c(K_u - 1)(1 - \frac{\beta}{4}) + N\frac{\eta_J}{2} + \frac{N\eta_0}{2},\ i = 1, \ldots, K_s, \\ &= \frac{N}{2}E_c(K_u - 1)(1 - \frac{\beta}{4}) + \frac{N\eta_0}{2},\ i = K_s + 1, \ldots, M. \end{aligned} \tag{3.6}$$

We note that the total jammer power is given by $P_J = \eta_J K_s W_1 = \eta_J W(K_s/M)$. By defining JSR $= P_J/(E_c/T_c)$ as the JSR, we can solve for η_J as $\eta_J =$ JSR $\times \frac{E_c}{\rho_J(1+\beta)}$, where $\rho_J = K_s/M$ is the fraction of the carriers affected by the jammer.

For each code symbol, the M outputs, $z_m, m = 1, \ldots, M$, are processed using the maximal ratio combiner (MRC) to result in an output Z. Since each z_m is affected by the fade $\alpha_m^{(1)}$ and has a noise variance of σ_m^2, the MRC weights should be proportional to $\alpha_m^{(1)}/\sigma_m^2$ to yield maximum SNR. Assuming perfect knowledge of $\{\alpha_m^{(1)}\}$ and $\{\sigma_m^2\}$ at the receiver, the output of the MRC, Z, can then be expressed as

$$Z = \sum_{m=1}^{M} \frac{\alpha_m^{(1)}}{\sigma_m^2} z_m = d^{(1)} N \sqrt{E_c} \sum_{m=1}^{M} (\frac{\alpha_m^{(1)}}{\sigma_m})^2 + \xi, \tag{3.7}$$

where ξ, conditioned on $(\alpha_1^{(1)}, \ldots, \alpha_M^{(1)})$, is zero-mean Gaussian with variance $\sigma_\xi^2 = \sum_{m=1}^{M} (\alpha_m^{(1)}/\sigma_m)^2$. The instantaneous SNR r.v, γ, at the output of MRC is given by

$$\gamma = \frac{(E[Z|\alpha_1^{(1)}, \ldots, \alpha_M^{(1)}])^2}{2\text{Var}\{Z|\alpha_1^{(1)}, \ldots, \alpha_M^{(1)}\}} = \sum_{m=1}^{M} [\alpha_m^{(1)}]^2 \overline{\gamma}_m, \tag{3.8}$$

where $\overline{\gamma}_m = N^2 E_c/(2\sigma_m^2)$ is the average SINR on the mth carrier. Using (3.6) we can simplify $\overline{\gamma}_m$ as

$$\begin{aligned} \overline{\gamma}_m &= \frac{1}{M} \frac{r_c \gamma_b}{1 + \frac{r_c}{\mathcal{S}_F} \gamma_b (K_u - 1)(1 - \beta/4) + \frac{r_c}{\mathcal{S}_F} \gamma_b \frac{\text{JSR}}{\rho_J (1+\beta)}}, \ m = 1, \ldots, K_s \\ &= \frac{1}{M} \frac{r_c \gamma_b}{1 + \frac{r_c}{\mathcal{S}_F} \gamma_b (K_u - 1)(1 - \beta/4)}, \ m = K_s + 1, \ldots, M. \end{aligned} \tag{3.9}$$

For convenience, define $\mathbf{a} = r_c \gamma_b / M$, $\Delta_0 = \gamma_b (K_u - 1)(1 - \beta/4) + \gamma_b \frac{\text{JSR}}{\rho_J (1+\beta)}$ and $\Delta_1 = \gamma_b (K_u - 1)(1 - \beta/4)$. Clearly, $\Delta_0 \geq \Delta_1$ and $\overline{\gamma}_m$ can be expressed in terms of $\mathbf{a}$, Δ_0, Δ_1, r_c, and $\mathcal{S}_F$ as

$$\begin{aligned} \overline{\gamma}_m &= \frac{\mathbf{a}}{1 + r_c \Delta_0 / \mathcal{S}_F}, \ m = 1, \ldots, K_s, \\ &= \frac{\mathbf{a}}{1 + r_c \Delta_1 / \mathcal{S}_F}, \ m = K_s + 1, \ldots, M. \end{aligned} \tag{3.10}$$

3.2.1 Frame Error Rate with Convolutional Coding

The MRC outputs, $\{Z_n\}$, corresponding to a given coded frame are passed to the deinterleaver and then to the Viterbi decoder for soft-decision decoding. It is well known that at high SNR regions, the key performance metric with channel coding is the PEP between two codewords [37]. The PEP between two codewords $\mathbf{x} = (x_1, \ldots, x_{N_F})$ and $\mathbf{y} = (y_1, \ldots, y_{N_F})$ which differ in d positions, when $\mathbf{x}$ is the transmitted codeword, is given by

$$\begin{aligned} P_2(d|\underline{\alpha}) &= \text{Prob}\left(\sum_{n=1}^{N_F}(Z_n - x_n)^2 > \sum_{n=1}^{N_F}(Z_n - y_n)^2\right) \\ &= \text{Prob}\Big(\sum_{n=1}^{N_F}\xi_n(x_n - y_n) < -\sum_{n=1}^{N_F} N\sqrt{E_c}x_n \times \\ &\quad \sum_{m=1}^{M}(\alpha_{m,n}^{(1)}/\sigma_m)^2(x_n - y_n)\Big), \end{aligned} \tag{3.11}$$

where in the last step of (3.11) we have used (3.7), N_F is the coded frame length of the terminated convolutional code, and the additional subscript n in $\alpha_{m,n}^{(1)}$ shows the time index of the code symbol. Without loss of generality, we assume that the codewords $\mathbf{x}$ and $\mathbf{y}$ differ in the first d positions. Then, using the Chernoff bound, $Q(x) \leq 1/2\exp(-x^2/2)$ for $x \geq 0$, we can upper bound (3.11) as

$$P_2(d|\underline{\alpha}) \leq \frac{1}{2}\exp\left(-\sum_{n=1}^{d}\sum_{m=1}^{M}(\alpha_{m,n}^{(1)})^2\overline{\gamma}_m\right). \tag{3.12}$$

Upon taking the expectation of (3.12) over the distribution of $\{\alpha_{m,n}^{(1)}\}$, we obtain

$$\begin{aligned} \overline{P}_2(d) &= E\left\{P_2(d|\underline{\alpha})\right\} \\ &\leq \frac{1}{2}\prod_{m=1}^{M}\left(\frac{1}{1+\overline{\gamma}_m}\right)^d \end{aligned}$$

$$< \frac{1}{2}\prod_{m=1}^{M}\overline{\gamma}_m^{-d}$$
$$= \frac{1}{2\mathbf{a}^{Md}}(1+r_c\Delta_0/\mathcal{S}_F)^{K_s d}(1+r_c\Delta_1/\mathcal{S}_F)^{(M-K_s)d}, \quad (3.13)$$

where (3.10) was used in (3.13).

Following an approach similar to that of Section 2.2.4 in Chapter 2, an upper bound on the FER for our system can be expressed as

$$P_B \leq \sum_d t(d)\overline{P}_2(d)$$
$$< \sum_d \frac{t(d)}{2\mathbf{a}^{Md}}(1+r_c\Delta_0/\mathcal{S}_F)^{K_s d}(1+r_c\Delta_1/\mathcal{S}_F)^{(M-K_s)d}, \quad (3.14)$$

where $t(d)$ is a function of the weight spectrum [37] of the underlying convolutional code. We are also interested in a lower bound on the FER. Following the same steps as outlined in Appendix-A, and using the dominant term of (3.14), a lower bound on the FER can be obtained as

$$P_B \geq t(d_{free})C(M,d_{free})\prod_{m=1}^{M}(1+\overline{\gamma}_m)^{-d_{free}}, \quad (3.15)$$

where d_{free} is the free distance of the code, $C(M,d) = \frac{1}{2\pi}\beta\left(Md+\frac{1}{2},\frac{1}{2}\right)$, and $\beta(p,q)$ is the standard beta integral [36].

3.3 End-to-End Average Distortion

We assume that the information source is Gaussian-distributed with independent and identically distributed source samples, each with unit variance. If r_s denotes the number of bits-per-source sample, then the average source distortion with minimum mean square error scalar quantization on a noise-free channel is given by $D(r_s) = \epsilon 2^{-2r_s}$, where ϵ depends on the quantizer [38]. Note that each coded frame of length N_F contains $N_F r_c/r_s$ source samples. Then, the average distortion per source sample can be written as [39,

Eqn. (10)]

$$\begin{aligned}\mathcal{D}(r_s, r_c, \mathcal{S}_F) &= (1 - P_B(r_c, \mathcal{S}_F))\epsilon 2^{-2r_s} + P_B(r_c, \mathcal{S}_F) \\ &\leq \epsilon 2^{-2r_s} + P_B(r_c, \mathcal{S}_F) \\ &\leq \epsilon 2^{-2r_s} + \sum_d \frac{t(d)}{2\mathbf{a}^{Md}}(1 + r_c\Delta_0/\mathcal{S}_F)^{K_s d}(1 + r_c\Delta_1/\mathcal{S}_F)^{(M-K_s)d} \\ &\triangleq D_u(r_s, r_c, \mathcal{S}_F), \end{aligned} \tag{3.16}$$

where the above upper bound is quite accurate in the high SNR region.

A lower bound on the end-to-end average distortion can be obtained by first lower bounding the frame error rate, $P_B(r_c, \mathcal{S}_F)$ by the term with minimum free distance d_{free} as $P_B(r_c, \mathcal{S}_F) \geq t(d_{free})P_2(d_{free})$. With this a lower bound on the average distortion can be obtained as

$$\begin{aligned}\mathcal{D}(r_s, r_c, \mathcal{S}_F) &\geq \epsilon 2^{-2r_s} + t(d_{free})P_2(d_{free})(1 - \epsilon 2^{-2r_s}) \\ &\geq \epsilon 2^{-2r_s} + (1 - \epsilon 2^{-2r_s})t(d_{free})C(M, d_{free}) \prod_{m=1}^{M}(1 + \overline{\gamma}_m)^{-d_{free}} \\ &\triangleq D_l(r_s, r_c, \mathcal{S}_F), \end{aligned} \tag{3.17}$$

where in the second step of (3.17) we have used (3.15). In what follows, we consider both the upper bound and lower bounds on the average distortion of (3.16) and (3.17), respectively, as our objective functions.

3.4 Optimum Bandwidth Allocation

If we denote by $\mathcal{U}$ the number of source samples-per-second available to the source coder, then the chip rate at the output of the spread-spectrum modulator is given by $\mathcal{U}r_s\frac{1}{r_c}\mathcal{S}_F$, which is limited to $W/(1 + \beta)$, where W is the spread-spectrum bandwidth and β is the excess fractional bandwidth due to Nyquist chip wave-shaping filtering. That

is, the variables r_s, r_c and $\mathcal{S}_F$ are related by $r_s\mathcal{S}_F/r_c \leq C_0$, where $C_0 = W/((1+\beta)\mathcal{U})$. The distortion function is given by $\mathcal{D}(r_s, r_c, \mathcal{S}_F)$, which can also be written as $\mathcal{D}(r_s, r_c, C_0 r_c/r_s)$. We notice that by fixing the channel code rate, r_c, the distortion can be expressed only as a function of the source rate r_s, together with the bandwidth constraint C_0. In this section, we minimize the objective functions, $D_u(r_s, r_c, \mathcal{S}_F)$ of (3.16) and $D_l(r_s, r_c, \mathcal{S}_F)$ of (3.17), as a function of the source code rate r_s.

3.4.1 Upper Bound Based Optimal Allocation

With r_c fixed, we substitute $\mathcal{S}_F = C_0 r_c/r_s$ in (3.16) and rewrite (3.16) as a function of only r_s as follows:

$$D_u(r_s) = \epsilon 2^{-2r_s} + \sum_d \frac{t(d)}{2\mathbf{a}^{Md}}(1+\frac{\Delta_0}{C_0}r_s)^{dK_s}(1+\frac{\Delta_1}{C_0}r_s)^{(M-K_s)d}. \tag{3.18}$$

The first derivative of (3.18) with respect to r_s can be obtained as

$$\begin{aligned}\frac{d}{dr_s}D_u(r_s) = (-2\epsilon\ln 2)2^{-2r_s} + \sum_d \frac{t(d)}{2\mathbf{a}^{Md}}\Bigg\{ \frac{K_s d\Delta_0}{C_0} \times \\ \left(1+\frac{\Delta_0}{C_0}r_s\right)^{K_s d-1}\left(1+\frac{\Delta_1}{C_0}r_s\right)^{(M-K_s)d} + \frac{(M-K_s)d\Delta_1}{C_0} \times \\ \left(1+\frac{\Delta_0}{C_0}r_s\right)^{K_s d}\left(1+\frac{\Delta_1}{C_0}r_s\right)^{(M-K_s)d-1}\Bigg\}\end{aligned} \tag{3.19}$$

By taking the derivative of (3.19) we arrive at

$$\begin{aligned}&\frac{d^2}{dr_s^2}D_u(r_s) = 4\epsilon(\ln 2)^2 2^{-2r_s} + \\ &\sum_d \frac{t(d)}{2\mathbf{a}^{Md}}(1+\Delta_0 r_s/C_0)^{K_s d}(1+\Delta_1 r_s/C_0)^{(M-K_s)d} \times \\ &\Bigg\{\left(\frac{K_s d\Delta_0}{C_0+r_s\Delta_0} + \frac{(M-K_s)d\Delta_1}{C_0+r_s\Delta_1}\right)^2 -\end{aligned}$$

$$\frac{K_s d\Delta_0^2}{(C_0+\Delta_0 r_s)^2} - \frac{(M-K_s)d\Delta_1^2}{(C_0+\Delta_1 r_s)^2}\Bigg\}. \tag{3.20}$$

Since $1 \leq K_s \leq M$, both the terms within $(\cdot)^2$ of (3.20) are positive. Using $(x+y)^2 \geq x^2+y^2$ for $x \geq 0$ and $y \geq 0$, we can simplify (3.20) as

$$\begin{aligned}
&\frac{d^2}{dr_s^2} D_u(r_s) \geq 4\epsilon(\ln 2)^2 2^{-2r_s} + \\
&\sum_d \frac{t(d)}{2\mathbf{a}^{Md}} (1+\Delta_0 r_s/C_0)^{K_s d} (1+\Delta_1 r_s/C_0)^{(M-K_s)d} \times \\
&\left\{ \frac{K_s d(K_s d-1)\Delta_0^2}{(C_0+\Delta_0 r_s)^2} + \frac{(M-K_s)d((M-K_s)d-1)\Delta_1^2}{(C_0+\Delta_1 r_s)^2} \right\}.
\end{aligned} \tag{3.21}$$

By noting that the expression inside $\{\cdot\}$ of (3.21) is non-negative, we conclude that $D_u(r_s)$ is a convex function of r_s. The optimal 2-tuple is then given by $(r_s^*, r_c, C_0 r_c/r_s^*)$, where r_s^* uniquely solves $\frac{d}{dr_s} D_u(r_s) = 0$.

3.4.2 Lower Bound Based Optimal Allocation

By fixing r_c, and, as before, substituting $\mathcal{S}_F = C_0 r_c/r_s$ we express $D_{lower}(\cdot,\cdot,\cdot)$ of (3.17) as a function of only r_s. For convenience, let us define

$$f(r_s) \triangleq t(d_{free}) C(m, d_{free}) \left(1 + \frac{\mathbf{a}}{1+\frac{\Delta_0 r_s}{C_0}}\right)^{-K_s d_{free}} \left(1 + \frac{\mathbf{a}}{1+\frac{\Delta_1 r_s}{C_0}}\right)^{-(M-K_s)d_{free}} \tag{3.22}$$

so that (3.17) can be expressed as

$$D_l(r_s) = \epsilon 2^{-2r_s} + (1-\epsilon 2^{-2r_s}) f(r_s). \tag{3.23}$$

Notice that since $f(r_s)$ is a lower bound on the frame error rate, we have $0 \leq f(r_s) \leq 1$. The first derivative of (3.23) with respect to r_s can then be computed as

$$\frac{d}{dr_s} D_l(r_s) = -\epsilon(2\ln 2)2^{-2r_s} + f(r_s)\epsilon(2\ln 2)2^{-2r_s} + (1-\epsilon 2^{-2r_s})\frac{d\, f(r_s)}{dr_s}, \tag{3.24}$$

where, after some simplification, we can show that

$$\frac{d}{dr_s} f(r_s) = f(r_s) \times \left[\frac{K_s d_{free} \mathbf{a} \Delta_0 C_0}{(C_0 + r_s\Delta_0)((1+\mathbf{a})C_0 + r_s\Delta_0)} + \frac{(M-K_s) d_{free} \mathbf{a} \Delta_1 C_0}{(C_0 + r_s\Delta_1)((1+\mathbf{a})C_0 + r_s\Delta_1)} \right], \tag{3.25}$$

which is positive for all r_s. Upon equating (3.24) to zero, and solving for r_s, we arrive at the following implicit equation:

$$r_s^* = \frac{1}{2}\log_2 \left(\frac{\epsilon \times \left[\frac{d}{dr_s} f(r_s)\big|_{r_s=r_s^*} + (2\ln 2)\left(1 - f(r_s)\big|_{r_s=r_s^*}\right)\right]}{\frac{d}{dr_s} f(r_s)\big|_{r_s=r_s^*}} \right). \tag{3.26}$$

Since $\frac{d}{dr_s} f(r_s)|_{r_s=r_s^*} > 0$, the argument of the logarithm in (3.26) is always positive.

3.5 Results and Discussion

In this section, we present some numerical results based on the analysis presented in Sections 3.2-3.4. First, Fig. 3.2 shows the tightness of the lower and the upper bounds on the PEP on Rayleigh fading channel with $M = 4$ carriers. Also shown is the true PEP, which is numerically evaluated. We conclude from Fig. 3.2 that the bounds are sufficiently tight. In particular, for SNR-per-bit, γ_b, values less than 15 dB, the upper bound is within 2 dB of the true PEP.

The lower and upper bounds on the average end-to-end source distortion, as derived

Table 3.1 *Optimum source code rate, spreading factor, and the minimum distortion, for a fixed channel code rate, based on both upper and lower bounds on the end-to-end average distortion. Number of sub-carriers $M = 4$. The JSR is 10 dB with the jammer completely overlapping one sub-carrier (i.e., $K_s = 1$). $K_u = 5$, $\gamma_b = 10$ dB and frame length = 500 bits.*

r_c	Lower Bound			Upper Bound		
	r_s^*	$\mathcal{S}_F$	$D(r_s^*)$	r_s^*	$\mathcal{S}_F$	$D(r_s^*)$
$\frac{1}{2}$	9.15	27	$1.07 \cdot 10^{-5}$	8.40	29	$2.68 \cdot 10^{-5}$
$\frac{1}{3}$	10.48	15	$1.57 \cdot 10^{-6}$	9.69	17	$4.23 \cdot 10^{-6}$
$\frac{1}{4}$	10.65	11	$1.16 \cdot 10^{-6}$	10.18	12	$2.11 \cdot 10^{-6}$

in Section 3.3, are plotted in Fig. 3.3. For a fixed spread bandwidth and channel code rate, the average distortion is plotted as a function of the source code rate. A family of such curves is obtained for varying levels of channel code complexity, as measured by its constraint length. We notice from Fig. 3.3 that $i)$ there exists a source code rate at which the distortion can be minimized, $ii)$ the minimum source code rate shifts to the right for increasing values of the channel code complexity, since a stronger channel code enables the spread-spectrum modulator to use a small value of the spread factor, $iii)$the lower and the upper bounds coincide at all r_s that are below the r_s at which the distortion is minimized, after which the bounds differ by an order of magnitude. This difference in the lower and the upper bounds can be explained as follows: Notice that for a fixed channel code rate with moderate constraint lengths, increasing source code rate limits the available spread factor. This results in increasing variances for both the MAI and the PBI, which makes the Chernoff based union upper bound ineffective and is not comparable with the dominant term-based lower bound.

In Table 3.1, we present the optimum source code rate, the optimum spreading factor, and the resulting average distortion for various channel code rates. For all the channel codes, the complexity of the encoder is fixed at a constraint length of 6. Both lower and upper bounds on the distortion are considered with the constraint on the bandwidth expansion factor set to 500 (i.e., $r_s \frac{1}{r_c} \mathcal{S}_F = 500$). The number of users is fixed at $K_u = 5$. From

Table 3.2 *Optimum source code rate, spreading factor, and the minimum distortion, for a fixed channel code rate, based on both upper and lower bounds on the end-to-end average distortion. The other system parameters are as follows: SNR-per-bit, $\gamma_b = 20$ dB, JSR = 0 dB, $\rho_J = 0.25$. The bandwidth constraint, C_0, is set to 500. The constraint length of the channel code is fixed to 6.*

r_c	K_u	Lower Bound			Upper Bound		
		r_s^*	$\mathcal{S}_F$	$D(r_s^*)$	r_s^*	$\mathcal{S}_F$	$D(r_s^*)$
$\frac{1}{2}$	5	10.30	24	$2.146 \cdot 10^{-6}$	9.66	25	$4.776 \cdot 10^{-6}$
	10	7.93	31	$4.536 \cdot 10^{-5}$	7.20	34	$1.104 \cdot 10^{-4}$
	25	5.26	47	$1.481 \cdot 10^{-3}$	4.43	56	$3.909 \cdot 10^{-3}$
	50	3.65	68	$1.203 \cdot 10^{-2}$	2.79	89	$3.142 \cdot 10^{-2}$
$\frac{1}{3}$	5	11.75	14	$2.658 \cdot 10^{-7}$	11.06	15	$6.410 \cdot 10^{-7}$
	10	8.93	18	$1.081 \cdot 10^{-5}$	8.15	20	$2.836 \cdot 10^{-5}$
	25	5.87	28	$6.197 \cdot 10^{-4}$	5.00	33	$1.754 \cdot 10^{-3}$
	50	4.08	40	$6.598 \cdot 10^{-3}$	3.18	52	$1.851 \cdot 10^{-2}$
$\frac{1}{4}$	5	11.98	10	$1.805 \cdot 10^{-7}$	11.56	10	$3.095 \cdot 10^{-7}$
	10	8.96	13	$9.805 \cdot 10^{-6}$	8.49	14	$1.751 \cdot 10^{-5}$
	25	5.75	21	$6.939 \cdot 10^{-4}$	5.21	23	$1.312 \cdot 10^{-3}$
	50	3.90	32	$7.935 \cdot 10^{-3}$	3.33	37	$1.516 \cdot 10^{-2}$

Table 3.1, we observe that both the lower and the upper bounds result in approximately the same optimum bandwidth allocation. Table 3.1 also indicates that with decreasing channel code rates, it is beneficial to allocate more bandwidth to the source coder than to the spread-spectrum modulator. This can be explained as follows: For a given constraint length, a low rate channel code provides higher free distance, and hence large diversity order, which, together with the M-fold diversity provided by the MRC, helps to reduce the burden on the spread-spectrum modulator in combating the interference.

The effect of increasing system load (i.e., the number of users, K_u) on the bandwidth allocation is also investigated. The results are summarized in Table 3.2, which corresponds to $M = 4$ carriers, $\gamma_b = 20$ dB and JSR = 0 dB. The bandwidth constraint is set to 500. From Table 3.2, for a given channel code rate, it is seen that the source code rate has to be decreased as the number of users increases to allow sufficient processing gain to suppress the additional MAI. Also, for a given number of users, the best performance is seen to be achieved at the lowest channel code rate (with the exception of the lower bound

Table 3.3 *Comparison between SC-CDMA with a RAKE receiver and MC-CDMA for the same system bandwidth and channel code rate. The number of carriers in MC-CDMA system is set to 4 whereas an equal number of multipath components, with i.i.d Rayleigh fading, are assumed to be resolved by the single-carrier CDMA system. An upper bound on the average distortion is minimized and the resulting optimal allocation is tabulated. The other system parameters are as follows: SNR-per-bit, $\gamma_b = 10$ dB, $\rho_J = 0.25$ and $K_u = 5$. The bandwidth constraint, C_0, is set to 500. The constraint length of the channel code is fixed to 6.*

r_c	JSR	MC-CDMA			SC-CDMA		
	(dB)	r_s^*	$\mathcal{S}_F$	$D(r_s^*)$	r_s^*	$\mathcal{S}_F$	$D(r_s^*)$
$\frac{1}{2}$	0	9.66	25	$4.776 \cdot 10^{-6}$	9.85	25	$3.710 \cdot 10^{-6}$
	10	8.40	29	$2.668 \cdot 10^{-5}$	7.90	31	$4.458 \cdot 10^{-5}$
	20	7.72	32	$7.530 \cdot 10^{-5}$	3.14	79	0.02012
	25	7.65	32	$8.540 \cdot 10^{-5}$	1.31	190	0.1995
$\frac{1}{3}$	0	11.06	15	$6.410 \cdot 10^{-7}$	11.27	14	$4.778 \cdot 10^{-7}$
	10	9.69	17	$4.233 \cdot 10^{-6}$	8.97	18	$9.735 \cdot 10^{-6}$
	20	9.04	18	$1.126 \cdot 10^{-5}$	3.57	46	0.0112
	25	8.97	18	$1.258 \cdot 10^{-5}$	1.52	108	0.1502
$\frac{1}{4}$	0	11.56	10	$3.095 \cdot 10^{-7}$	11.79	10	$2.276 \cdot 10^{-7}$
	10	10.18	12	$2.114 \cdot 10^{-6}$	9.35	13	$5.673 \cdot 10^{-6}$
	20	9.55	13	$5.401 \cdot 10^{-6}$	3.73	33	0.009006
	25	9.49	13	$5.988 \cdot 10^{-6}$	1.62	77	0.13402

result for $K_u = 25$ and 50 users, where the use of a rate $1/3$ code yielded slightly better performance than the use of a rate $1/4$ code).

Finally, we compare the performance of a single-carrier CDMA system employing a RAKE receiver against the performance of a MC-CDMA system in terms of the optimum bandwidth allocation. We assume that the number of multipaths resolved by the SC-CDMA system is the same as the number of carriers in an MC-CDMA system. Furthermore, we assume that the multipath fading in SC-CDMA is Rayleigh distributed with uniform intensity profile. The two systems are compared by varying the JSR, and the results are tabulated in Table 3.3. It is evident, from Table 3.3, that the single-carrier version performs worse than the MC-CDMA system for increasing values of the JSR. Also, as the JSR increases, the source coding rate is reduced in the SC-CDMA system and more bandwidth is allocated to spreading in order to combat the jammer. However, as we

notice from the resulting minimum distortion in Table 3.3, even with increasing spread factor the SC-CDMA cannot reach the performance of the MC-CDMA. This is due to the fact that no additional signal processing is employed in SC-CDMA, apart from a simple RAKE processing, whereas the MC-CDMA system has effectively nullified the effect of the jammer using the MRC receiver, in a simple way, by attenuating all the carriers that are affected by the PBI. We also note that, by incorporating a notch-filter, although at a higher complexity, to mitigate the effects of the jammer, the tradeoff performance of SC-CDMA can be expected to improve.

3.6 Conclusions

For a fixed total bandwidth expansion factor, and for a fixed channel code rate, we studied the problem of optimal bandwidth allocation between the source coder and the spread-spectrum unit for an MC-CDMA system operating over a frequency-selective fading channel with NBI. By assuming a Gaussian source with the optimum scalar quantizer and a binary convolutional code with soft-decision decoding, we obtained both a lower and an upper bound on the end-to-end average source distortion. The optimal bandwidth allocation was then numerically obtained by minimizing upper and lower bounds on the average distortion. We have shown that the upper bound-based cost function is a convex function of the source code rate, and the optimal allocation depends on the system and the channel conditions, such as the total number of active users, the number of carriers, and the average jammer-to-signal power ratio.

CHAPTER 4

Cooperative Diversity with Optimum Noncoherent Reception

4.1 Introduction

More than two decades after the seminal works of van der Meulen [23], and Cover and El Gamal [25] on the capacity limits of relay channels, recently, there is a renewed interest in the area of relay-assisted cooperative communication for mobile ad hoc wireless networks. By sharing the transmission resources efficiently in a collaborative manner, mobile nodes with single-antenna transceivers can increase their data rate, range and reliability by forming virtual antenna arrays [45]. Sendonaris *et al.* in [46] showed that, with transmitter CSI, the sum-capacity of an ergodic fading channel can be improved with user cooperation, whereas in [47] Laneman showed that reliability can be improved with the knowledge of CSI only at the receiver.

The performance of coherent binary PSK (BPSK) signaling with an amplify-and-forward protocol and receiver CSI was studied in [48], whereas an improved analysis of error probability, using the moment generating function approach, was presented in [49]. Recently, the performance of multi-branch, multi-hop, relay channels was considered in [50] and [51]. The analyses of [48]-[51] showed that with M relay nodes, a direct link between the source and destination, and perfect CSI at the receiver, coherent multi-branch AF reception over independent channels achieves the full diversity order of $M + 1$.

To acquire the CSI, the relay channel has to be trained (typically with the help of pilot signaling), which results in a throughput penalty. If the variation of the channel over time is high relative to the signaling duration, then the estimates become outdated and are not useful for signal detection. In such a scenario, one is inclined to employ noncoherent detection techniques which do not require the knowledge of the instantaneous channel realization. In this context, Chen and Laneman in [52] and [53] studied the performance of noncoherent binary FSK (BFSK) signaling with a decode-and-forward protocol. In [52] and [53], it was shown that, with M relays, the diversity order achievable with a noncoherent DF protocol is at most $(M/2)+1$ when M is even, and $(M+1)/2$ when M is odd. That is, with the DF protocol, noncoherent signaling loses approximately half of the available diversity order.

In this chapter, we consider noncoherent communication over Rayleigh fading relay channels with an AF protocol. While neither the relays nor the destination have knowledge of the instantaneous CSI, we assume that the statistical averages of the channel gains are known to them. This is a reasonable assumption, as an example, for a slowly varying relay network topology. The amplification gain of the relay is chosen to satisfy an average power constraint. We consider both on-off keying (OOK) and BFSK modulation schemes, and derive the maximum likelihood (ML) noncoherent AF (NCAF) receiver structures at the destination. Unfortunately, even for the case of single relay node, no closed-form expression for the ML NCAF receiver is available, and the ML metric computation requires numerical evaluation of certain integrals. To gain some understanding of the receiver performance, we assume that the relay-to-destination link is unfaded[1]. This is reasonable when there is a strong line-of-sight path from the relay to the destination. With this, we are able to derive simple closed-form expressions for the average bit error rate (BER), with an arbitrary number of relay nodes, that serve as lower bounds on the optimal performance. We derive the Upper bounds on the average BER by employing the Bhattacharyya bound [29]. We propose simple suboptimum receivers, for both OOK and

[1]Similar assumption is made in [54] for diversity analysis.

BFSK, along with their performance evaluations. We also show that, using asymptotic diversity order analysis [55], with M relay nodes plus a link between the source and the destination, the OOK achieves a diversity order of at least $(M+1)/2$, but never $M+1$, whereas BFSK achieves the full diversity of $M+1$. However, one of our more surprising results is that for OOK system, without relay, the asymptotic diversity analysis predicts a diversity order of less than unity. Since we could not find a good physical interpretation of this result, it suggests that the use of asymptotic diversity analysis should be used with caution.

The rest of this chapter is organized as follows. We present the system model in Section 4.2. Optimum NCAF receiver structures for OOK and BFSK are formulated in Sections 4.2.1 and 4.2.2, respectively. With the assumption that the relay-to-destination link is unfaded, Sections 4.3.1 and 4.3.2, respectively, derive the average BER expressions for both OOK and BFSK modulations, whereas Bhattacharyya distance-based upper bounds on the BER are discussed in Section 4.4. Suboptimum receiver structures are presented in Section 4.5. In Section 4.6 we study the asymptotic diversity order analysis, whereas numerical and simulation results are presented in Section 4.7. Finally, we conclude this work in Section 4.8.

4.2 System Model

Consider a source node S that wishes to communicate with an intended destination node D with the help of M relay nodes, $R_1, \ldots, R_M$, as shown in Fig. 4.1. We assume frequency-flat fading on the links between the source and the destination, between the source and the relays, and between the relays and the destination. Let g_1 denote the channel gain on the path from the source to the destination D, and, for $j = 1, \ldots, M$, g_2^j denote the channel gain on the path from the source to the relay node R_j. Also, let g_3^j denotes the channel gain on the path from the relay R_j to the destination. We assume that g_1, $\{g_2^j\}$, and $\{g_3^j\}$, $j = 1, \ldots, M$, are zero-mean complex Gaussian random variables

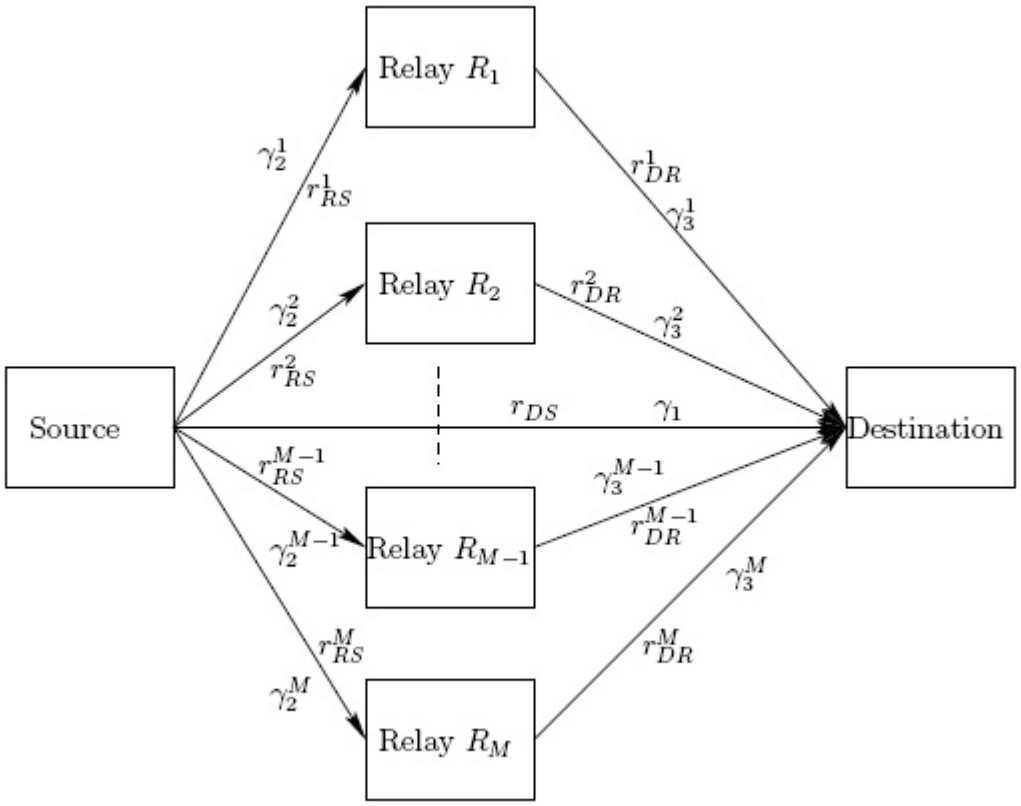

Figure 4.1 *Block diagram of the system with M relays. Here, r_{DS} is the received signal from the source to the destination on the direct path, whereas r_{RS}^j and r_{DR}^j respectively denote the signal received from the source to the jth relay, and from the jth relay to the destination. The random variables γ_1, γ_2^j and γ_3^j, respectively denote the instantaneous link SNRs on the path from the source to the destination, from the source to the relay R_j, and from the relay R_j to the destination.*

(r.vs) with variances $E[|g_1|^2] = \Omega_1$, and $E[|g_2^j|^2] = \Omega_2^j$, and $E[|g_3^j|^2] = \Omega_3^j$, $j = 1, \ldots, M$, respectively.

The source employs a binary signal constellation, $\mathcal{X}$, and neither the relays nor the destination know the instantaneous channel gains, and hence employ noncoherent demodulation. We also assume that the relays amplify the signal received from the source in such a way that they meet their respective average power constraints. Even though the relays and the destination do not have instantaneous knowledge of the gains $\{g_2^j, g_3^j\}_{j=1}^M$

and g_1, we do assume that they have the knowledge of the statistical averages, $\{\Omega_2^j, \Omega_3^j\}_{j=1}^M$ and Ω_1. Our communication protocol is the same as that of [56], where in the first time slot the source broadcasts its signal to the destination and the relays, whereas in the second time slot the relays forward their copies to the destination. That is, if T and W, respectively, denote the message duration and bandwidth required for a single-hop system, then the message duration and bandwidth requirements with M relays are $2T$ and MW, respectively.

Throughout this chapter, we employ low-pass equivalent complex baseband signal models so that $\mathcal{X}$, in general, represents a complex-valued constellation. Let $X \in \mathcal{X}$ be the symbol transmitted by the source in the first time slot. Then, the matched-filer (MF) output at the jth relay is then given by

$$r_{RS}^j = g_2^j X + \eta_{RS}^j, \tag{4.1}$$

where η_{RS}^j is a complex-valued Gaussian noise random variable (r.v) with zero-mean and variance $E[|\eta_{RS}^j|^2] = \sigma_N^2$. The output of MF at the destination due to the direct link is given by

$$r_{DS} = g_1 X + \eta_{DS}, \tag{4.2}$$

where η_{DS} is a complex-valued Gaussian noise r.v with zero-mean and variance $E[|\eta_{DS}|^2] = \sigma_N^2$. The relay R_j amplifies the signal r_{RS}^j by a factor A_j, where A_j is chosen in such a way that the constraint $E[|A_j r_{RS}^j|^2] = E_s$ is satisfied. Clearly, $A_j = \sqrt{\frac{E_s}{E_s \Omega_2^j + \sigma_N^2}}$. In the second time slot, the relays transmit their respective signals to the destination. The output of the MF at the destination due to the relay R_j is given by

$$r_{DR}^j = A_j g_3^j r_{RS}^j + \eta_{DR}^j = A_j g_3^j g_2^j X + A_j g_3^j \eta_{RS}^j + \eta_{DR}^j, \tag{4.3}$$

where η_{DR}^j is a complex-valued Gaussian noise r.v with zero-mean and variance $E[|\eta_{DR}^j|^2] = \sigma_N^2$. One of the main goals in this chapter is to derive the optimal receiver structure at the

destination, based only on the statistical knowledge of $\Omega_1, \{\Omega_2^j, \Omega_3^j\}_{j=1}^M$. In what follows, we consider two kinds of binary signal constellations that are amenable to noncoherent detection: 1)OOK modulation, and 2)BFSK modulation.

4.2.1 On-Off Keying

With OOK, the signal set is given by $\mathcal{X} = \{0, \sqrt{2E_s}\}$. The signal 0 is transmitted when the bit $b = 0$, whereas $\sqrt{2E_s}$ is transmitted when the bit $b = 1$. The information bits '0' and '1' are assumed to be equally likely, so that the average transmit energy at the output of the source is E_s.

When the information bit $b = 1$ is transmitted, the joint pdf of $\{r_{DR}^j\}_{j=1}^M$, and r_{DS}, conditioned on $X = \sqrt{2E_s}$, is given by

$$\begin{aligned} f_{r_{DR}^1,\ldots,r_{DR}^M,r_{DS}|X=\sqrt{2E_s}} &= E_{g_1}\left[f_{n_{DS}|g_1}\left(r_{DS} - \sqrt{2E_s}g_1\right)\right] \times \\ &\quad \prod_{j=1}^{M} E_{g_2^j,g_3^j}\left[f_{\tilde{n}_{DR}^j|g_2^j,g_3^j}\left(r_{DR}^j - A_j g_2^j g_3^j \sqrt{2E_s}\right)\right], \quad (4.4) \end{aligned}$$

where $E_U[\cdot]$ denotes the expectation over the r.v U, and $\tilde{n}_{DR}^j$, conditioned on g_2^j and g_3^j, is a zero-mean complex Gaussian r.v with variance $E[|\tilde{n}_{DR}^j|^2|g_2^j, g_3^j] = \sigma_N^2(1 + A_j^2|g_3^j|^2)$. Also, $f_{n_{DS}|g_1}(\cdot)$ and $f_{\tilde{n}_{DR}^j|g_2^j,g_3^j}(\cdot)$ are the conditional density functions of n_{DS} and $\tilde{n}_{DR}^j$, respectively. For simplicity, we define the following variables. We define $\gamma_1 \triangleq |g_1|^2E_s/\sigma_N^2$, $\gamma_2^j \triangleq |g_2^j|^2E_s/\sigma_N^2$, and $\gamma_3^j \triangleq |g_3^j|^2E_s/\sigma_N^2$, and their respective statistical averages by $\overline{\gamma}_1 \triangleq E[\gamma_1] = \Omega_1 E_s/\sigma_N^2$, $\overline{\gamma}_2^j \triangleq E[\gamma_2^j] = \Omega_2^j E_s/\sigma_N^2$, and $\overline{\gamma}_3^j \triangleq E[\gamma_3^j] = \Omega_3^j E_s/\sigma_N^2$. In order to proceed further, we need the following lemma:

Lemma 1. *If Z is a complex Gaussian r.v, having independent real and imaginary parts, with mean $E[Z] = \mathfrak{m}$ and variance $E[|Z - \mathfrak{m}|^2] = \mathcal{N}$, then the expected value of*

$\exp(-|Z|^2)$ *is given by*

$$E[\exp(-|Z|^2)] \;=\; \frac{1}{1+\mathcal{N}}\exp\left(-\frac{|\mathfrak{m}|^2}{1+\mathcal{N}}\right). \tag{4.5}$$

Proof. Refer to [57, Eqn. (2.1-117)]. □

Since $(r_{DS}-\sqrt{2E_s}g_1)/\sqrt{\sigma_N^2}$ is complex Gaussian with mean $r_{DS}/\sqrt{\sigma_N^2}$ and variance $(2E_s/\sigma_N^2)E[|g_1|^2] = 2E_s\Omega_1/\sigma_N^2 = 2\overline{\gamma}_1$, using Lemma 1, the first term in (4.4) can be simplified to

$$E_{g_1}\left[f_{n_{DS}|g_1}\left(r_{DS}-\sqrt{2E_s}g_1\right)\right] = \frac{1}{\pi\sigma_N^2}\times\frac{1}{1+2\overline{\gamma}_1}\exp\left(-\frac{Z_{DS}}{1+2\overline{\gamma}_1}\right), \tag{4.6}$$

where $Z_{DS} = |r_{DS}|^2/\sigma_N^2$. Following a similar argument as that for (4.6), the jth term in the product of the second term in (4.4) can now be simplified to

$$\begin{aligned}
&E_{g_2^j,g_3^j}\left[f_{\tilde{n}_{DR}^j|g_2^j,g_3^j}\left(r_{DR}^j - A_j g_2^j g_3^j\sqrt{2E_s}\right)\right] = \\
&E_{g_2^j,g_3^j}\left[\frac{1}{\pi\sigma_N^2(1+A_j^2|g_3^j|^2)}\exp\left(-\frac{|r_{DR}^j - A_j g_2^j g_3^j\sqrt{2E_s}|^2}{\sigma_N^2(1+A_j^2|g_3^j|^2)}\right)\right] \\
&= E_{g_3^j}\left[\frac{1}{\pi\sigma_N^2}\frac{\exp\left(-\frac{|r_{DR}^j|^2/\sigma_N^2}{1+A_j^2|g_3^j|^2(1+2\overline{\gamma}_2^j)}\right)}{(1+A_j^2|g_3^j|^2(1+2\overline{\gamma}_2^j))}\right].
\end{aligned} \tag{4.7}$$

By defining $\lambda(\overline{\gamma}_2^j) = (1+2\overline{\gamma}_2^j)/(1+\overline{\gamma}_2^j)$, and $Z_{DR}^j = |r_{DR}^j|^2/\sigma_N^2$, we can express (4.7) by the following integral:

$$\begin{aligned}
&E_{g_2^j,g_3^j}\left[f_{\tilde{n}_{DR}^j|g_2^j,g_3^j}\left(r_{DR}^j - A_j g_2^j g_3^j\sqrt{2E_s}\right)\right] \\
&= \frac{1}{\pi\sigma_N^2}\int_{x=0}^{\infty}\frac{\exp(-x)}{1+\lambda(\overline{\gamma}_2^j)\overline{\gamma}_3^j x}\exp\left(-\frac{Z_{DR}^j}{1+\lambda(\overline{\gamma}_2^j)\overline{\gamma}_3^j x}\right)dx.
\end{aligned} \tag{4.8}$$

Note that, unfortunately, the integral in (4.8) does not have a closed-form solution.

When $X = 0$ is transmitted, we have

$$f_{r^1_{DR},\ldots,r^M_{DR},r_{DS}|X=0} = E_{g_1}\left[f_{n_{DS}}\left(r_{DS}\right)\right] \times \prod_{j=1}^{M} E_{g_2^j,g_3^j}\left[f_{\tilde{n}^j_{DR}|g_2^j,g_3^j}\left(r^j_{DR}\right)\right]. \tag{4.9}$$

Following the analysis of (4.6) and (4.7), we can simplify the terms in (4.9) to

$$E_{g_1}\left[f_{n_{DS}}\left(r_{DS}\right)\right] = \frac{1}{\pi\sigma_N^2}\exp\left(-Z_{DS}\right) \tag{4.10}$$

$$\text{and} \quad E_{g_2^j,g_3^j}\left[f_{\tilde{n}^j_{DR}}\left(r^j_{DR}\right)\right] = E_{g_2^j,g_3^j}\left[\frac{1}{\pi\sigma_N^2(1+A_j^2|g_3^j|^2)}\exp\left(-\frac{|r^j_{DR}|^2}{\sigma_N^2(1+A_j^2|g_3^j|^2)}\right)\right]$$

$$= \frac{1}{\pi\sigma_N^2}\int_{x=0}^{\infty}\frac{\exp(-x)}{1+\mu(\overline{\gamma}_2^j)\overline{\gamma}_3^j x}\exp\left(-\frac{Z^j_{DR}}{1+\mu(\overline{\gamma}_2^j)\overline{\gamma}_3^j x}\right)dx, \tag{4.11}$$

where $\mu(\overline{\gamma}_2^j) = 1/(1+\overline{\gamma}_2^j)$.

Finally, the log-likelihood ratio of the transmitted bit at the destination is given by

$$\begin{aligned}\mathrm{LLR}(b) &\triangleq \log\left(\frac{f_{r^1_{DR},\ldots,r^M_{DR},r_{DS}|X=\sqrt{2E_s}}}{f_{r^1_{DR},\ldots,r^M_{DR},r_{DS}|X=0}}\right)\\ &= \mathcal{F}\left(Z_{DS},\overline{\gamma}_1\right) + \sum_{j=1}^{M}\mathcal{G}\left(Z^j_{DR},\overline{\gamma}_2^j,\overline{\gamma}_3^j\right),\end{aligned} \tag{4.12}$$

where

$$\mathcal{F}\left(Z_{DS},\overline{\gamma}_1\right) = -\log\left(1+2\overline{\gamma}_1\right) + \left(\frac{2\overline{\gamma}_1}{1+2\overline{\gamma}_1}\right)Z_{DS} \tag{4.13}$$

$$\text{and} \quad \mathcal{G}\left(Z^j_{DR},\overline{\gamma}_2^j,\overline{\gamma}_3^j\right) = \log\left(\int_{x=0}^{\infty}\frac{\exp\left(-x-\frac{Z^j_{DR}}{1+\lambda(\overline{\gamma}_2^j)\overline{\gamma}_3^j x}\right)}{1+\lambda(\overline{\gamma}_2^j)\overline{\gamma}_3^j x}dx\right) -$$

$$\log\left(\int_{x=0}^{\infty}\frac{\exp\left(-x-\frac{Z^j_{DR}}{1+\mu(\overline{\gamma}_2^j)\overline{\gamma}_3^j x}\right)}{1+\mu(\overline{\gamma}_2^j)\overline{\gamma}_3^j x}dx\right). \tag{4.14}$$

The optimum receiver at the destination, implementing (4.12), is shown in Fig. 4.2. The

destination decodes $\widehat{b} = 1$ if $\text{LLR} \geq 0$ and $\widehat{b} = 0$ otherwise.

4.2.2 Binary FSK

With BFSK signaling, the signal constellation is given by $\mathcal{X} = \{\sqrt{E_s}e^{j2\pi f_1 t}, \sqrt{E_s}e^{j2\pi f_2 t}\}$, where f_1 and f_2 are two orthogonal frequency tones. When $b = 1$ is the transmitted bit, we have $X = \sqrt{E_s}e^{2\pi f_1 t}$. After matched filtering of the received signals r_{DS} and r_{DR}^j, $j = 1, \ldots, M$, by $e^{-2\pi f_1 t}$ and $e^{-j2\pi f_2 t}$ over the signaling duration, we obtain the following low-pass equivalent complex-valued outputs as

$$\begin{aligned}
r_{DS,1} &\triangleq r_{DS,c,1} + jr_{DS,s,1} = \sqrt{E_s}g_1 + \eta_{DS,1} && (4.15)\\
r_{DS,2} &\triangleq r_{DS,c,2} + jr_{DS,s,2} = \eta_{DS,2} && (4.16)\\
r_{DR,1}^k &\triangleq r_{DR,c,1}^k + jr_{DR,s,1}^k \\
&= A_k\sqrt{E_s}g_2^k g_3^k + A_k g_3^k \eta_{RS,1}^k + \eta_{DR,1}^k \; k = 1, \ldots, M && (4.17)\\
r_{DR,2}^k &\triangleq r_{DR,c,2}^k + jr_{DR,s,2}^k = A_k g_3^k \eta_{RS,2}^k + \eta_{DR,2}^k \quad k = 1, \ldots, M. && (4.18)
\end{aligned}$$

In (4.15)-(4.18), the subscripts 1 and 2 represent the outputs due to correlating with frequencies f_1 and f_2, respectively, whereas the subscripts c and s denote the in-phase and quadrature components, respectively.

Conditioned on f_1 being transmitted, the conditional probability density of $r_{DS,1}$, $r_{DS,2}$, $r_{DR,1}^k$, $r_{DR,2}^k$, $k = 1, \ldots, M$, is given by

$$\begin{aligned}
&f_{r_{DS,1}, r_{DS,2}, r_{DR,1}^1, r_{DR,2}^1, \ldots, r_{DR,1}^M, r_{DR,2}^M | f_1} = E_{g_1}[f_{\eta_{DS,1}|g_1}(r_{DS,1} - \sqrt{E_s}g_1)] f_{\eta_{DS,2}}(r_{DS,2}) \\
&\times \prod_{k=1}^{M} E_{g_2^k, g_3^k}\left[f_{\tilde{\eta}_{DR,1}^k | g_2^k, g_3^k}(r_{DR,1}^k - A_k\sqrt{E_s}g_2^k g_3^k) f_{\tilde{\eta}_{DR,2}^k | g_2^k, g_3^k}(r_{DR,2}^k) \right], \qquad (4.19)
\end{aligned}$$

where $\tilde{\eta}_{DR,1}^k = A_k g_3^k \eta_{RS,1}^k + \eta_{DR,1}^k$ and $\tilde{\eta}_{DR,2}^k = A_k g_3^k \eta_{RS,2}^k + \eta_{DR,2}^k$, conditioned on g_2^k and g_3^k, are two independent complex Gaussian r.vs with zero-mean and variances $E[|\tilde{\eta}_{DR,1}^k|^2 | g_2^k, g_3^k] = E[|\tilde{\eta}_{DR,2}^k|^2 | g_2^k, g_3^k] = \sigma_N^2(1 + A_k^2 |g_3^k|^2)$.

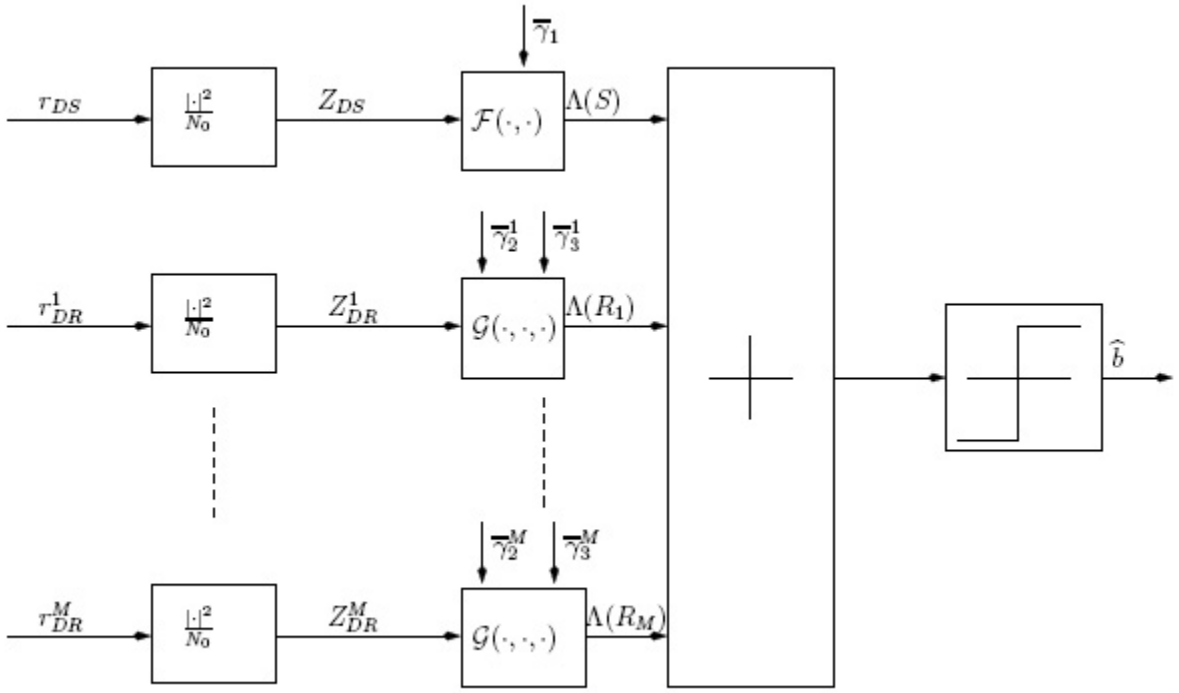

Figure 4.2 *Optimum receiver for OOK modulation. The functions $\mathcal{F}(\cdot,\cdot)$ and $\mathcal{G}(\cdot,\cdot,\cdot)$ are respectively defined in Eqns. (4.13) and (4.14).*

Using Lemma 1, the terms of (4.19) can be simplified to

$$E_{g_1}[f_{\eta_{DS,1}|g_1}(r_{DS,1}-\sqrt{E_s}g_1)] = \frac{1}{\pi\sigma_N^2}\times\frac{1}{1+\frac{E_s\Omega_1}{\sigma_N^2}}\exp\left(-\frac{|r_{DS,1}|^2/\sigma_N^2}{1+E_s\Omega_1/\sigma_N^2}\right)$$
$$= \frac{1}{\pi\sigma_N^2}\times\frac{1}{1+\overline{\gamma}_1}\exp\left(-\frac{Z_{DS,1}}{1+\overline{\gamma}_1}\right). \tag{4.20}$$

$$f_{\eta_{DS,2}}(r_{DS,2}) = \frac{1}{\pi\sigma_N^2}\exp\left(-\frac{|r_{DS,2}|^2}{\sigma_N^2}\right) = \frac{1}{\pi\sigma_N^2}\exp\left(-Z_{DS,2}\right) \tag{4.21}$$

$$E_{g_2^k,g_3^k}\left[f_{\tilde{\eta}^k_{DR,1}|g_2^k,g_3^k}(r^k_{DR,1}-A_k\sqrt{E_s}g_2^kg_3^k)f_{\tilde{\eta}^k_{DR,2}|g_2^k,g_3^k}(r^k_{DR,2})\right] =$$
$$E_{g_3^k}\left[\frac{1}{\pi^2N_0^2(1+A_k^2|g_2^k|^2)^2}\times\exp\left(-\frac{|r^k_{DR,2}|^2}{\sigma_N^2(1+A_k^2|g_3^k|^2)}\right)\right.$$
$$\left.\frac{1}{1+\frac{A_k^2E_s|g_3^k|^2\Omega_2^k}{\sigma_N^2(1+A_k^2|g_3^k|^2)}}\exp\left(-\frac{\frac{|r^k_{DR,2}|^2}{\sigma_N^2(1+A_k^2|g_3^k|^2)}}{1+\frac{A_k^2E_s|g_3^k|^2\Omega_2^k}{\sigma_N^2(1+A_k^2|g_3^k|^2)}}\right)\right]$$
$$= \frac{1}{\pi^2N_0^2}E_{\gamma_2^k}\left[\frac{1}{1+\mu(\overline{\gamma}_2^k)\gamma_3^k}\times\frac{1}{1+\gamma_3^k}\exp\left(-\frac{Z^k_{DR,1}}{1+\gamma_3^k}-\frac{Z^k_{DR,2}}{1+\mu(\overline{\gamma}_2^k)\gamma_3^k}\right)\right]$$
$$= \frac{1}{\pi^2N_0^2}\underbrace{\int_{x=0}^{\infty}\frac{dx}{1+\mu(\overline{\gamma}_2^k)\overline{\gamma}_3^kx}\times\frac{\exp(-x)}{1+\overline{\gamma}_3^kx}\exp\left(-\frac{Z^k_{DR,1}}{1+\overline{\gamma}_3^kx}-\frac{Z^k_{DR,2}}{1+\mu(\overline{\gamma}_2^k)\overline{\gamma}_3^kx}\right)}_{\triangleq\Psi(Z^k_{DR,1},Z^k_{DR,2},\overline{\gamma}_2^k,\overline{\gamma}_3^k)}$$
$$= \frac{1}{\pi^2N_0^2}\Psi(Z^k_{DR,1},Z^k_{DR,2},\overline{\gamma}_2^k,\overline{\gamma}_3^k). \tag{4.22}$$

In (4.22), we have $Z_{DS,1} = |r_{DS,1}|^2/\sigma_N^2$, $Z_{DS,2} = |r_{DS,2}|^2/\sigma_N^2$, $Z^k_{DR,1} = |r^k_{DR,1}|^2/\sigma_N^2$, $Z^k_{DR,2} = |r^k_{DR,2}|^2/\sigma_N^2$, and $\Psi(Z^k_{DR,1},Z^k_{DR,2},\overline{\gamma}_2^k,\overline{\gamma}_3^k)$ is given by the integral of (4.22).

When frequency f_2 is transmitted, the above analysis remains valid but, since the correlation with $e^{-j2\pi f_1t}$ would yield only the noise, and the correlation with $e^{-j2\pi f_2t}$ would yield signal-plus-noise, we need to exchange $Z^k_{DR,1}$ and $Z^k_{DR,2}$, and $Z_{DS,1}$ and

$Z_{DS,2}$. With this, the LLR of the transmitted bit at the destination is then given by

$$\begin{aligned}
\mathrm{LLR}(b) &= \log\left(\frac{f_{r_{DS,1},r_{DS,2},r^1_{DR,1},r^1_{DR,2},\ldots,r^M_{DR,1},r^M_{DR,2}|f_1}}{f_{r_{DS,1},r_{DS,2},r^1_{DR,1},r^1_{DR,2},\ldots,r^M_{DR,1},r^M_{DR,2}|f_2}}\right) \\
&= \log\left(\frac{\exp\left(-\frac{Z_{DS,1}}{1+\overline{\gamma}_1}-Z_{DS,2}\right)\prod_{k=1}^{M}\Psi(Z^k_{DR,1},Z^k_{DR,2},\overline{\gamma}^k_2,\overline{\gamma}^k_3)}{\exp\left(-\frac{Z_{DS,2}}{1+\overline{\gamma}_1}-Z_{DS,1}\right)\prod_{k=1}^{M}\Psi(Z^k_{DR,2},Z^k_{DR,1},\overline{\gamma}^k_2,\overline{\gamma}^k_3)}\right) \\
&= \left(\frac{\overline{\gamma}_1}{1+\overline{\gamma}_1}\right)[Z_{DS,1}-Z_{DS,2}]+\sum_{j=1}^{M}\mathcal{H}\left(Z^j_{DR,1},Z^j_{DR,2},\overline{\gamma}^j_2,\overline{\gamma}^j_3\right), \quad (4.23)
\end{aligned}$$

where, using the definition of $\Psi(\cdot,\cdot,\cdot,\cdot)$ in (4.22), we have

$$\begin{aligned}
\mathcal{H}\left(Z^j_{DR,1},Z^j_{DR,2},\overline{\gamma}^j_2,\overline{\gamma}^j_3\right) &= \log\left(\int_0^\infty \frac{dx\exp\left(-x-\frac{Z^j_{DR,1}}{1+\overline{\gamma}^j_3 x}-\frac{Z^j_{DR,2}}{1+\mu(\overline{\gamma}^j_2)\overline{\gamma}^j_3 x}\right)}{(1+\overline{\gamma}^j_3 x)(1+\mu(\overline{\gamma}^j_2)\overline{\gamma}^j_3 x)}\right) \\
&\quad -\log\left(\int_0^\infty \frac{dx\exp\left(-x-\frac{Z^j_{DR,2}}{1+\overline{\gamma}^j_3 x}-\frac{Z^j_{DR,1}}{1+\mu(\overline{\gamma}^j_2)\overline{\gamma}^j_3 x}\right)}{(1+\overline{\gamma}^j_3 x)(1+\mu(\overline{\gamma}^j_2)\overline{\gamma}^j_3 x)}\right). \quad (4.24)
\end{aligned}$$

The optimum receiver at the destination, implementing (4.23), is shown in Fig. 4.3. The destination decodes $\widehat{b}=1$ if $\mathrm{LLR}\geq 0$ and $\widehat{b}=0$ otherwise.

4.3 Lower Bounds on the Average BER

Due to the complicated nature of the detection metrics of (4.12) and (4.23), an analysis of the performance of the optimum NCAF is difficult to perform. As a consequence, we now consider a simple case of having a strong line-of-sight path on the relay-to-destination link. An example scenario could be terrestrial communication from the relay to the destination in a rural environment. In this case, we assume that the channel gain from the relay to the destination is unfaded. That is, we have $f_{\gamma^j_3}(x)=\delta(x-\overline{\gamma}^j_3)$, where $\delta(x)$ is the Dirac delta function. With this assumption, we derive simple closed-form

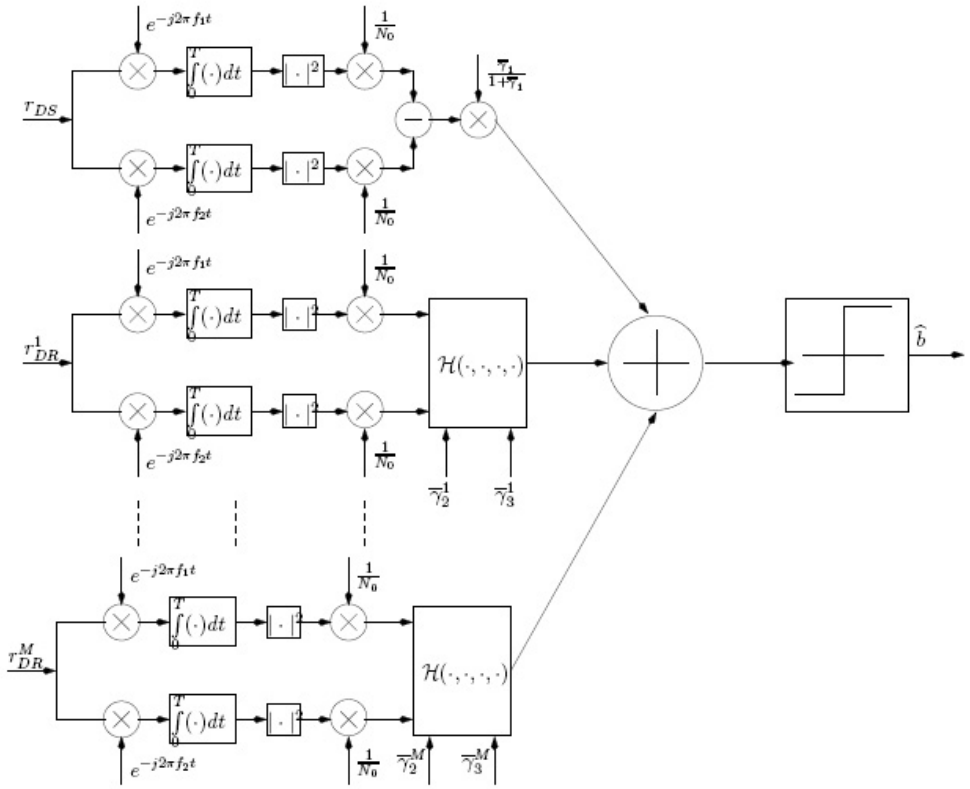

Figure 4.3 *Optimum receiver for BFSK modulation. The function $\mathcal{H}(\cdot,\cdot,\cdot,\cdot)$ is defined in (4.24).*

expressions for the average probability of bit error. It is to be noted that, even if this assumption is not satisfied in practice, the resulting expressions can still serve as lower bounds on the average error performance.

4.3.1 On-Off Keying

We first realize that the term $\exp(-x)$ in the integrands of (4.11) and (4.22) is due to the fact that we are averaging $E_{\gamma_2^j}[\cdot]$ over the pdf of $\gamma_2^j/\overline{\gamma}_2^j$, which is exponentially distributed with unity mean. Upon replacing $\exp(-x)$ in the integrands of (4.11) by $\delta(x-1)$, we can simplify the optimum receiver for this special case as

$$\begin{aligned}\mathrm{LLR}(b) &= -\log\left(1+2\overline{\gamma}_1\right) + \left(\frac{2\overline{\gamma}_1}{1+2\overline{\gamma}_1}\right) Z_{DS} + \\ &\sum_{j=1}^{M}\left\{\log\left(\frac{1}{1+\lambda(\overline{\gamma}_2^j)\overline{\gamma}_3^j}\exp\left(-\frac{Z_{DR}^j}{1+\lambda(\overline{\gamma}_2^j)\overline{\gamma}_3^j}\right)\right) - \right. \\ &\left.\log\left(\frac{1}{1+\mu(\overline{\gamma}_2^j)\overline{\gamma}_3^j}\exp\left(-\frac{Z_{DR}^j}{1+\mu(\overline{\gamma}_2^j)\overline{\gamma}_3^j}\right)\right)\right\}. \qquad (4.25)\end{aligned}$$

Eqn. (4.25) can be expressed in a convenient form as

$$\mathrm{LLR}(b) = c_1 Z_{DS} + \sum_{j=1}^{M} c_2^j Z_{DR}^j - \mathrm{T_h} \qquad (4.26)$$

where

$$\begin{aligned}\text{where} \quad c_1 &= \frac{2\overline{\gamma}_1}{1+2\overline{\gamma}_1} \qquad (4.27)\\ c_2^j &= \frac{2\overline{\gamma}_2^j\overline{\gamma}_3^j}{(1+\overline{\gamma}_2^j+\overline{\gamma}_3^j)(1+\lambda(\overline{\gamma}_2^j)\overline{\gamma}_3^j)} \qquad j=1,\ldots,M \qquad (4.28)\\ \text{and} \quad \mathrm{T_h} &= \log(1+2\overline{\gamma}_1) + \\ &\sum_{j=1}^{M}\left\{\log(1+\lambda(\overline{\gamma}_2^j)\overline{\gamma}_3^j) - \log\left(1+\mu(\overline{\gamma}_2^j)\overline{\gamma}_3^j\right)\right\}. \qquad (4.29)\end{aligned}$$

In Appendix-C, we present a closed-form expression for the average BER of the detector of (4.26) which is given by

$$\begin{aligned}\overline{P}_{e,\text{On-Off}} &= \frac{1}{2}\left(1 - F\left(\overline{X}_0, \overline{Y}_0^1, \ldots, \overline{Y}_0^M, \mathrm{T_h}\right)\right) + \\ &\quad \frac{1}{2}F\left(\overline{X}_1, \overline{Y}_1^1, \ldots, \overline{Y}_1^M, \mathrm{T_h}\right), \end{aligned} \tag{4.30}$$

where

$$F(\overline{U}_1, \overline{U}_2, \ldots, \overline{U}_N, \mathrm{T_h}) = \sum_{j=1}^{N}\left\{\prod_{i=1, i\neq j}^{N}\frac{\overline{U}_j}{\overline{U}_j - \overline{U}_i}\right\}\left(1 - e^{-\frac{\mathrm{T_h}}{\overline{U}_j}}\right) \tag{4.31}$$

$$\overline{X}_0 = \frac{2\overline{\gamma}_1}{1 + 2\overline{\gamma}_1} \tag{4.32}$$

$$\overline{Y}_0^j = \frac{2\overline{\gamma}_2^j\overline{\gamma}_3^j}{(1+\overline{\gamma}_2^j)(1+\lambda(\overline{\gamma}_2^j)\overline{\gamma}_3^j)} \quad j = 1, \ldots, M \tag{4.33}$$

$$\overline{X}_1 = 2\overline{\gamma}_1 \tag{4.34}$$

$$\text{and} \quad \overline{Y}_1^j = \frac{2\overline{\gamma}_2^j\overline{\gamma}_3^j}{1 + \overline{\gamma}_2^j + \overline{\gamma}_3^j} \quad j = 1, \ldots, M. \tag{4.35}$$

In (4.31), the function $F(\overline{U}_1, \overline{U}_2, \ldots, \overline{U}_N, \mathrm{T_h})$ is defined as the probability of $U_1 + U_2 + \ldots + U_N$ less than $\mathrm{T_h}$, where $U_1, \ldots, U_N$ are independent exponentially distributed r.vs with the mean of U_i being $\overline{U}_i$.

We now study the behavior of (4.30) at high SNR. Similar to [53], we let $\overline{\gamma}_1 = \mathsf{t}_1\overline{\gamma}$, and, for $j = 1, \ldots, M$, $\overline{\gamma}_2^j = \mathsf{t}_2^j\overline{\gamma}$ and $\overline{\gamma}_3^j = \mathsf{t}_3^j\overline{\gamma}$, so that the average link SNR goes to infinity with $\overline{\gamma}$, while still maintaining a fixed proportionality among them. The variables t_1 and $\{\mathsf{t}_2^j, \mathsf{t}_3^j\}_{j=1}^M$ capture the relay placement and path-loss variability in the relay network. As $\overline{\gamma} \to \infty$, (4.32)-(4.35) approach

$$\overline{X}_0 = 1 \tag{4.36}$$

$$\overline{Y}_0^j = 1 \qquad j = 1, \ldots, M \tag{4.37}$$

$$\overline{X}_1 = 2\mathsf{t}_1\overline{\gamma} \tag{4.38}$$

$$\text{and} \quad \overline{Y}_1^j = \frac{2\mathsf{t}_2^j \mathsf{t}_3^j}{\mathsf{t}_2^j + \mathsf{t}_3^j}\overline{\gamma} \qquad j = 1, \ldots, M, \tag{4.39}$$

respectively. As $\overline{\gamma} \to \infty$, the threshold $\mathrm{T_h}$ in (4.29) can be approximated as $(M+1)\log(\overline{\gamma})$. In view of (4.36) and (4.37), the first term, $\Big(1 - F(\overline{X}_0, \overline{Y}_0^1, \ldots, \overline{Y}_0^M, \mathrm{T_h})\Big)$, in (4.30) is nothing but the probability that the sum of $M+1$ independent and identically distributed (i.i.d.) exponential r.vs, each having unity mean, exceeds $\mathrm{T_h}$. This has a well-known closed form, which is given by [57]

$$\begin{aligned}
\Big(1 - F(\overline{X}_0, \overline{Y}_0^1, \ldots, \overline{Y}_0^M, \mathrm{T_h})\Big) &= \int_{\mathrm{T_h}}^{\infty} \frac{e^{-x} x^M}{\Gamma(M+1)} dx \\
&\approx \frac{e^{-\mathrm{T_h}} {\mathrm{T_h}}^M}{\Gamma(M+1)} \quad (\mathrm{T_h} \to \infty) \\
&\approx \frac{(M+1)^M}{M!} \times \frac{(\log(\overline{\gamma}))^M}{(\overline{\gamma})^{M+1}} \quad (\overline{\gamma} \to \infty),
\end{aligned} \tag{4.40}$$

where in the second step of (4.40) we employed the asymptotic behavior of incomplete Gamma function [36]. The third step in (4.40) is due to $\mathrm{T_h} \approx (M+1)\log(\overline{\gamma})$. To characterize the behavior of $F(\overline{X}_1, \overline{Y}_1^1, \ldots, \overline{Y}_1^M, \mathrm{T_h})$ in (4.30), we notice that the constituent r.vs $\overline{X}_1, \overline{Y}_1^1, \ldots, \overline{Y}_1^M$ have a linear growth in their expected values with $\overline{\gamma}$ (see (4.38) and (4.39)). Let us define $\mathsf{t}_{\max} = \max(\mathsf{t}_1, \frac{\mathsf{t}_2^1 \mathsf{t}_3^1}{\mathsf{t}_2^1 + \mathsf{t}_3^1}, \ldots, \frac{\mathsf{t}_2^M \mathsf{t}_3^M}{\mathsf{t}_2^M + \mathsf{t}_3^M})$. The probability $F(\overline{X}_1, \overline{Y}_1^1, \ldots, \overline{Y}_1^M, \mathrm{T_h})$ can be lower bounded as

$$\begin{aligned}
&F(\overline{X}_1, \overline{Y}_1^1, \ldots, \overline{Y}_1^M, \mathrm{T_h}) = \text{Prob}\left(X_1 + Y_1^1 + \cdots + Y_1^M < \mathrm{T_h}\right) \\
&\geq \text{Prob}\left(\max\left[\overline{X}_1, \overline{Y}_1^1, \ldots, \overline{Y}_1^M\right] \times \left(\frac{X_1}{\overline{X}_1} + \frac{Y_1^1}{\overline{Y}_1^1} + \cdots + \frac{Y_1^M}{\overline{Y}_1^M}\right) < \mathrm{T_h}\right) \\
&= \text{Prob}\left(\frac{X_1}{\overline{X}_1} + \frac{Y_1^1}{\overline{Y}_1^1} + \cdots + \frac{Y_1^M}{\overline{Y}_1^M} < \frac{\mathrm{T_h}}{2\mathsf{t}_{\max}\overline{\gamma}}\right).
\end{aligned} \tag{4.41}$$

Observe that the r.vs $X_1/\overline{X}_1, Y_1^1/\overline{Y}_1^1, \ldots, Y_1^M/\overline{Y}_1^M$ are i.i.d. r.vs each with unity mean. That is, the sum $\frac{X_1}{\overline{X}_1} + \sum_{j=1}^{M} \frac{Y_1^j}{\overline{Y}_1^j}$ is Gamma distributed [57]. As a result, (4.41) simplifies

to [57]

$$\begin{aligned} F(\overline{X}_1, \overline{Y}_1^1, \ldots, \overline{Y}_1^M, \mathrm{T_h}) &\geq \int_{x=0}^{\frac{\mathrm{T_h}}{2\mathsf{t}_{\max}\overline{\gamma}}} \frac{e^{-x}x^M}{\Gamma(M+1)}dx \\ &= 1 - e^{-\frac{\mathrm{T_h}}{2\mathsf{t}_{\max}\overline{\gamma}}} \sum_{j=0}^{M} \frac{1}{j!}\left(\frac{\mathrm{T_h}}{2\mathsf{t}_{\max}\overline{\gamma}}\right)^j \\ &\geq \frac{(M+1)^{M+1}}{(2\mathsf{t}_{\max})^{M+1}(M+1)!}\left(\frac{\log(\overline{\gamma})}{\overline{\gamma}}\right)^{M+1} (\overline{\gamma} \to \infty). \quad (4.42) \end{aligned}$$

Combining (4.42) with (4.40), we have

$$\begin{aligned} \overline{P}_{e,\text{On-Off}} &\geq \frac{(M+1)^M}{M!} \times \frac{(\log(\overline{\gamma}))^M}{2(\overline{\gamma})^{M+1}} + \frac{(M+1)^{M+1}}{2(2\mathsf{t}_1)^{M+1}(M+1)!}\left(\frac{\log(\overline{\gamma})}{\overline{\gamma}}\right)^{M+1} \\ &> \frac{(M+1)^{M+1}}{2(2\mathsf{t}_1)^{M+1}(M+1)!}\left(\frac{1}{\overline{\gamma}}\right)^{M+1} \qquad (\overline{\gamma} \to \infty). \quad (4.43) \end{aligned}$$

4.3.2 Binary FSK

By replacing $\exp(-x)$ in the integrals of (4.22) by $\delta(x-1)$, we can simplify the function $\mathcal{H}(\cdot,\cdot,\cdot,\cdot)$ to

$$\mathcal{H}\left(Z_{DR,1}^j, Z_{DR,2}^j, \overline{\gamma}_2^j, \overline{\gamma}_3^j\right) = \left(Z_{DR,1}^j - Z_{DR,2}^j\right) \frac{\overline{\gamma}_2^j \overline{\gamma}_3^j}{(1+\overline{\gamma}_3^j)(1+\overline{\gamma}_2^j+\overline{\gamma}_3^j)}. \quad (4.44)$$

With this, we can simplify $\mathrm{LLR}(b)$ of (4.23) to

$$\begin{aligned} \mathrm{LLR}(b) &= \left(\frac{\overline{\gamma}_1}{1+\overline{\gamma}_1}\right)[Z_{DS,1} - Z_{DS,2}] + \\ &\quad \sum_{j=1}^{M}\left(\frac{\overline{\gamma}_2^j\overline{\gamma}_3^j}{(1+\overline{\gamma}_3^j)(1+\overline{\gamma}_2^j+\overline{\gamma}_3^j)}\right)\left(Z_{DR,1}^j - Z_{DR,2}^j\right). \quad (4.45) \end{aligned}$$

An analysis of the average error rate for the detector of (4.45) can be performed as follows: Without loss of generality, we assume that the frequency f_1 is transmitted. Then $Z_{DS,1}$ is exponentially distributed with mean $1+\overline{\gamma}_1$, whereas $Z_{DS,2}$ is exponentially distributed

with mean 1. Similarly, $Z^j_{DR,1}$ is exponentially distributed with mean $1+\overline{\gamma}^j_3$, whereas $Z^j_{DR,2}$ is exponentially distributed with mean $1+\mu(\overline{\gamma}^j_2)\overline{\gamma}^j_3$. Also, note that $Z_{DS,1}, Z_{DS,2}$, $Z^j_{DR,1}$, $Z^j_{DR,2}$, $j=1,\ldots,M$, are independent r.vs. With this, we can define the following r.vs:

$$\begin{aligned} U_1 &= \frac{\overline{\gamma}_1}{1+\overline{\gamma}_1} Z_{DS,1} \\ U_{j+1} &= \left(\frac{\overline{\gamma}^j_2\overline{\gamma}^j_3}{(1+\overline{\gamma}^j_3)(1+\overline{\gamma}^j_2+\overline{\gamma}^j_3)}\right) Z^j_{DR,1} \qquad j=1,\ldots,M, \quad (4.46) \\ V_1 &= \frac{\overline{\gamma}_1}{1+\overline{\gamma}_1} Z_{DS,2} \\ \text{and} \qquad V_{j+1} &= \left(\frac{\overline{\gamma}^j_2\overline{\gamma}^j_3}{(1+\overline{\gamma}^j_3)(1+\overline{\gamma}^j_2+\overline{\gamma}^j_3)}\right) Z^j_{DR,2} \qquad j=1,\ldots,M. \quad (4.47) \end{aligned}$$

The r.vs of (4.46) and (4.47), respectively, have the following mean values:

$$\begin{aligned} \overline{U}_1 &= \overline{\gamma}_1 \quad (4.48) \\ \overline{U}_{j+1} &= \frac{\overline{\gamma}^j_2\overline{\gamma}^j_3}{1+\overline{\gamma}^j_2+\overline{\gamma}^j_3} \qquad j=1,\ldots,M, \quad (4.49) \\ \overline{V}_1 &= \frac{\overline{\gamma}_1}{1+\overline{\gamma}_1} = \frac{\overline{U}_1}{1+\overline{U}_1} \quad (4.50) \\ \text{and} \qquad \overline{V}_{j+1} &= \frac{\overline{\gamma}^j_2\overline{\gamma}^j_3}{(1+\overline{\gamma}^j_2)(1+\overline{\gamma}^j_3)} = \frac{\overline{U}_{j+1}}{1+\overline{U}_{j+1}} \qquad j=1,\ldots,M. \quad (4.51) \end{aligned}$$

The average BER is then given by

$$\overline{P}_{e,\text{BFSK}} = \text{Prob}\left(\sum_{j=1}^{M+1} U_j < \sum_{j=1}^{M+1} V_j\right) = \sum_{i=1}^{M+1}\sum_{j=1}^{M+1} \kappa_i\zeta_j \left(\frac{\overline{V}_i}{\overline{V}_i+\overline{U}_j}\right), \quad (4.52)$$

where the details of (4.52) can be found in Appendix-D, and the ζ_j and κ_j of (4.52) are given by

$$\zeta_j = \prod_{i=1,i\neq j}^{M+1} \frac{\overline{U}_j}{\overline{U}_j-\overline{U}_i} \text{ and } \kappa_i = \prod_{j=1,j\neq i}^{M+1} \frac{\overline{V}_i}{\overline{V}_i-\overline{V}_j}. \quad (4.53)$$

We now consider the behavior of (4.52) at high SNR. With $\overline{\gamma}_1 = \mathsf{t}_1\overline{\gamma}$, and for $j = 1, \ldots, M$, $\overline{\gamma}_2^j = \mathsf{t}_2^j\overline{\gamma}$ and $\overline{\gamma}_3^j = \mathsf{t}_3^j\overline{\gamma}$, and upon letting $\overline{\gamma} \to \infty$, the mean values in (4.48)-(4.51) simplify to

$$\begin{aligned} \overline{U}_1 &= \mathsf{t}_1\overline{\gamma} && (4.54)\\ \overline{U}_{j+1} &= \frac{\mathsf{t}_2^j\mathsf{t}_3^j}{\mathsf{t}_2^j + \mathsf{t}_3^j}\overline{\gamma} \qquad j = 1, \ldots, M, && (4.55)\\ \overline{V}_1 &= 1 && (4.56)\\ \text{and} \qquad \overline{V}_{j+1} &= 1 \qquad j = 1, \ldots, M. && (4.57) \end{aligned}$$

Define $V = \sum_{j=1}^{M+1} V_j$. At high SNR, from (4.56) and (4.57), V is a sum of $M+1$ i.i.d. exponential random variables of unity mean, and hence V is Gamma distributed [57]. Using (4.54)-(4.57), the expression in (4.52) can be simplified as

$$\begin{aligned} \overline{P}_{e,\text{BFSK}} &= \text{Prob}\left(\sum_{j=1}^{M+1} U_j < V\right) \\ &\geq E\left[\text{Prob}\left(\max\left(\overline{U}_1, \ldots, \overline{U}_{M+1}\right) \times \left\{\sum_{j=1}^{M+1} \frac{U_j}{\overline{U}_j}\right\} < v\right) \Big| V = v\right]. \end{aligned} \quad (4.58)$$

Since $\max\left(\overline{U}_1, \ldots, \overline{U}_{M+1}\right) = \mathsf{t}_{\max}\overline{\gamma}$, and $\sum_{j=1}^{M+1} \frac{U_j}{\overline{U}_j}$ is again Gamma distributed, (4.58) can be simplified as

$$\begin{aligned} \overline{P}_{e,\text{BFSK}} &\geq \int_{v=0}^{\infty} dv \frac{e^{-v}v^M}{\Gamma(M)} \times \int_{u=0}^{\frac{v}{\mathsf{t}_{\max}\overline{\gamma}}} du \frac{e^{-u}u^M}{\Gamma(M+1)} \\ &= \int_{v=0}^{\infty} dv \frac{e^{-v}v^M}{\Gamma(M)} \times e^{-\frac{v}{\mathsf{t}_{\max}\overline{\gamma}}} \sum_{j=M+1}^{\infty} \frac{1}{j!}\left(\frac{v}{\mathsf{t}_{\max}\overline{\gamma}}\right)^j \\ &= \frac{1}{\Gamma(M+1)} \sum_{j=M+1}^{\infty} \frac{1}{j!} \frac{1}{(\mathsf{t}_{\max}\overline{\gamma})^j} \times \frac{\Gamma(M+j+1)}{(1+\frac{1}{\mathsf{t}_{\max}\overline{\gamma}})^{M+j+1}} \\ &\geq \frac{(2M+1)!}{M!(M+1)!}\left(\frac{1}{\mathsf{t}_{\max}\overline{\gamma}}\right)^{M+1} \qquad (\overline{\gamma} \to \infty). \end{aligned} \quad (4.59)$$

4.4 Upper Bounds on the Average BER

In this section, we present upper bounds on the average BER for both OOK and BFSK signals on noncoherent relay channels. To accomplish this task, we use the likelihood functions of the transmitted bits along with the Bhattacharyya bound. The Bhattacharyya upper bound on the probability of error in discriminating two hypotheses, H_0 and H_1, is given by [29]

$$\overline{P}_b \leq \int_{z=-\infty}^{\infty} \sqrt{f_{\mathrm{H}_1}(z) f_{\mathrm{H}_0}(z)} dz, \tag{4.60}$$

where $f_{\mathrm{H}_j}(z)$ is the likelihood function for the hypothesis H_j, $j \in \{0, 1\}$.

For OOK, when the signal is present, the conditional density function, f_{H_1}, takes the form of $f_{Z_{DS}, Z_{DR}^1, \ldots, Z_{DR}^M | X=\sqrt{2E_s}}$, whereas f_{H_0}, when the signal is absent, takes the form of $f_{Z_{DS}, Z_{DR}^1, \ldots, Z_{DR}^M | X=0}$. Since $f_{Z_{DS}, Z_{DR}^1, \ldots, Z_{DR}^M | X=\sqrt{2E_s}} = f_{Z_{DS}|X=\sqrt{2E_s}} \times \prod_{j=1}^{M} f_{Z_{DR}^j | X=\sqrt{2E_s}}$ and $f_{Z_{DS}, Z_{DR}^1, \ldots, Z_{DR}^M | X=0} = f_{Z_{DS}|X=0} \times \prod_{j=1}^{M} f_{Z_{DR}^j | X=0}$, the integral in (4.60) can be expressed as

$$\begin{aligned} \overline{P}_{b,\mathrm{On-Off}} \leq & \int_{Z_{DS}=0}^{\infty} \sqrt{\frac{1}{1+2\overline{\gamma}_1} \exp\left(-\frac{Z_{DS}}{1+2\overline{\gamma}_1} - Z_{DS}\right)} dZ_{DS} \times \\ & \prod_{j=1}^{M} \int_{Z_{DR}^j=0}^{\infty} \sqrt{\mathsf{A}(Z_{DR}^j, 1, \lambda(\overline{\gamma}_2^j)\overline{\gamma}_3^j) \mathsf{A}(Z_{DR}^j, 1, \mu(\overline{\gamma}_2^j)\overline{\gamma}_3^j)} dZ_{DR}^j, \end{aligned} \tag{4.61}$$

where

$$\begin{aligned} \mathsf{A}(Z, a, b) &= \int_{x=0}^{\infty} \frac{\exp(-ax)}{1+bx} \exp\left(-\frac{Z}{1+bx}\right) dx \\ &= \frac{1}{b} \int_{t=0}^{\infty} \frac{\exp(-at/b)}{1+t} \exp\left(-\frac{Z}{1+t}\right) dt \\ &= \frac{1}{b} \mathsf{A}(Z, a/b, 1). \end{aligned} \tag{4.62}$$

Except for the first term, which can be evaluated as $\sqrt{1+2\overline{\gamma}_1}/(1+\overline{\gamma}_1)$, (4.61) does not appear to have a closed-from. As a result, one must resort to numerical integration. At high SNR, using (4.36)-(4.39), the functions $\mathsf{A}(Z_{DR}^j, 1, \lambda(\overline{\gamma}_2^j)\overline{\gamma}_3^j)$ and $\mathsf{A}(Z_{DR}^j, 1, \mu(\overline{\gamma}_2^j)\overline{\gamma}_3^j)$ in the jth integral of the product of (4.61) can be approximated as

$$\begin{aligned} \mathsf{A}(Z_{DR}^j, 1, \lambda(\overline{\gamma}_2^j)\overline{\gamma}_3^j) &\approx \frac{1}{2\overline{\gamma}_3^j}\mathsf{A}\left(Z_{DR}^j, \frac{1}{2\overline{\gamma}_3^j}, 1\right) \\ &\approx \frac{1}{2\mathsf{t}_3^j\overline{\gamma}}\mathsf{A}\left(Z_{DR}^j, 0, 1\right) \qquad (4.63) \\ \text{and} \quad \mathsf{A}(Z_{DR}^j, 1, \mu(\overline{\gamma}_2^j)\overline{\gamma}_3^j) &\approx \mathsf{A}\left(Z_{DR}^j, 1, \frac{\mathsf{t}_3^j}{\mathsf{t}_2^j}\right). \qquad (4.64) \end{aligned}$$

The first term of (4.61), $\sqrt{1+2\overline{\gamma}_1}/(1+\overline{\gamma}_1)$, at high SNR, can be approximated as $\sqrt{2/\overline{\gamma}_1} = \sqrt{2/\mathsf{t}_1}/\sqrt{\overline{\gamma}}$. Using this, along with (4.63) and (4.64), the high SNR version of (4.61) can be written as

$$\begin{aligned} \overline{P}_{b,\mathrm{On-Off}} &\leq \frac{1}{\sqrt{\overline{\gamma}}}\sqrt{\frac{2}{\mathsf{t}_1}} \times \\ &\quad \prod_{j=1}^{M} \frac{1}{\sqrt{2\mathsf{t}_3^j\overline{\gamma}}} \int_{Z_{DR}^j=0}^{\infty} \sqrt{\mathsf{A}\left(Z_{DR}^j, 0, 1\right)\mathsf{A}\left(Z_{DR}^j, 1, \frac{\mathsf{t}_3^j}{\mathsf{t}_2^j}\right)}\, dZ_{DR}^j \\ &= \frac{1}{(\overline{\gamma})^{\frac{M+1}{2}}} \times \left[\sqrt{\frac{2}{\mathsf{t}_1}} \times \right. \\ &\quad \left. \prod_{j=1}^{M} \frac{1}{\sqrt{2\mathsf{t}_3^j}} \int_{Z_{DR}^j=0}^{\infty} \sqrt{\mathsf{A}\left(Z_{DR}^j, 0, 1\right)\mathsf{A}\left(Z_{DR}^j, 1, \frac{\mathsf{t}_3^j}{\mathsf{t}_2^j}\right)}\, dZ_{DR}^j\right]. \qquad (4.65) \end{aligned}$$

Note that the term in square brackets of (4.65) is not a function of $\overline{\gamma}$.

For the case of BFSK, the Bhattacharyya bound, analogous to (4.61), can be written as

$$\overline{P}_{b,\mathrm{BFSK}} \leq \int_0^{\infty}\int_0^{\infty} \sqrt{\frac{1}{(1+\overline{\gamma}_1)^2}\exp\left(-[Z_{DS,1}+Z_{DS,2}]\frac{(2+\overline{\gamma}_1)}{(1+\overline{\gamma}_1)}\right)} \times$$

$$dZ_{DS,1}\, dZ_{DS,2} \times$$
$$\prod_{j=1}^{M} \int_0^{\infty} \int_0^{\infty} \sqrt{\Psi(Z^j_{DR,1}, Z^j_{DR,2}, \overline{\gamma}^j_2, \overline{\gamma}^j_3)\Psi(Z^j_{DR,2}, Z^j_{DR,1}, \overline{\gamma}^j_2, \overline{\gamma}^j_3)} \times$$
$$dZ^j_{DR,1}\, dZ^j_{DR,2}, \tag{4.66}$$

where the function $\Psi(\cdot,\cdot,\cdot,\cdot)$ is given in (4.22). Only the first term in (4.66) has a closed-form solution, and is given by $4(1+\overline{\gamma}_1)/(2+\overline{\gamma}_1)^2$. However, similar to (4.61), (4.66) must be evaluated numerically. At high SNR, the first term $4(1+\overline{\gamma}_1)/(2+\overline{\gamma}_1)^2$ in (4.66) behaves as $\frac{4}{\mathsf{t}_1\overline{\gamma}}$, and the functions $\Psi(Z^j_{DR,1}, Z^j_{DR,2}, \overline{\gamma}^j_2, \overline{\gamma}^j_3)$ and $\Psi(Z^j_{DR,2}, Z^j_{DR,1}, \overline{\gamma}^j_2, \overline{\gamma}^j_3)$, with the help of (4.22) and (4.36)-(4.39), can be simplified to

$$\begin{aligned} \Psi(Z^j_{DR,1}, Z^j_{DR,2}, \overline{\gamma}^j_2, \overline{\gamma}^j_3) &\approx \frac{1}{\mathsf{t}^j_3\overline{\gamma}} \int_{u=0}^{\infty} \frac{e^{-Z^j_{DR,1} - \frac{Z^j_{DR,2}}{1+u}}}{1+u} du \\ &= \frac{1}{\mathsf{t}^j_3\overline{\gamma}} \Theta(Z^j_{DR,1}, Z^j_{DR,2}) \end{aligned} \tag{4.67}$$

$$\begin{aligned} \text{and } \Psi(Z^j_{DR,2}, Z^j_{DR,1}, \overline{\gamma}^j_2, \overline{\gamma}^j_3) &\approx \frac{1}{\mathsf{t}^j_3\overline{\gamma}} \int_{u=0}^{\infty} \frac{e^{-Z^j_{DR,2} - \frac{Z^j_{DR,1}}{1+u}}}{1+u} dt \\ &= \frac{1}{\mathsf{t}^j_3\overline{\gamma}} \Theta(Z^j_{DR,2}, Z^j_{DR,1}), \end{aligned} \tag{4.68}$$

where

$$\Theta(Z_1, Z_2) = \int_{t=0}^{\infty} \frac{e^{-Z_1 - \frac{Z_2}{1+t}}}{1+t} dt. \tag{4.69}$$

Using (4.67) and (4.68), (4.66) becomes

$$\begin{aligned} \overline{P}_{b,\mathrm{BFSK}} &\leq \frac{4}{\mathsf{t}_1\overline{\gamma}} \times \\ &\quad \prod_{j=1}^{M} \int_0^{\infty} \int_0^{\infty} \frac{1}{\mathsf{t}^j_3\overline{\gamma}} \sqrt{\Theta(Z^j_{DR,1}, Z^j_{DR,2})\Theta(Z^j_{DR,2}, Z^j_{DR,1})} dZ^j_{DR,1}\, dZ^j_{DR,2} \\ &= \frac{1}{(\overline{\gamma})^{M+1}} \times \left[\frac{4}{\mathsf{t}_1} \prod_{j=1}^{M} \frac{1}{\mathsf{t}^j_3} \times \right. \end{aligned}$$

$$\prod_{j=1}^{M} \int_{0}^{\infty} \int_{0}^{\infty} \sqrt{\Theta(Z_{DR,1}^{j}, Z_{DR,2}^{j})\Theta(Z_{DR,2}^{j}, Z_{DR,1}^{j})} dZ_{DR,1}^{j}\, dZ_{DR,2}^{j} \Bigg]. \quad (4.70)$$

Note that, in (4.70) the term in square brackets is not a function of $\overline{\gamma}$.

4.5 Suboptimum Receivers

In this section, we present easy to implement suboptimum receivers for both OOK and BFSK. For OOK, we propose the following detector:

$$\mathrm{LLR}(b)_{\text{Subopt}}\,(\text{OOK}) = c_1 Z_{DS} + \sum_{j=1}^{M} c_2^j Z_{DR}^j - \mathrm{T_h}, \quad (4.71)$$

where c_1, c_2^j, $j = 1, \ldots, M$, and $\mathrm{T_h}$ are given by (4.27), (4.28) and (4.29), respectively. It is to be noted that (4.71) is optimum only when the relay-to-destination link is unfaded. Performance analysis of (4.71) is carried out in Appendix-E.

For BFSK, we propose the following suboptimum receiver:

$$\begin{aligned} \mathrm{LLR}_{\text{Subopt}}(b) \;=\; & \left(\frac{\overline{\gamma}_1}{1+\overline{\gamma}_1}\right)[Z_{DS,1} - Z_{DS,2}] + \\ & \sum_{j=1}^{M} \left(\frac{\overline{\gamma}_2^j \overline{\gamma}_3^j}{(1+\overline{\gamma}_3^j)(1+\overline{\gamma}_2^j+\overline{\gamma}_3^j)}\right)\left(Z_{DR,1}^j - Z_{DR,2}^j\right). \end{aligned} \quad (4.72)$$

Again, (4.72) is optimal only when the relay-to-destination link is unfaded. In Appendix-F, we present an analysis on the performance of (4.72).

4.6 Asymptotic Diversity Order Analysis

In this section, we consider the use of the expression from [55] for the asymptotic diversity orders of the systems discussed in this chapter. As will be seen, it is unclear as to how much credence one should put on the results of this type of analysis. However, we

present them because similar results for other systems are prevalent in the literature (see, e.g., [53], [54]).

From [55], the asymptotic diversity order of a system with M relay nodes is taken as

$$\mathsf{d}_M \triangleq -\lim_{\overline{\gamma}\to\infty} \frac{\log \overline{P}_b^{(M)}(\overline{\gamma})}{\log(\overline{\gamma})}, \tag{4.73}$$

where $\overline{\gamma}$ is the average SNR, and $\overline{P}_b^{(M)}(\overline{\gamma})$ is the average BER for M-relay system with an SNR of $\overline{\gamma}$. The use of this expression yields the following results for the noncoherent relay channels discussed in Sections 4.3 and 4.4: Using the lower bound on the BER for OOK, (4.43), in (4.73) yields the following upper bound on the diversity order:

$$\mathsf{d}_{M,OOK} < M + 1, \tag{4.74}$$

Also, the upper bound on the BER of (4.65) yields the following lower bound on the diversity order:

$$\mathsf{d}_{M,OOK} \geq \frac{M+1}{2}. \tag{4.75}$$

Taken together, (4.74) and (4.75) show that OOK achieves a diversity order of at least $(M+1)/2$, but cannot achieve the full diversity of $M+1$. For BFSK, using the lower bound of (4.58) and the upper bound of (4.70), on the BER, in (4.73), we conclude that

$$\begin{aligned} \mathsf{d}_{M,BFSK} &\leq M+1, \\ \text{and} \qquad \mathsf{d}_{M,BFSK} &\geq M+1, \end{aligned} \tag{4.76}$$

respectively. That is, BFSK achieves a full diversity order of $M+1$. Furthermore, using (F.11) in (4.73), we conclude that the suboptimum BFSK receiver of (4.72) also achieves a full diversity of $M+1$ as $\overline{\gamma} \to \infty$. Note, in particular, that for a noncoherent OOK system without the relay, upon setting $M = 0$ in (4.74), the asymptotic diversity order is less than unity. This result seemingly makes no sense in the context of physical diversity,

and thus suggests that the conclusions drawn from the use of the above expressions should be viewed with at least some degree of skepticism.

4.7 Results and Discussion

We now present some numerical and simulation results to illustrate the performance of the receivers for OOK and BFSK signal sets that were derived in the previous sections. First, notice that for OOK modulation, the ML receiver at the destination has to compute two integrals per relay node, as given by $\mathcal{G}(\cdot,\cdot,\cdot)$ of Eqn. (4.14), totaling $2M$ integrals for the M-relay channel. For BFSK, from Eqn. (4.24), the number of required integral computations is also $2M$. In order to reduce this computational complexity, we would like to approximate these integrals. Fortunately, each integral in Eqns. (4.14) and (4.24) is of the form $\int_0^\infty \exp(-x)h(x)dx$, which can be approximated with high accuracy using the Gauss-Laguerre quadrature (GLQ) rule [58] as $\sum_{n=1}^{N} w_n h(x_n)$, where $\{x_1,\ldots,x_N\}$ is a set of abscissae, and $\{w_1,\ldots,w_N\}$ is a set of weighting coefficients. Throughout this section, unless otherwise stated, we assume the following: $i)M = 1$ relay node placed on the path from the source to the destination, at a distance d_{RS} from the source, $ii)$the distance d_{DS} between the source and the destination is set to unity, whereas the location of the relay is varied, and $iii)$the path loss exponent δ is set to 4. If $\overline{\gamma}$ denotes the average received SNR for a system without the relay, then we have $\overline{\gamma}_1 = 0.5\overline{\gamma}$, $\overline{\gamma}_2^1 = 0.5\overline{\gamma}d_{RS}^{-\delta}$, and $\overline{\gamma}_3^1 = 0.5\overline{\gamma}d_{DR}^{-\delta}$, where $d_{DR} = d_{DS} - d_{RS}$. Here, the factor 0.5 is chosen to ensure that the total transmit power of the source plus the relay is equal to the source transmit power without the relay.

Fig. 4.4 plots the exact and the GLQ-based approximate LLR with $N = 5$ points for a run of 100 randomly generated information bits with $\overline{\gamma} = 10$ dB. From Fig. 4.4, we conclude that even with a small number of points, the approximation-based LLR provides almost the same performance as that of the exact integral-based one, and the sign of the LLR is preserved, thus maintaining the detection accuracy. Negligible performance im-

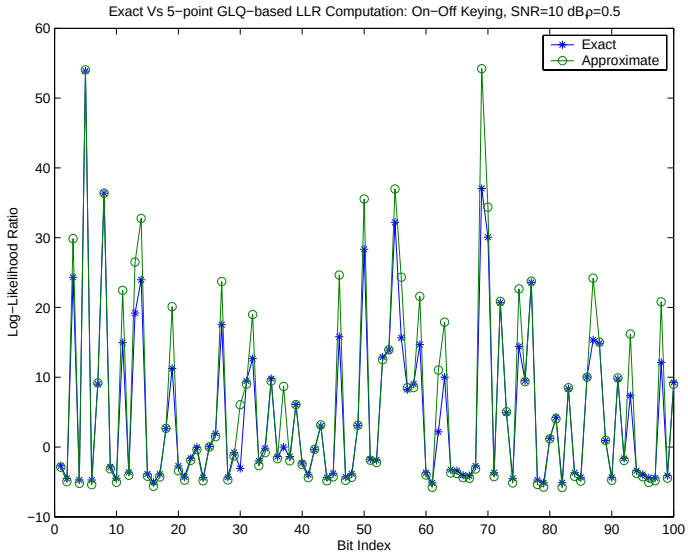

Figure 4.4 *Comparison of the exact and the GLQ-based log-likelihood ratio computation for noncoherent OOK modulation.* $\rho = d_{RS}$.

provement is observed (not shown in Fig. 4.4) by increasing N. However, for guaranteed accuracy, in all the subsequent plots we show the results with $N = 100$.

Fig. 4.5 shows the average BER of the optimum OOK receiver of Eqn. (4.12) as a function of $\overline{\gamma}$. Three scenarios of the relay placement are considered: 1)relay is closer to the source than to the destination, with $d_{RS} = 0.1$, 2)relay is closer to the destination than to the source, with $d_{RS} = 0.9$, and 3)relay at the midpoint between the source and the destination with $d_{RS} = 0.5$. Also shown is the average BER for single-hop transmission, which is obtained analytically by evaluating Eqn. (4.30) with $M = 0$, and the BER performance obtained by using the suboptimum detector of Eqn. (4.71). From Fig. 4.5, we observe that placement of the relay at the midpoint uniformly minimizes the average BER, whereas relay placement close to the destination results in worse BER performance. In fact, at lower values of $\overline{\gamma}$, single-hop transmission performs slightly better than the case with $d_{RS} = 0.9$, which can be attributed to an increase in the noise amplification at the relay, power split between the source and the relay, and, consequently, a reduction in the average SNR at the destination. Compared with single-hop performance, as $\overline{\gamma}$ increases,

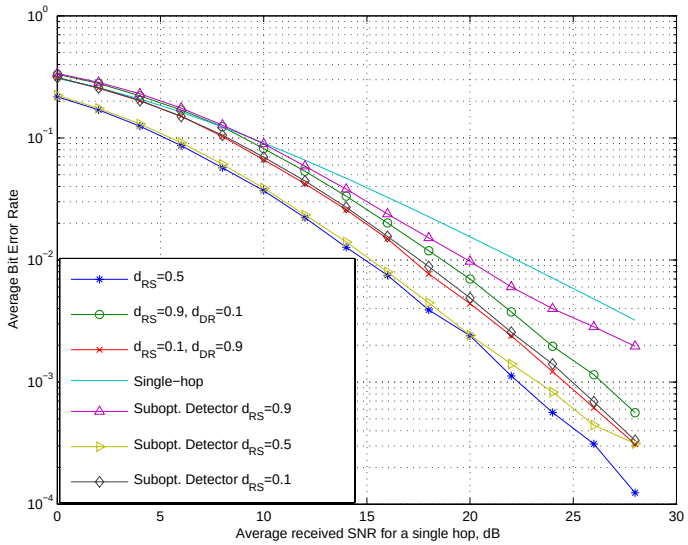

Figure 4.5 *Average probability of error for OOK modulation with noncoherent demodulation. Three cases of relay placements are considered:* a*)Relay close to the source,* b*)relay at the midpoint between the source and the destination, and* c*)relay close to the destination. Also shown is the analytical error probability performance of a system with no relay and the performance with the suboptimum detector of Eqn. (4.71).*

we notice from Fig. 4.5 an improved performance with a single relay node. We also conclude from Fig. 4.5 that the suboptimum detector performs reasonably well, compared with the ML NCAF receiver, when the relay is close to the source. This can be explained by the fact that noise amplification at the relay is less severe when the relay is close to the source.

The average BER for the optimum BFSK receiver of Eqn. (4.23) is plotted in Fig. 4.6 as a function of $\overline{\gamma}$. The placement of the relay is the same as that of Fig. 4.5. The suboptimum receiver as given in (4.72) is also considered. The following observations can be made from Fig. 4.6. First, with optimum reception, BER performance with $\rho = 0.5$ is uniformly better than with $\rho = 0.1$ and 0.9, which is due to the fact that, with $\rho = 0.5$, the noise amplification at the relay is roughly balanced by the strong signal from the relay to the destination. The suboptimum receiver of (4.71) has identical performance to that of the optimum one (over the plotted range of SNR values) at $\rho = 0.1$ and performs very close to the optimum one at $\rho = 0.5$, whereas its performance is inferior to the

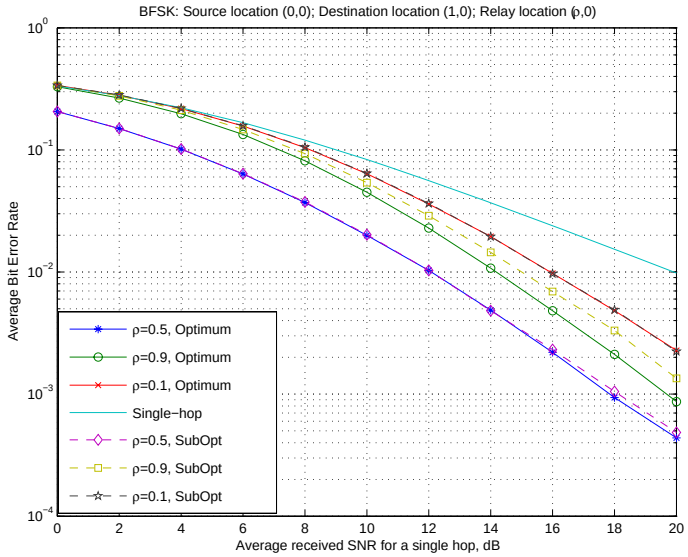

Figure 4.6 *Average probability of error for FSK modulation with noncoherent demodulation. Three cases of relay placements are considered: a)Relay close to the source, b)relay at the midpoint between the source and the destination, and c)relay close to the destination. Also shown is the analytical error probability performance of a system with no relay and the performance achieved by the suboptimum detector of Eqn. (4.72).*

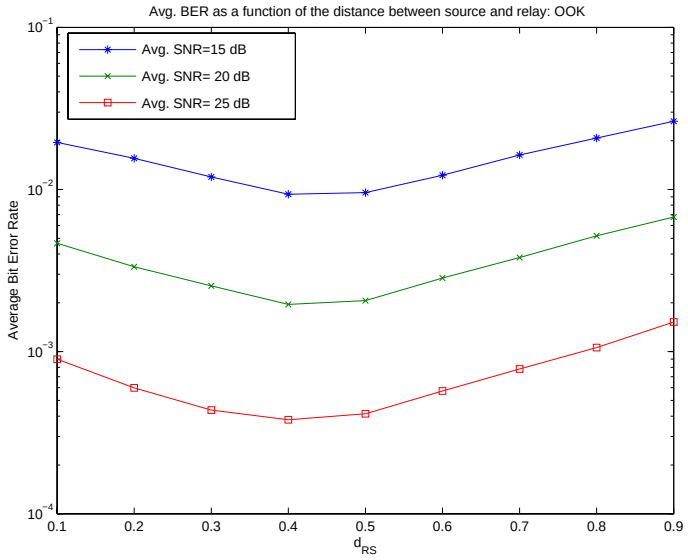

Figure 4.7 *Average probability of error for OOK modulation with noncoherent demodulation, as a function of the normalized distance between the source and the relay. It is assumed that the source and the destination are separated by unit distance.*

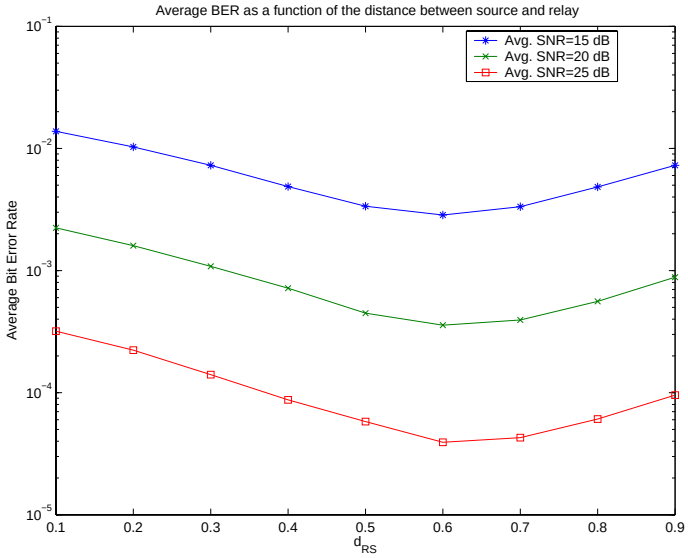

Figure 4.8 *Average probability of error for FSK modulation with noncoherent demodulation, as a function of the normalized distance between the source and the relay. It is assumed that the source and the destination are separated by unit distance.*

optimum one at $\rho = 0.9$. We conjecture that, for relay placement closer to the destination than to the source, the suboptimum receiver suffers from more noise amplication than the optimum one. Also, notice from Fig. 4.6 that, over the range of the plotted average SNR, $\overline{\gamma}$, performance with the relay is uniformly better than the single-hop transmission. We also study the effect of relay placement on the average BER performance. We choose $\overline{\gamma} \in \{15, 20, 25\}$ dB, and vary d_{RS} from 0.1 to 0.9. The average BER curves for OOK and BFSK are plotted, as a function of d_{RS}, in Figs. 4.7 and 4.8, respectively. For both OOK and BFSK, relay placement in the vicinity of $d_{RS} = 0.5$ minimizes the average BER.

Finally, we present upper and lower bounds on the average BER performance of the NCAF receivers. Fig. 4.9 shows the average BER performance with OOK modulation. In Fig. 4.9, the upper bound is obtained by evaluating (4.61), whereas the lower bound is given by (4.30). Fig. 4.10 plots the average BER for BFSK using the upper bound of (4.66), and the lower bound of (4.52). The average BER is parameterized by $\rho = d_{RS} \in \{0.1, 0.5, 0.9\}$ in Fig. 4.9, and by $\rho \in \{0.2, 0.5, 0.8\}$ in Fig. 4.10. The lower bounds in Figs. 4.9 and 4.10 show that the placement of relay at the midpoint between the source

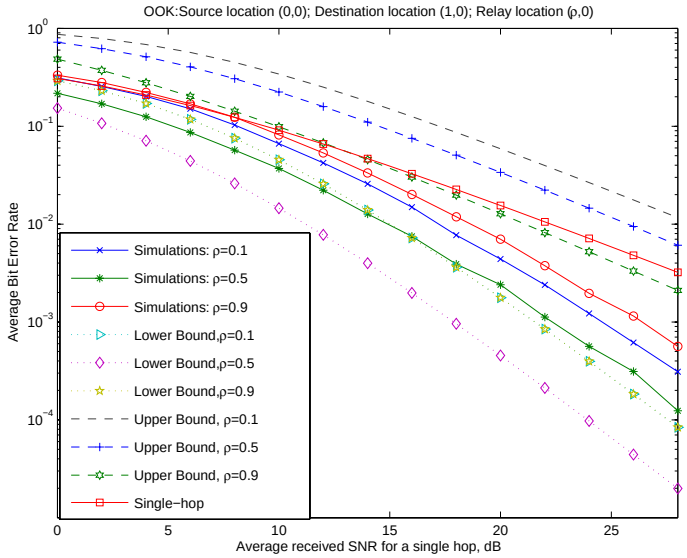

Figure 4.9 *Comparison of the average BER for OOK modulation with noncoherent demodulation. The plots with legend "Upper Bound" correspond to Bhattacharyya distance between the likelihood functions, whereas the plots with legend "Lower Bound" correspond to the assumption that the link between the relay and the destination is unfaded. The plots with legend "Simulations" are essentially the same as that of the simulation results of Fig. 4.5.*

and the destination is optimal, whereas relay placement close to the source yields the same performance as that of placement close to the destination. This can be explained with the observation that (4.30) and (4.52) are symmetric with respect to $\overline{\gamma}_2^j$ and $\overline{\gamma}_3^j$. That is, by exchanging $\overline{\gamma}_2^j$ and $\overline{\gamma}_3^j$, the resulting average BER does not change. For OOK, the upper bounds in Fig. 4.9 indicate that single-hop transmission has better performance over the relay-based one when $\rho \in \{0.1, 0.5\}$, whereas with BFSK Fig. 4.10 shows that, at high SNR, the relay-based system performs better than the single-hop system.

4.8 Conclusion

We have presented ML receiver structures for noncoherent amplify-and-forward communication when multiple relay nodes are employed. We considered both OOK and BFSK modulation schemes on Rayleigh fading channels with no receiver CSI. It was

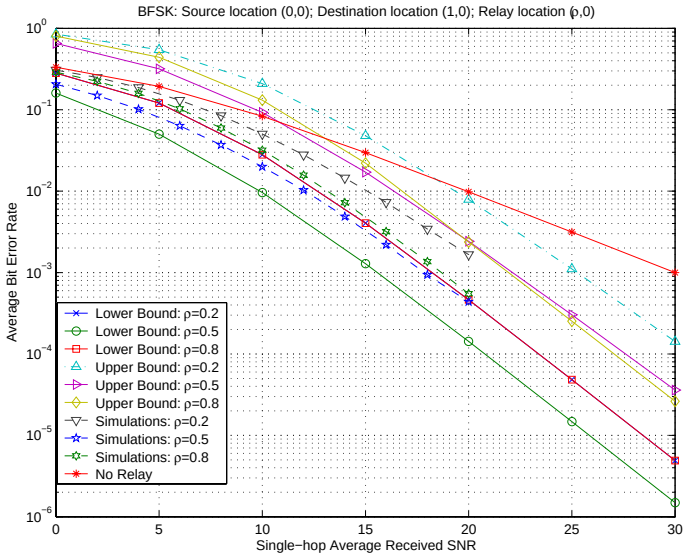

Figure 4.10 *Comparison of the average BER for BFSK modulation with noncoherent demodulation. The plots with legend "Upper Bound" correspond to Bhattacharyya distance between the likelihood functions, whereas the plots with legend "Lower Bound" correspond to the assumption that the link between the relay and the destination is unfaded.*

observed that, even for the simplest case of having only one relay node, the optimum noncoherent receiver is quite involved, and the ML metric computation requires evaluation of certain integrals. Next, we presented lower and upper bounds on the average BER, and also proposed simple suboptimum receivers along with their performance evaluation. Our asymptotic diversity analysis showed that, with M relay nodes, and a link between the source and the destination, OOK achieves a diversity order of atleast $(M+1)/2$, whereas BFSK achieves the full diversity of $M+1$.

CHAPTER 5

Transmit Power Allocation in a Parallel Relay Network

5.1 Introduction

The lifetime [59] of a wireless ad hoc network crucially depends on how efficiently the transmission power is utilized [60]. Conservation of transmit power not only increases the network lifetime, but also reduces undesirable interference to the other nodes in the network, thereby improving the communication reliability as well. This chapter is concerned with optimizing the reliability performance of a power constrained cooperative network with various relaying protocols. With receiver CSI (or CSIR) alone, we consider the decode-and-forward and distributed space-time coded (DSTC) protocols of [61], and the amplify-and-forward protocol of [48] and [56].

Numerous works have shown that with perfect CSI at both the transmitters and the receivers (denoted by CSI-TR), the relay channel performance can be improved significantly through optimal transmit power allocation. In [62], subject to short term power constraint, the authors presented an information theoretic study of the channel capacity as well as the outage probability of wireless relay channels with perfect CSI-TR. Outage behavior of various relaying protocols with optimal power control and CSI-TR is investigated in [63]. In [64], subject to individual long term power constraints on the source and the relay, Liang and Veeravalli consider transmitter power allocation on a Gaussian relay channel with perfect CSI-TR. With an average total energy constraint, Larsson and

Cao in [65] consider the possibility of adapting not only the transmission power but also the time slot and bandwidth allocation for the source and the relay. In [66], the authors report the impact of relay gain allocation on the performance of an AF protocol. Adaptive transmit power allocation schemes are proposed in [67] and [68] for maximizing the instantaneous capacity of a two-hop Rayleigh fading relay channel. In [67], a regenerative (i.e., the relay decodes and then re-encodes the source bits) system is analyzed, whereas the performance of a non-regenerative system is considered in [68]. With an Alamouti space-time block code (STBC) [69], adaptive transmit power allocation based on perfect CSIT is investigated in [70].

While the above works assume that perfect CSI is available at the transmitters for optimum power allocation, power allocation can still be performed even when perfect CSIT is not available (which, for example, is true on a fast varying fading channel), provided some statistical knowledge of the channel gains is available to the transmitting nodes. With the knowledge of the mean channel power gains (or simply, mean channel gains) alone, this idea is explored in [71] in the context of a multihop diversity system, whereas the authors in [72] investigate the optimal power allocation problem for a transmit diversity system. Recently, [73] presented both SNR maximizing and outage probability minimizing optimal power allocation schemes with the knowledge of the mean channel gains. However, the main limitations of [73] are that the results are valid for only AF protocol with a single relay node. The coding gain of AF and DF protocols, with equal power allocation, is computed in [74], wherein it is shown that when the average channel gain between the source and the relay is smaller than the average channel gain between the relay and the destination, the DF protocol is inferior to the AF protocol, in terms of the asymptotic coding gain (ACG) [75].

In this chapter, building upon the equal power allocation-based information theoretic results presented in [61] and [56], we study the optimal transmit power allocation problem for AF, DF and DSTC protocols with multiple relay nodes. Similar to [71],[72], and [73], we assume that only knowledge of the mean channel gains is known to the nodes in

the network, which can easily be realized with a low-rate feedback for a slowly varying network topology, and obtain the optimum transmit power vector that minimizes the outage probability of mutual information (or simply, outage probability) at the destination. We show that, at high SNR, the outage probability expressions for various protocols are convex functions of the transmit power vector, and the optimal power allocation depends on whether or not a direct link exists between the source and the destination. Additionally, for AF and DF protocols, this allocation depends only on the ratio of the mean channel gains (i.e., the ratio of the source-to-relay channel gain to the relay-to-destination channel gain), whereas with a DSTC protocol with a direct link this allocation also depends on the transmission rate. Interestingly, our results without a direct link show that both the DF and DSTC protocols have identical optimal power vector and identical asymptotic coding gain ratio (CGR, i.e., the ratio of the ACG with optimal power allocation to the ACG with equal power allocation). Our analysis reveals that, in addition to the outage probability improvements, optimal power allocation also brings impressive coding gains over equal power allocation. Furthermore, with a single relay, our results show that optimal power allocation can also reduce the ACG gap between the DF and AF protocols. While our optimization is performed with a sum power constraint, our results can be modified to account for a per-node maximum power constraint by simply clipping the excess power of a given node, and reallocating the remaining power to the nodes satisfying the constraints in an optimal manner [71].

The rest of this chapter is organized as follows. In Section 5.2, we describe the system and the channel model. High SNR approximations for the outage probabilities expressions with AF, DF and DSTC protocols are developed, and validated through simulations, in Section 5.3. We formulate the optimum power allocation problem in Section 5.4, and derive the optimum power allocation vector for AF, DF and DSTC protocols. The coding gain improvements with power allocation are presented in Section 5.5. We provide numerical results and discussions in Section 5.6, and conclude our work in Section 5.7.

5.2 System Model

We assume a single source communicating with a single destination with the help of M relay nodes. The channels between all the nodes are assumed to be random, independent, frequency-flat, and constant over the signaling duration. We employ low-pass equivalent complex-valued representation for the transmit and receive signals, for the channel gains and for background additive noise. Specifically, the channel gain between the source and the destination is denoted by g_1, which is assumed to be a zero-mean, circularly symmetric, complex Gaussian r.v with variance $E[|g_1|^2] = \Omega_1$. In a similar fashion, for the jth relay, the gain from the source to the relay is denoted by g_2^j, and the gain from the relay to the destination by g_3^j, with variances $E[|g_2^j|^2] = \Omega_2^j$ and $E[|g_3^j|^2] = \Omega_3^j$. The noise r.v on each link is assumed to be zero-mean, independent, additive, and Gaussian distributed. In this chapter, we consider three relaying protocols, namely $a)$ amplify-and-forward, $b)$ decode-and-forward, and $c)$ distributed space-time coded protocols. The description of these protocols can be found in [61] and [56]. While [61] and [56], in their mutual information (MI) analysis, always assume the existence of a direct link between the source and destination, in this chapter we separately analyze the two systems with/without a direct link. When there is no direct link (NDL) between the source and the destination, which is true, for example, when there is an obstruction on the source-destination path, mathematically, we set $\Omega_1 = 0$ for all the analysis with NDL. On the other hand, when there exists a direct link (DL) between the source and the destination Ω_1 is non-zero. The total bandwidth available for the source transmission without cooperation is denoted by W. Similar to [61] and [56], half-duplex constraints are imposed on the relay nodes (i.e., the relays cannot transmit and receive simultaneously). With repetition-based AF and DF protocols, we assume that the total bandwidth is divided into $M + 1$ equi-width, disjoint channels, so that the bandwidth available for the source and for each one of the M relay nodes is $W/(M + 1)$. Throughout this chapter, the transmission rate of the source, $\tilde{R}$, is normalized by the bandwidth, W. That is, $R = \tilde{R}/W$. In a similar way, the MI is also

normalized by W. Let us denote by $\tilde{P}_s$ the average transmit power of the source, and by $\tilde{P}_{r,j}$ the average transmit power of the jth relay. The single-sided power spectral density of the additive Gaussian noise is denoted by N_0, so that noise power in a bandwidth W is $\sigma_N^2 = N_0 W$.

We assume that the transmitted baseband samples of the nodes are independent Gaussian distributed r.vs with zero-mean and variance equal to the respective average transmit power. When the source transmits at a power level of $\tilde{P}_s$, the instantaneous SNR at the destination is $\tilde{P}_s|g_1|^2/(N_0W/(M+1)) = (M+1)\tilde{P}_s|g_1|^2/\sigma_N^2$, which is denoted by γ_1. In a similar manner, the instantaneous received SNR at the jth relay from the source is denoted by γ_2^j, which is given by $\gamma_2^j = (M+1)\tilde{P}_s|g_2^j|^2/\sigma_N^2$. When the relays transmit their respective signals to the destination, the SNR at the destination from the jth relay is $\gamma_3^j = (M+1)\tilde{P}_{r,j}|g_3^j|^2/\sigma_N^2$. Let us define $P_s = (M+1)\tilde{P}_s$, and, for $j = 1, \ldots, M$, $P_{r,j} = (M+1)\tilde{P}_{r,j}$; also, we denote by $\underline{P} = [P_s, P_{r,1}, \ldots, P_{r,M}]$, the transmit power vector. Finally, we define the following variables: $\overline{\gamma}_1 \stackrel{\triangle}{=} E[\gamma_1] = P_s\Omega_1/\sigma_N^2$, and for $j = 1, \ldots, M$, $\overline{\gamma}_2^j \stackrel{\triangle}{=} E[\gamma_2^j] = P_s\Omega_2^j/\sigma_N^2$ and $\overline{\gamma}_3^j \stackrel{\triangle}{=} E[\gamma_3^j] = P_{r,j}\Omega_3^j/\sigma_N^2$.

5.3 High SNR Outage Analysis

In this section we develop high SNR approximations for the outage probability of MI with AF, DF and DSTC protocols, which is defined as the probability that the instantaneous MI at the destination falls below a target rate of R [76].

5.3.1 AF Protocol

With the AF protocol, assuming a direct link between the source and the destination, the output SNR at the destination, with maximal ratio combining, is [50],[51]

$$\gamma_{AF,DL} = \gamma_1 + \sum_{j=1}^{M} \frac{\gamma_2^j \gamma_3^j}{1 + \gamma_2^j + \gamma_3^j}.$$

The instantaneous MI at the destination can be written as

$$\begin{aligned} I_{AF,DL} &= \frac{1}{M+1}\log_2\left(1+\gamma_{AF,DL}\right) \\ &= \frac{1}{M+1}\log_2\left(1+\gamma_1+\sum_{j=1}^{M}\frac{\gamma_2^j\gamma_3^j}{1+\gamma_2^j+\gamma_3^j}\right). \end{aligned} \tag{5.1}$$

The fraction $1/(M+1)$ in (5.1) is due to the fact that the source uses only $1/(M+1)$ of the total bandwidth W. This outage probability with AF protocol, $P_{Out,AF,DL}(\underline{P})$, is given by

$$\begin{aligned} P_{Out,AF,DL}(\underline{P}) &= \text{Prob}(I_{AF,DL} < R) \\ &= \text{Prob}\left(\gamma_1+\sum_{j=1}^{M}\frac{\gamma_2^j\gamma_3^j}{1+\gamma_2^j+\gamma_3^j} < 2^{(M+1)R}-1\right). \end{aligned} \tag{5.2}$$

At high SNR, following the approach of [51], we can approximate (5.2) as[1]

$$\begin{aligned} P_{Out,AF,DL}(\underline{P}) &\approx \frac{\left[2^{(M+1)R}-1\right]^{M+1}}{(M+1)!}\frac{1}{\overline{\gamma}_1}\prod_{j=1}^{M}\left(\frac{1}{\overline{\gamma}_2^j}+\frac{1}{\overline{\gamma}_3^j}\right) \\ &= \frac{\left[(2^{(M+1)R}-1)\sigma_N^2\right]^{M+1}}{(M+1)!}\frac{1}{\Omega_1 P_s}\prod_{j=1}^{M}\left(\frac{1}{P_s\Omega_2^j}+\frac{1}{P_{r,j}\Omega_3^j}\right). \end{aligned} \tag{5.3}$$

Upon defining $\alpha_j = \Omega_2^j/\Omega_3^j$ and a constant $\mathsf{C}_{AF,DL} = \left[(2^{(M+1)R}-1)\sigma_N^2\right]^{M+1}/((M+1)!\Omega_1\prod_{j=1}^{M}\Omega_2^j)$, (5.3) simplifies to the following compact form:

$$P_{Out,AF,DL}(\underline{P}) \approx \mathsf{C}_{AF,DL}\frac{1}{P_s}\prod_{j=1}^{M}\left(\frac{1}{P_s}+\frac{\alpha_j}{P_{r,j}}\right). \tag{5.4}$$

In the absence of a direct link, since $\Omega_1 = 0$ the source to the destination SNR r.v γ_1 does not contribute to the MI expression of (5.1). As a result, analogous (5.3) and (5.4), we

[1]Note that the steps required to arrive at (5.3) are very similar to those in [51] and hence are skipped for brevity.

can write the outage probability as

$$P_{Out,AF,NDL}(\underline{P}) \approx \mathsf{C}_{AF,NDL} \prod_{j=1}^{M} \left(\frac{1}{P_s} + \frac{\alpha_j}{P_{r,j}} \right), \tag{5.5}$$

where $\mathsf{C}_{AF,NDL} = \left[(2^{(M+1)R} - 1)\sigma_N^2 \right]^M / (M! \prod_{j=1}^{M} \Omega_2^j)$.

5.3.2 DF Protocol

With a DF protocol, a relay is assumed to correctly decode the source transmission if the instantaneous MI is above the attempted transmission rate R. Assuming a direct link, the instantaneous SNR at the destination, conditioned on a set $\mathcal{D}$ of correctly decoded relays, is given by $\gamma_{DF,DL} = \gamma_1 + \sum_{j \in \mathcal{D}} \gamma_3^j$, where we assumed that the destination performs MRC of the received signals. The instantaneous MI at the destination, conditioned on $\mathcal{D}$, can be written as

$$I_{DF,DL}(\mathcal{D}) = \frac{1}{M+1} \log_2 \left(1 + \gamma_{DF,DL}\right) = \frac{1}{M+1} \log_2 \left(1 + \gamma_1 + \sum_{j \in \mathcal{D}} \gamma_3^j \right). \tag{5.6}$$

The outage probability at the destination can then be written as

$$\begin{aligned} P_{Out,DF,DL}(\underline{P}) &= \text{Prob}(I_{DF,DL} < R) \\ &= \sum_{\mathcal{D}} \text{Prob}(\mathcal{D}) \text{Prob}\left(I_{DF,DL} < R | \mathcal{D}\right) \\ &= \sum_{\mathcal{D}} \text{Prob}(\mathcal{D}) \text{Prob}\left(\gamma_1 + \sum_{j \in \mathcal{D}} \gamma_3^j < 2^{(M+1)R} - 1 \right). \end{aligned} \tag{5.7}$$

The probability of the decoding set, $\text{Prob}(\mathcal{D})$, is simply the probability that a subset $\mathcal{D}$ of relays correctly decodes the source signals. This event happens when all the relays in $\mathcal{D}$ have their conditional MI above the target rate R, and the relays outside $\mathcal{D}$ have their

conditional MI below the rate R. That is,

$$\begin{aligned}
\text{Prob}(\mathcal{D}) &= \left[\prod_{j\in\mathcal{D}} \text{Prob}\left(\frac{1}{M+1}\log_2(1+\gamma_2^j) > R\right)\right] \times \\
&\quad \prod_{k\notin\mathcal{D}} \text{Prob}\left(\frac{1}{M+1}\log_2(1+\gamma_2^k) < R\right) \\
&= \left[\prod_{j\in\mathcal{D}} e^{-\frac{2^{(M+1)R}-1}{\overline{\gamma}_2^j}}\right] \times \prod_{k\notin\mathcal{D}}\left(1-e^{-\frac{2^{(M+1)R}-1}{\overline{\gamma}_2^k}}\right) \\
&\approx \prod_{k\notin\mathcal{D}} \frac{2^{(M+1)R}-1}{\overline{\gamma}_2^k}, \qquad (5.8)
\end{aligned}$$

where the approximation in the last step of (5.8) is valid for high SNR, and is due to the fact that, for small x, $\exp(-x) \approx 1$ and $1-\exp(-x) \approx x$ [61], [56], [72], [75]. With the help of Appendix-G, the second term of (5.7) can be approximated as

$$\text{Prob}\left(\gamma_1 + \sum_{j\in\mathcal{D}} \gamma_3^j < 2^{(M+1)R}-1\right) \approx \frac{\left[2^{(M+1)R}-1\right]^{|\mathcal{D}|+1}}{(|\mathcal{D}|+1)!}\frac{1}{\overline{\gamma}_1}\prod_{j\in\mathcal{D}}\frac{1}{\overline{\gamma}_3^j}. \qquad (5.9)$$

Using (5.8) and (5.9) in (5.7), we arrive at the following high SNR approximation:

$$\begin{aligned}
P_{Out,DF,DL}(\underline{P}) &\approx \sum_{\mathcal{D}}\left[\prod_{k\notin\mathcal{D}}\frac{2^{(M+1)R}-1}{\overline{\gamma}_2^k}\right] \times \frac{\left[2^{(M+1)R}-1\right]^{|\mathcal{D}|+1}}{(|\mathcal{D}|+1)!}\frac{1}{\overline{\gamma}_1}\prod_{j\in\mathcal{D}}\frac{1}{\overline{\gamma}_3^j} \\
&= \mathsf{C}_{DF,DL}\sum_{\mathcal{D}}\frac{1}{(|\mathcal{D}|+1)!}\left(\frac{1}{P_s}\right)^{M+1-|\mathcal{D}|}\prod_{j\in\mathcal{D}}\frac{\alpha_j}{P_{r,j}}, \qquad (5.10)
\end{aligned}$$

where $\mathsf{C}_{DF,DL} = \left[(2^{(M+1)R}-1)\sigma_N^2\right]^{M+1}/(\Omega_1\prod_{j=1}^{M}\Omega_2^j)$. In the absence of a direct link, (5.10) can be modified as follows: First, the probability $\text{Prob}(\mathcal{D})$ in (5.8) is not related to the existence of a direct link, and hence it remains unchanged. However, since there is no direct link, the r.v γ_1 does not contribute to the outage expression of (5.9), and the

modified expression, with the help of Appendix-G, is

$$\text{Prob}\left(\sum_{j\in\mathcal{D}}\gamma_3^j < 2^{(M+1)R}-1\right) \approx \frac{\left[2^{(M+1)R}-1\right]^{|\mathcal{D}|}}{(|\mathcal{D}|)!}\prod_{j\in\mathcal{D}}\frac{1}{\overline{\gamma}_3^j}. \tag{5.11}$$

Using (5.8) and (5.11) in (5.7), and following the steps in (5.10) for the simplification, we arrive at

$$\begin{aligned} P_{Out,DF,NDL}(\underline{P}) &\approx \frac{\left[(2^{(M+1)R}-1)\sigma_N^2\right]^M}{\prod_{j=1}^M \Omega_2^j}\sum_{\mathcal{D}}\frac{1}{(|\mathcal{D}|)!}\left(\frac{1}{P_s}\right)^{M-|\mathcal{D}|}\prod_{j\in\mathcal{D}}\frac{\Omega_2^j}{\Omega_3^j P_{r,j}} \\ &= \mathsf{C}_{DF,NDL}\sum_{\mathcal{D}}\frac{1}{(|\mathcal{D}|)!}\left(\frac{1}{P_s}\right)^{M-|\mathcal{D}|}\prod_{j\in\mathcal{D}}\frac{\alpha_j}{P_{r,j}}, \end{aligned} \tag{5.12}$$

where $\mathsf{C}_{DF,NDL} = \left[(2^{(M+1)R}-1)\sigma_N^2\right]^M/(\prod_{j=1}^M \Omega_2^j)$.

5.3.3 Distributed STC Protocol

Let us now turn our attention to a DSTC protocol. With a DSTC protocol, the bandwidth is divided into two disjoint bands of width $W/2$ each. In the first phase of the protocol, the source transmits over a bandwidth of $W/2$. Each relay node independently attempts to decode the source transmission. In the event that multiple relay nodes able to successfully decode the source information, they collaborate their transmissions by forming a virtual orthogonal STBC[2] and simultaneously transmit over the remaining bandwidth of $W/2$. Practical issues such as construction of distributed STBCs, channel feedback requirements, and communication theoretic performances can be found, for example, in [77] and [78]. Compared with the repetition based AF/DF protocols, a DSTC protocol is bandwidth efficient by a factor of $(M+1)/2$. When a direct link exists, Laneman and Wornell [61] showed that a DSTC protocol achieves a full spatial diversity order

[2] Note that very low rate but highly reliable side channels are assumed to exist between the relays to communicate which nodes have successfully decoded, and to convey the choice of the space-time block code to be used.

equal to the total number of nodes (in our case, it is $M+1$). In the presence of a direct link, conditioned on the set of decoding nodes $\mathcal{D}$, the conditional MI at the destination with DSTC is

$$\begin{aligned} I_{DTSC,DL}(\mathcal{D}) &= \frac{1}{2}\log_2\left(1+\frac{\tilde{P}_s}{N_0W/2}|g_1|^2\right)+\frac{1}{2}\log_2\left(1+\sum_{j\in\mathcal{D}}\frac{\tilde{P}_{r,j}}{N_0W/2}|g_3^j|^2\right) \\ &= \frac{1}{2}\log_2\left(1+\frac{2}{M+1}\gamma_1\right)+\frac{1}{2}\log_2\left(1+\frac{2}{M+1}\sum_{j\in\mathcal{D}}\gamma_3^j\right), \end{aligned} \quad (5.13)$$

which is the sum of MIs of two independent parallel channels, the first one from the source to the destination, and the second one from the successfully decoded relays to the destination. Eqn. (5.13) is achievable when relays re-encode the decoded source information using independent code books, and when the all code books are available to the destination [25]. The factor $1/2$ in front of the logarithm in (5.13) is due to the fact that the nodes transmit in half of the available bandwidth.

In the absence of a direct link, (5.13) reduces to

$$I_{DTSC,NDL}(\mathcal{D}) = \frac{1}{2}\log_2\left(1+\frac{2}{M+1}\sum_{j\in\mathcal{D}}\gamma_3^j\right). \quad (5.14)$$

Similar to (5.7), the outage probability with DSTC is

$$\begin{aligned} P_{Out,DSTC,DL}(\underline{P}) &= \text{Prob}(I_{DSTC,DL}<R) \\ &= \sum_{\mathcal{D}}\text{Prob}(\mathcal{D})\text{Prob}\left(I_{DSTC,DL}<R|\mathcal{D}\right) \\ &= \sum_{\mathcal{D}}\text{Prob}(\mathcal{D})\times \\ &\quad \text{Prob}\left((1+\frac{2}{M+1}\gamma_1)\times(1+\frac{2}{M+1}\sum_{j\in\mathcal{D}}\gamma_3^j)<2^{2R}\right) \end{aligned} \quad (5.15)$$

with a direct link, and

$$P_{Out,DSTC,NDL}(\underline{P}) = \sum_{\mathcal{D}} \text{Prob}(\mathcal{D})\text{Prob}\left(\frac{2}{M+1}\sum_{j\in\mathcal{D}}\gamma_3^j < 2^{2R}-1\right) \tag{5.16}$$

without a direct link. Analogous to (5.8), the probability $\text{Prob}(\mathcal{D})$ is

$$\begin{aligned}\text{Prob}(\mathcal{D}) &= \left[\prod_{j\in\mathcal{D}}\text{Prob}\left(\frac{1}{2}\log_2(1+\frac{2}{M+1}\gamma_2^j) > R\right)\right]\times \\ &\quad \prod_{k\notin\mathcal{D}}\text{Prob}\left(\frac{1}{2}\log_2(1+\frac{2}{M+1}\gamma_2^k) < R\right) \\ &\approx \prod_{k\notin\mathcal{D}}\frac{(2^{2R}-1)(M+1)}{2\overline{\gamma}_2^k},\end{aligned} \tag{5.17}$$

whereas the second term of (5.15) can be approximated as[3].

$$\begin{aligned}&\text{Prob}\left((1+\frac{2}{M+1}\gamma_1)\times(1+\frac{2}{M+1}\sum_{j\in\mathcal{D}}\gamma_3^j) < 2^{2R}\right) \approx \\ &\left(\frac{(2^{2R}-1)(M+1)}{2}\right)^{|\mathcal{D}|+1}\times\mathcal{A}_{|\mathcal{D}|}(2^{2R}-1)\frac{1}{\overline{\gamma}_1}\prod_{j\in\mathcal{D}}\frac{1}{\overline{\gamma}_3^j},\end{aligned} \tag{5.18}$$

where

$$\mathcal{A}_n(t) = \frac{1}{(n-1)!}\int_{u=0}^{1}\frac{u^{n-1}(1-u)}{1+tu}du \qquad n>0, \tag{5.19}$$

and $\mathcal{A}_0(t) = 1$. Without a direct link, using (G.9) of Appendix-G, the second term of (5.16) approximately equals

$$\text{Prob}\left(\frac{2}{M+1}\sum_{j\in\mathcal{D}}\gamma_3^j < 2^{2R}-1\right) \approx \left(\frac{(2^{2R}-1)(M+1)}{2}\right)^{|\mathcal{D}|}\frac{1}{(|\mathcal{D}|)!}\prod_{j\in\mathcal{D}}\frac{1}{\overline{\gamma}_3^j}. \tag{5.20}$$

[3]Eqn. (5.18) can be obtained from [61] by setting the variables $\mathsf{SNR}=1$, $\lambda_{s,d(s)} = 1/\overline{\gamma}_1$, and $\lambda_{r,d(s)} = 1/\overline{\gamma}_3^r$ in [61, Eqn. (19)].

Plugging (5.17) and (5.18) in (5.15), we have

$$\begin{aligned} P_{Out,DSTC,DL}(\underline{P}) &\approx \left(\frac{(2^{2R}-1)(M+1)}{2}\right)^{M+1} \\ &\quad \sum_{\mathcal{D}} \mathcal{A}_{|\mathcal{D}|}(2^{2R}-1)\frac{1}{\overline{\gamma}_1}\left[\prod_{k\notin\mathcal{D}}\frac{1}{\overline{\gamma}_2^k}\right]\prod_{j\in\mathcal{D}}\frac{1}{\overline{\gamma}_3^j} \\ &= \mathsf{C}_{DSTC,DL}\sum_{\mathcal{D}}\mathcal{A}_{|\mathcal{D}|}(2^{2R}-1)\prod_{j\in\mathcal{D}}\frac{\alpha_j}{P_{r,j}}\left(\frac{1}{P_s}\right)^{M+1-|\mathcal{D}|}, \end{aligned} \quad (5.21)$$

where $\mathsf{C}_{DSTC,DL} = \left((2^{2R}-1)(M+1)\sigma_N^2/2\right)^{M+1}/(\Omega_1\prod_{j=1}^{M}\Omega_2^j)$. Using (5.17) and (5.20) in (5.16), the approximate outage probability without a direct link is

$$P_{Out,DSTC,NDL}(\underline{P}) \approx \mathsf{C}_{DSTC,NDL}\sum_{\mathcal{D}}\frac{1}{(|\mathcal{D}|)!}\left(\frac{1}{P_s}\right)^{M-|\mathcal{D}|}\prod_{j\in\mathcal{D}}\frac{\alpha_j}{P_{r,j}}, \quad (5.22)$$

where $\mathsf{C}_{DSTC,NDL} = \left((2^{2R}-1)(M+1)\sigma_N^2/2\right)^{M}/(\prod_{j=1}^{M}\Omega_2^j)$. It is worth noticing the similarity between (5.22) and (5.12), which can be explained by the fact that the same number, $|\mathcal{D}|$, of relay nodes are employed in both DF and DSTC protocols[4].

5.3.4 Accuracy of High SNR Outage Probability Approximations

We now compare the high SNR approximations of (5.4), (5.5), (5.10), (5.12), (5.21), and (5.22) against their respective exact outage expressions. One hundred million (10^8) channel realizations, for each SNR value, were simulated to evaluate the exact outage expressions. We used $M = 3$ relay nodes, both with and without a direct link between the source and the destination. Due to lack of consensus on the relay network topology, we assumed that the source, the destination, and the relay nodes were placed on a circle with radius $1/2$. The source was located at $(0,0)$, the destination at $(1,0)$, and the jth relay at $((1+\cos\theta_j)/2, (\sin\theta_j)/2)$, $j = 1,2,3$, with $\theta_1 = \pi/3$, $\theta_2 = \pi/4$ and $\theta_3 = \pi/6$. For a

[4]Eqns. (5.12) and (5.22) differ only in the scale factor, which captures the bandwidth efficiency of a given protocol.

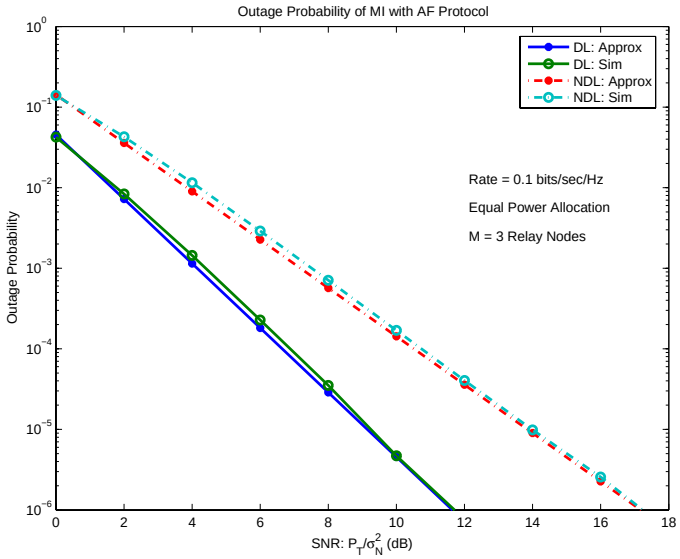

Figure 5.1 *Comparison of exact outage probability against the high SNR approximation for an amplify-and-forward protocol.* $M = 3$ *relay nodes are considered both without and with a direct link between the source and the destination. Equal power allocation is assumed with* $R = 0.1$ *bits/sec/Hz.*

given path loss exponent η, we have $\Omega_1 = 1$, $\Omega_2^j = [\cos(\theta_j/2)]^{-\eta}$, and $\Omega_3^j = [\sin(\theta_j/2)]^{-\eta}$, $j = 1, 2, 3$. Throughout this paper, we use $\eta = 4$. For simplicity, we assumed equal power allocation among the source and the 3 relays. Then, $P_s = P_T/4$, and $P_{r,j} = P_T/4$, $j = 1, \ldots, 4$, where P_T is the average total power. The target information rate was set to $R \in \{0.1, 1.0\}$ bits/sec/Hz. The outage probability results are shown, as a function of P_T/σ_N^2, in Figs. 5.1, 5.2 and 5.3 for AF, DF, and DSTC protocols, respectively, with $R = 0.1$. Figs. 5.4, 5.5 and 5.6 show a similar outage behavior with $R = 1.0$ for AF, DF, and DSTC protocols, respectively. From Figs. 5.1, 5.2 and 5.3 we conclude that the high SNR approximations are quite accurate. When the information rate is increased to ten folds, from $R = 0.1$, Figs. 5.4, 5.5 and 5.6 show that the outage performance degrades signficantly, and a large value of SNR is needed to maintain a desired level of outage probability.

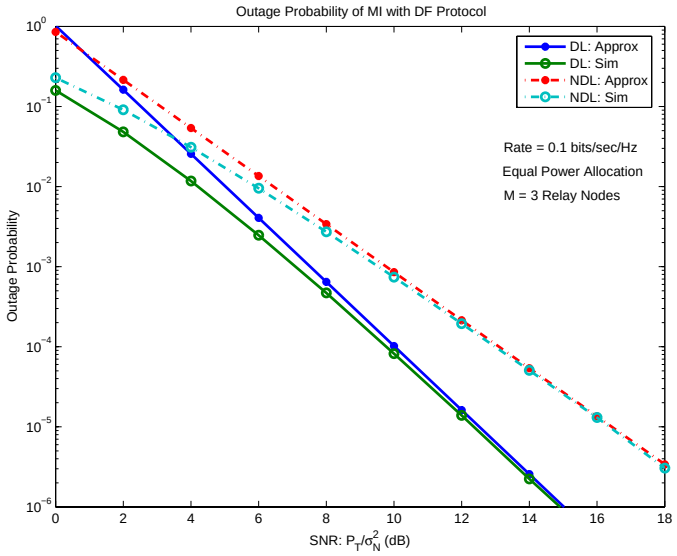

Figure 5.2 *Comparison of exact outage probability against the high SNR approximation for a decode-and-forward protocol.* $M = 3$ *relay nodes are considered both without and with a direct link between the source and the destination. Equal power allocation is assumed with* $R = 0.1$ *bits/sec/Hz.*

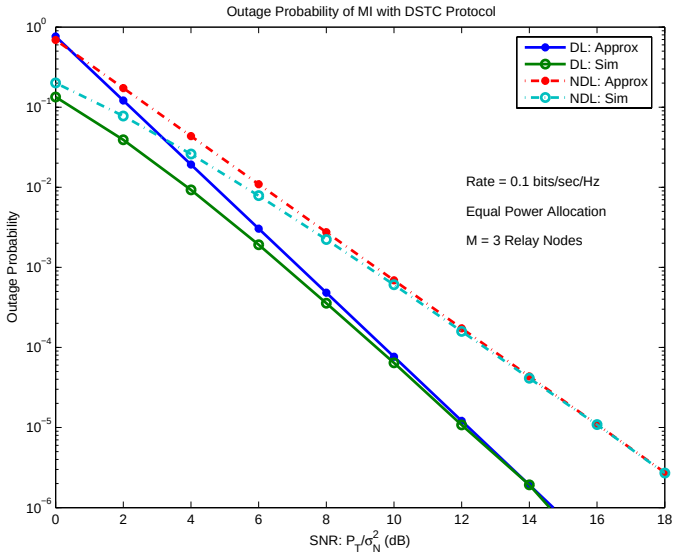

Figure 5.3 *Comparison of exact outage probability against the high SNR approximation for a distributed space-time code protocol.* $M = 3$ *relay nodes are considered both without and with a direct link between the source and the destination. Equal power allocation is assumed with* $R = 0.1$ *bits/sec/Hz.*

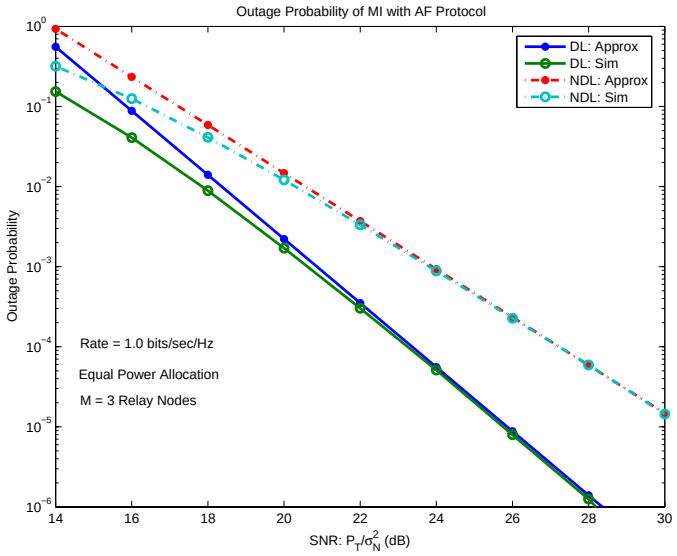

Figure 5.4 *Comparison of exact outage probability against the high SNR approximation for an amplify-and-forward protocol.* $M = 3$ *relay nodes are considered both without and with a direct link between the source and the destination. Equal power allocation is assumed with* $R = 1.0$ *bits/sec/Hz.*

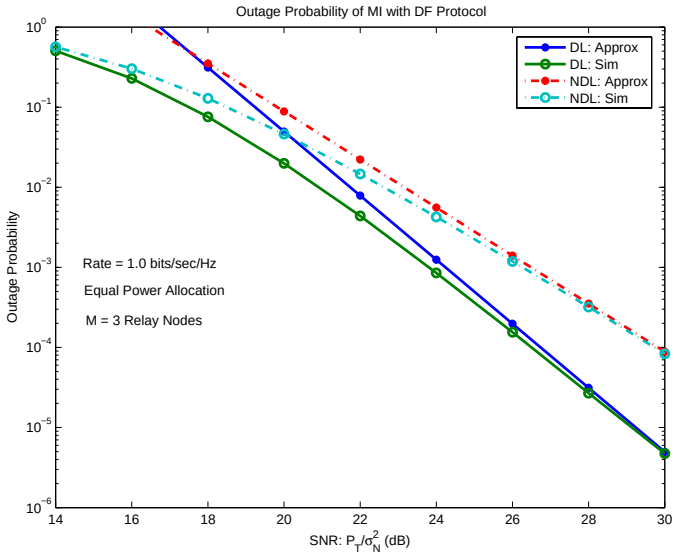

Figure 5.5 *Comparison of exact outage probability against the high SNR approximation for a decode-and-forward protocol.* $M = 3$ *relay nodes are considered both without and with a direct link between the source and the destination. Equal power allocation is assumed with* $R = 1.0$ *bits/sec/Hz.*

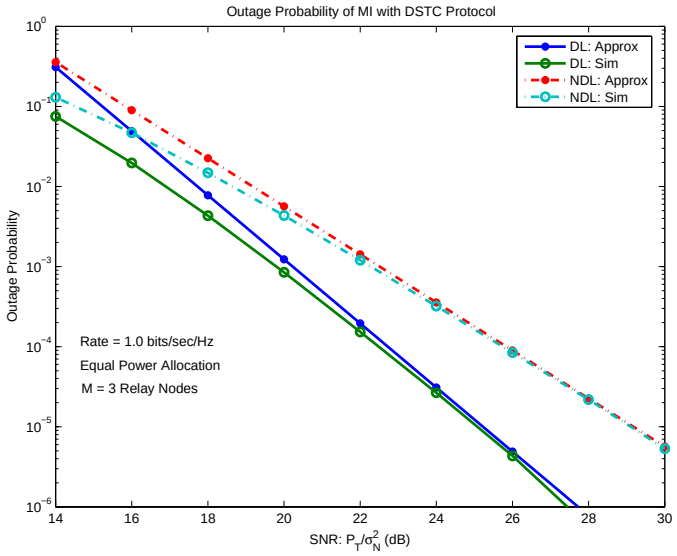

Figure 5.6 *Comparison of exact outage probability against the high SNR approximation for a distributed space-time code protocol. $M = 3$ relay nodes are considered both without and with a direct link between the source and the destination. Equal power allocation is assumed with $R = 1.0$ bits/sec/Hz.*

5.3.5 Convexity of High SNR Outage Probability Expressions

Upon examining (5.4), (5.5), (5.10), (5.12), (5.21), and (5.22), we notice that the outage probability of each protocol can be expressed as a linear combination (with positive weights) of the function

$$\Psi(\underline{P}) = \frac{1}{P_s^{n_0} \prod_{j=1}^{M} P_{r,j}^{n_j}}, \tag{5.23}$$

where $n_j \geq 0$ for $j = 0, 1, \ldots, M$. The determinant of the Hessian matrix of the objective function of (5.23) can be shown to be

$$\det\left(\nabla^2 \Psi(\underline{P})\right) = \Psi(\underline{P})^{M+1} \times \frac{\left(1 + \sum_{j=0}^{M} n_j\right) \prod_{j=0}^{M} n_j}{P_s^2 \prod_{j=1}^{M} P_{r,j}^2} \tag{5.24}$$

which is strictly positive. That is, (5.23) is a strictly convex function of $\underline{P}$. Since a linear combination (with positive weights) of convex functions is also convex, we conclude that (5.4), (5.5), (5.10), (5.12), (5.21), and (5.22) are also convex functions of $\underline{P}$. Since (5.23)

is in the form of a *monomial* [79], upon using the following change of variables

$$P_s = e^{x_0} \tag{5.25}$$

$$\text{and} \quad P_{r,j} = e^{x_j}, \quad j = 1, \ldots, M, \tag{5.26}$$

in (5.23), we can express our objective functions as *geometric programs* [79]. Since we have a linear constraint on the transmission powers, we can in fact efficiently solve the resulting geometric programs using commercial software, such as MOSEK [80].

5.4 Optimal Power Allocation

In this section, for AF, DF and DSTC protocols, we derive the optimal transmit power vector, $\underline{P}$, that minimizes the outage probability, subject to a sum power constraint. That is, our optimization problem is

$$\text{minimize} \quad P_{Out}(\underline{P}) \quad \text{subject to} \quad P_s + \sum_{j=1}^{M} P_{r,j} \leq P_T, \tag{5.27}$$

where P_T is the total transmit power. With equal power allocation, we have $P_s = P_{r,j} = P_T/(M+1)$, $j = 1, \ldots, M$. In our optimization, we devote equal attention to the cases without and with a direct link between the source and the destination. As will be clear at the end of this section, the presence or absence of a direct link significantly affects the optimum power vector, and the resulting performance gains. For all the protocols, we simply ignore the constants $\mathsf{C}_{AF,DL}, \mathsf{C}_{AF,NDL}, \mathsf{C}_{DF,DL}, \mathsf{C}_{DF,NDL}, \mathsf{C}_{DSTC,DL}$, and $\mathsf{C}_{DSTC,NDL}$, as they appear as multiplicative factors to the objective functions, and hence do not affect the resulting optimal power vector.

5.4.1 Amplify-and-Forward Protocol

When there is a direct link, using (5.4), the optimization problem of (5.27) is

$$\text{minimize} \quad \frac{1}{P_s}\prod_{j=1}^{M}\left(\frac{1}{P_s}+\frac{\alpha_j}{P_{r,j}}\right) \quad \text{subject to} \quad P_s+\sum_{j=1}^{M}P_{r,j}\leq P_T. \tag{5.28}$$

The Lagrange cost function can be written as

$$\mathcal{J}(\underline{P},\lambda)=\frac{1}{P_s}\prod_{j=1}^{M}\left(\frac{1}{P_s}+\frac{\alpha_j}{P_{r,j}}\right)+\lambda\left(P_s+\sum_{j=1}^{M}P_{r,j}-P_T\right), \tag{5.29}$$

where λ is the Lagrange parameter.

Upon setting the derivatives of $\mathcal{J}(\underline{P},\lambda)$ with respect to (w.r.t) P_s, $P_{r,j}$, $j=1,\ldots,M$, and λ, to zero, we have

$$\begin{aligned}
&-\frac{1}{P_s^2}\prod_{j=1}^{M}\left(\frac{1}{P_s}+\frac{\alpha_j}{P_{r,j}}\right)+\sum_{k=1}^{M}\frac{1}{P_s}\left(\prod_{j=1,j\neq k}^{M}\left(\frac{1}{P_s}+\frac{\alpha_j}{P_{r,j}}\right)\right)\left(-\frac{1}{P_s^2}\right)+\lambda=0\\
&\implies \qquad \lambda=\frac{P_{Out,AF,NDL}(\underline{P})}{P_s}\left(1+\sum_{k=1}^{M}\frac{P_{r,k}}{P_s\alpha_k+P_{r,k}}\right),
\end{aligned} \tag{5.30}$$

$$\begin{aligned}
&\frac{1}{P_s}\left[\prod_{k=1,k\neq j}^{M}\left(\frac{1}{P_s}+\frac{\alpha_k}{P_{r,k}}\right)\right]\left(-\frac{\alpha_j}{P_{r,j}}\right)+\lambda=0 \quad j=1,\ldots,M\\
&\implies \quad \lambda=\frac{P_{Out,AF,NDL}(\underline{P})\alpha_j P_s}{P_{r,j}(P_s\alpha_j+P_{r,j})}, \quad j=1,\ldots,M,
\end{aligned} \tag{5.31}$$

and

$$P_s+\sum_{j=1}^{M}P_{r,j}=P_T. \tag{5.32}$$

Using (5.31) and (5.32) in (5.30), we obtain

$$\frac{\lambda}{P_{Out,AF,NDL}(\underline{P})}=\frac{M+1}{P_T}. \tag{5.33}$$

Substituting (5.33) in (5.31), we arrive at the following quadratic equation over $P_{r,j}$:

$$P_{r,j}^2 + P_{r,j}P_s\alpha_j - \alpha_j P_s P_T/(M+1) = 0, \tag{5.34}$$

whose solution, in terms of P_s, is

$$P_{r,j} = \frac{-P_s\alpha_j + \sqrt{P_s^2\alpha_j^2 + 4P_s\alpha_j P_T/(M+1)}}{2}, \quad j = 1, \ldots, M. \tag{5.35}$$

Let $P_s = \delta_0 P_T$, and for $j = 1, \ldots, M$, $P_{r,j} = \delta_j P_T$, where $\delta_0 > 0$, $0 \leq \delta_j \leq 1$, $j = 1, \ldots, M$, and $\sum_{j=0}^{M} \delta_j = 1$. Then, by substituting (5.35) in (5.32), δ_0 can be expressed in the following transcendental equation:

$$\sum_{j=1}^{M} \sqrt{\delta_0^2\alpha_j^2 + 4\alpha_j\delta_0/(M+1)} = 2(1-\delta_0) + \delta_0 \sum_{j=1}^{M} \alpha_j. \tag{5.36}$$

Once δ_0 is found, P_s can be obtained as $P_s = \delta_0 P_T$ and (5.35) yields $P_{r,j}$. As a special case, let us assume $\alpha_j = \alpha, \forall\, j = 1, \ldots, M$, which might be thought of as a result of a symmetric relay placement. In this case, $\delta_j = (1-\delta_0)/M$, $j = 1, \ldots, M$, and we obtain the following closed-form expression for δ_0:

$$\delta_0 = \frac{1}{1-M\alpha}\left[1 - \frac{\alpha M}{2(M+1)}\left(1 + \sqrt{1 + 4\frac{M+1}{\alpha}}\right)\right]. \tag{5.37}$$

As $\alpha \to 0$, $\delta_0 \to 1$ indicating that all the power should be allocated to the source. Intuitively, this makes sense, since, when the relay is arbitrarily close to the destination, we expect the source to use as much of the available power as possible to reach the destination, and only a small amount of power is needed for the relay to reach the destination. On the other hand, when $\alpha \to \infty$ (i.e., the relay is arbitrarily close to the source) $\delta_0 \to \frac{1}{M+1}$. That is, equal power allocation is optimal only for large values of α. As $\alpha \to 1/M$, there is a discontinuity in the function, but using the L'Hospital rule in (5.37), we have $\delta_0 \to (M+1)/(1+2M)$.

In the absence of a direct link, with (5.5), the optimization problem is

$$\text{minimize} \quad \prod_{j=1}^{M}\left(\frac{1}{P_s}+\frac{\alpha_j}{P_{r,j}}\right) \quad \text{subject to} \quad P_s+\sum_{j=1}^{M}P_{r,j}\leq P_T. \tag{5.38}$$

The Lagrange cost function can be written as

$$\mathcal{J}(\underline{P},\lambda)=\prod_{j=1}^{M}\left(\frac{1}{P_s}+\frac{\alpha_j}{P_{r,j}}\right)+\lambda\left(P_s+\sum_{j=1}^{M}P_{r,j}-P_T\right). \tag{5.39}$$

Upon setting the derivatives of $\mathcal{J}(\underline{P},\lambda)$ w.r.t P_s, $P_{r,j}$, $j=1,\ldots,M$, and λ, to zero, we have

$$\begin{aligned}
&\sum_{k=1}^{M}\left(-\frac{1}{P_s^2}\right)\prod_{i=1,i\neq k}^{M}\left(\frac{1}{P_s}+\frac{\alpha_i}{P_{r,i}}\right)+\lambda=0\\
&\implies \quad \lambda=\frac{P_{Out,AF,NDL}(\underline{P})}{P_s}\sum_{k=1}^{M}\frac{P_{r,k}}{P_s(P_s\alpha_k+P_{r,k})} \qquad (5.40)\\
&\left[\prod_{i=1,i\neq j}^{M}\left(\frac{1}{P_s}+\frac{\alpha_i}{P_{r,i}}\right)\right]\left(-\frac{\alpha_j}{P_{r,j}^2}\right)+\lambda=0 \qquad j=1,\ldots,M\\
&\implies \quad \lambda=\frac{P_{Out,AF,NDL}(\underline{P})\alpha_j P_s}{P_{r,j}(P_s\alpha_j+P_{r,j})} \quad j=1,\ldots,M, \qquad (5.41)
\end{aligned}$$

and (5.32). Using (5.41) and (5.32) in (5.40), we obtain

$$\frac{\lambda}{P_{Out,AF,NDL}(\underline{P})}=\frac{M}{P_T}. \tag{5.42}$$

Substituting (5.42) in (5.41), we arrive at the quadratic

$$P_{r,j}^2+P_{r,j}P_s\alpha_j-\alpha_j P_s P_T/M=0, \tag{5.43}$$

whose solution, as a function of P_s, is

$$P_{r,j} = \frac{-P_s\alpha_j + \sqrt{P_s^2\alpha_j^2 + 4P_s\alpha_j P_T/M}}{2}, \quad j = 1, \ldots, M. \tag{5.44}$$

Let $P_s = \zeta_0 P_T$, and for $j = 1, \ldots, M$, $P_{r,j} = \zeta_j P_T$, where $\zeta_0 > 0$, $0 \leq \zeta_j \leq 1$, $j = 1, \ldots, M$, and $\sum_{j=0}^{M} \zeta_j = 1$. Then, by substituting (5.44) in (5.32), ζ_0 can be expressed in the following implicit equation:

$$\sum_{j=1}^{M} \sqrt{\zeta_0^2\alpha_j^2 + 4\alpha_j\zeta_0/M} = 2(1-\zeta_0) + \zeta_0 \sum_{j=1}^{M} \alpha_j. \tag{5.45}$$

Once ζ_0 is found, we get $P_s = \zeta_0 P_T$ and (5.44) yields $P_{r,j}$. As a special case, let us assume $\alpha_j = \alpha$, $\forall\, j = 1, \ldots, M$, so that $\zeta_j = (1-\zeta_0)/M$, $j = 1, \ldots, M$, where ζ_0 is given by

$$\zeta_0 = \frac{1}{1 + \sqrt{M\alpha}}. \tag{5.46}$$

As $\alpha \to 0$, $\zeta_0 \to 1$ indicating that a large fraction of the available power should be allocated to the source, consistent with the case with a direct link. On the other hand, unlike the case with a direct link, $\alpha \to \infty$ gives us $\zeta_0 \to 0$. That is, since the relay is arbitrarily close to the source, very little transmit power is needed by the source, and the rest of the available power has to be shared by the relays equally. Only when $\alpha = M$ does the equal power allocation become optimal.

5.4.2 Decode-and-Forward Protocol

Unlike the case with the AF protocol, due to the nature of (5.10) and (5.12), arriving at an optimal power vector for the DF protocol is rather cumbersome, even for a symmetric relay network with $\alpha_j = \alpha$, $\forall\, j = 1, \ldots, M$. In what follows, we restrict our attention to $M = 1$ and 2 relay nodes.

5.4.2.1 $M = 1$ Relay Node

Let us consider $M = 1$ first. The possible decoding sets are $\mathcal{D} = \phi$ (i.e., the relay is unable to decode) and $\mathcal{D} = \{1\}$ (the relay successfully decodes). Then, with a direct link, using (5.10), and ignoring the constant, the optimization problem of (5.27) reduces to

$$\begin{aligned} \text{minimize} \quad & \frac{1}{P_s^2} + \frac{1}{2}\frac{1}{P_s}\frac{\alpha_1}{P_{r,1}} = \frac{1}{P_s}\left(\frac{1}{P_s} + \frac{\widehat{\alpha}_1}{P_{r,1}}\right) \\ \text{subject to} \quad & P_s + P_{r,1} \leq P_T, \end{aligned} \tag{5.47}$$

where $\widehat{\alpha}_1 = \alpha_1/2$. Comparing (5.47) with (5.28) with $M = 1$, we notice that the DF protocol outage probability expression is very similar to that of the AF protocol. It then follows that, upon defining $P_s = \tau_0 P_T$ and $P_{r,1} = (1 - \tau_0)P_T$, $0 < \tau_0 \leq 1$, τ_0 can be obtained directly from (5.37) with $M = 1$ and α in (5.37) replaced by $\widehat{\alpha}_1 = \alpha_1/2$. That is,

$$\tau_0 = \frac{2}{2 - \alpha_1}\left[1 - \frac{\alpha_1}{8}\left(1 + \sqrt{1 + \frac{16}{\alpha_1}}\right)\right]. \tag{5.48}$$

As $\alpha_1 \to 2$, using the L'Hospital rule in (5.48), we have $\tau_0 \to 2/3$.

In the absence of a direct link, from (5.12) with $\mathcal{D} = \phi$ and $\{1\}$, the optimization problem is

$$\text{minimize} \quad \frac{1}{P_s} + \frac{\alpha_1}{P_{r,1}} \quad \text{subject to} \quad P_s + P_{r,1} \leq P_T. \tag{5.49}$$

Comparing (5.49) with (5.38) with $M = 1$, we notice that the DF protocol outage probability expression is exactly the same as that of the AF protocol. It then follows that, upon defining $P_s = \mu_0 P_T$ and $P_{r,1} = (1 - \mu_0)P_T$, $0 < \mu_0 \leq 1$, μ_0 can be obtained directly from (5.46) with $M = 1$ as

$$\mu_0 = \frac{1}{1 + \sqrt{\alpha_1}}, \tag{5.50}$$

which also coincides with [71, Eqn. (8)].

5.4.2.2 $M = 2$ Relay Nodes

With $M = 2$ relays, we have $\mathcal{D} = \phi, \{1\}, \{2\}$, and $\{1, 2\}$, and the optimization problem with a direct link is

$$\begin{aligned} &\text{minimize} \quad \frac{1}{P_s^3} + \frac{1}{2}\frac{1}{P_s^2}\left(\frac{\alpha_1}{P_{r,1}} + \frac{\alpha_2}{P_{r,2}}\right) + \frac{1}{6}\frac{1}{P_s}\frac{\alpha_1\alpha_2}{P_{r,1}P_{r,2}} \\ &\text{subject to} \quad P_s + P_{r,1} + P_{r,2} \leq P_T. \end{aligned} \tag{5.51}$$

Upon setting the derivatives of the Lagrange cost function w.r.t P_s, $P_{r,1}$, $P_{r,2}$, and λ to zero, we have

$$\begin{aligned} &-\frac{3}{P_s^4} - \frac{2}{P_s^3}\left(\frac{\alpha_1}{P_{r,1}} + \frac{\alpha_2}{P_{r,2}}\right) - \frac{1}{P_s^2}\frac{1}{6}\frac{\alpha_1\alpha_2}{P_{r,1}P_{r,2}} + \lambda = 0 \\ &\implies \lambda = \frac{3}{P_s^4} + \frac{2}{P_s^3}\left(\frac{\alpha_1}{P_{r,1}} + \frac{\alpha_2}{P_{r,2}}\right) + \frac{1}{P_s^2}\frac{1}{6}\frac{\alpha_1\alpha_2}{P_{r,1}P_{r,2}}, \end{aligned} \tag{5.52}$$

$$-\frac{1}{2P_s^2}\frac{\alpha_1}{P_{r,1}^2} - \frac{1}{6P_s}\frac{\alpha_1\alpha_2}{P_{r,1}^2P_{r,2}} + \lambda = 0 \quad \implies \lambda = \frac{1}{2P_s^2}\frac{\alpha_1}{P_{r,1}^2} + \frac{1}{6P_s}\frac{\alpha_1\alpha_2}{P_{r,1}^2P_{r,2}}, \tag{5.53}$$

$$-\frac{1}{2P_s^2}\frac{\alpha_2}{P_{r,2}^2} - \frac{1}{6P_s}\frac{\alpha_1\alpha_2}{P_{r,1}P_{r,2}^2} + \lambda = 0 \quad \implies \lambda = \frac{1}{2P_s^2}\frac{\alpha_2}{P_{r,2}^2} + \frac{1}{6P_s}\frac{\alpha_1\alpha_2}{P_{r,1}P_{r,2}^2}, \tag{5.54}$$

and

$$P_s + P_{r,1} + P_{r,2} = P_T. \tag{5.55}$$

Equating (5.53) with (5.52), and (5.53) with (5.54), we have

$$\begin{aligned} &P_s^3(\alpha_1\alpha_2/3) - P_s^2(\alpha_1\alpha_2P_{r,1}/3 - \alpha_1P_{r,2}) - \\ &P_s(2\alpha_1P_{r,1}P_{r,2} + 2\alpha_2P_{r,1}^2) - 6P_{r,1}^2P_{r,2} = 0 \end{aligned} \tag{5.56}$$

$$\text{and} \quad P_s(P_{r,2} - P_{r,1})\alpha_1\alpha_2/3 - (\alpha_2P_{r,1}^2 - \alpha_1P_{r,2}^2) = 0. \tag{5.57}$$

Eqns. (5.55), (5.56) and (5.57) constitute three equations in three unknowns, $P_s, P_{r,1}$, and $P_{r,2}$, and can be solved numerically to arrive at the optimal power vector. For the case of a symmetric relay network, we have $\alpha_1 = \alpha_2$. With this, (5.57) gives us $P_{r,1} = P_{r,2}$. Further, let $P_s = \epsilon P_{r,1} = \epsilon P_T/(2+\epsilon)$, $0 < \epsilon < 1$. Then substituting in (5.57) results in the following cubic equation[5] in ϵ:

$$\epsilon^3 - \epsilon^2(1 - 3/\alpha) - \epsilon(12/\alpha) - 18/\alpha^2 = 0 \tag{5.58}$$

which has at least one real root. Since the objective function is strictly convex in $\underline{P}$, it then follows that there exists only one positive root of (5.58). When $\alpha \to \infty$, (5.58) yields $\epsilon = 1$. That is, $P_s = P_{r,1} = P_{r,2} = P_T/3$, implying the optimality of equal power allocation as $\alpha \to \infty$.

In the absence of a direct link, with $M = 2$, the Lagrangian cost function is

$$\mathcal{J}(\underline{P}, \lambda) = \frac{1}{P_s^2} + \frac{1}{P_s}\frac{\alpha_1}{P_{r,1}} + \frac{1}{P_s}\frac{\alpha_2}{P_{r,2}} + \frac{1}{2}\frac{\alpha_1\alpha_2}{P_{r,1}P_{r,2}} + \lambda\left(P_s + \sum_{j=1}^{M} P_{r,j} - P_T\right). \tag{5.59}$$

Upon setting the derivatives of (5.59) w.r.t P_s, $P_{r,1}$, $P_{r,2}$, and λ to zero, we have

$$-\frac{2}{P_s^3} - \frac{1}{P_s^2}\frac{\alpha_1}{P_{r,1}} - \frac{1}{P_s^2}\frac{\alpha_2}{P_{r,2}} + \lambda = 0 \quad \Longrightarrow \quad \lambda = \frac{2}{P_s^3} + \frac{1}{P_s^2}\left(\frac{\alpha_1}{P_{r,1}} + \frac{\alpha_2}{P_{r,2}}\right), \tag{5.60}$$

$$-\frac{1}{P_s}\frac{\alpha_1}{P_{r,1}^2} - \frac{1}{2}\frac{\alpha_1\alpha_2}{P_{r,1}^2 P_{r,2}} + \lambda = 0 \quad \Longrightarrow \quad \lambda = \frac{1}{P_{r,1}}\left(\frac{1}{P_s}\frac{\alpha_1}{P_{r,1}} + \frac{1}{2}\frac{\alpha_1\alpha_2}{P_{r,1}P_{r,2}}\right), \tag{5.61}$$

$$-\frac{1}{P_s}\frac{\alpha_2}{P_{r,2}^2} - \frac{1}{2}\frac{\alpha_1\alpha_2}{P_{r,1}P_{r,2}^2} + \lambda = 0 \quad \Longrightarrow \quad \lambda = \frac{1}{P_{r,2}}\left(\frac{1}{P_s}\frac{\alpha_2}{P_{r,2}} + \frac{1}{2}\frac{\alpha_1\alpha_2}{P_{r,1}P_{r,2}}\right), \tag{5.62}$$

[5] In general, for a symmetric relay network with M relay nodes, one has to find the unique positive root of a polynomial of degree $M+1$.

and (5.55). Upon equating (5.61) with (5.62), and (5.61) with (5.60), we have

$$(\alpha_1 P_{r,2}^2 - \alpha_2 P_{r,1}^2) = \alpha_1\alpha_2 P_s(P_{r,1} - P_{r,2})/2 \tag{5.63}$$

$$\text{and} \quad P_s^3(\alpha_1\alpha_2/2) + P_s^2(\alpha_1 P_{r,2}) = P_s(\alpha_1 P_{r,1}P_{r,2} + \alpha_2 P_{r,1}^2) + 2P_{r,1}^2 P_{r,2}. \tag{5.64}$$

For a general (α_1, α_2), a numerical approach is needed to solve the above nonlinear equations. On the other hand, with $\alpha_1 = \alpha_2 = \alpha$, we once again have $P_{r,1} = P_{r,2}$ from (5.63). Upon letting $P_s = \kappa P_{r,1} = \kappa P_T/(2+\kappa)$, (5.64) results in

$$\kappa^3 + \kappa^2(2/\alpha) - \kappa(4/\alpha) - 4/\alpha^2 = 0. \tag{5.65}$$

Eqn. (5.65) is significantly different from (5.58) in the following way: While (5.58) shows that $\epsilon \to 1$ as $\alpha \to \infty$, (5.65) gives us $\kappa \to 0$ as $\alpha \to \infty$. That is, arbitrarily small power is needed for the source to transmit, instead of one-third of the total power allocation, when $\alpha \to \infty$.

5.4.3 Distributed Space-Time Coded Protocol

Upon comparing the outage probability expression for DSTC of (5.21) with that of (5.10) for the DF protocol, we notice that, in addition to differing in multiplicative constants, the factor $1/(|\mathcal{D}|+1)!$ in (5.10) is replaced by $\mathcal{A}_{|\mathcal{D}|}(2^{2R}-1)$ in (5.21). In fact,

$$\mathcal{A}_n(0) = \frac{1}{(n-1)!}\int_{u=0}^{1} u^{n-1}(1-u)du = \frac{1}{(n+1)!}, \tag{5.66}$$

which implies that the optimal power vector of the DF protocol is indeed a special case of that of the DSTC protocol. The important difference is that the optimal power allocation vector of the DSTC protocol *depends on the transmission rate* R. A simple, but interesting, case is that with $M = 2$ relay nodes, which forms a basis for implementing distributed Alamouti STBC.

With $M = 2$ relays, the analysis is very similar to that in Section 5.4.2, and hence we skip it for brevity. For a general (α_1, α_2), we obtain sets of equations very similar to (5.56) and (5.57), but with a dependence on $\mathcal{A}_1(2^{2R}-1)$ and $\mathcal{A}_2(2^{2R}-1)$. That is, we have

$$\begin{aligned}
&P_s^3(\mathcal{A}_2(2^{2R}-1)\alpha_1\alpha_2) - P_s^2(\mathcal{A}_2(2^{2R}-1)\alpha_1\alpha_2 P_{r,1} - \mathcal{A}_1(2^{2R}-1)\alpha_1 P_{r,2}) \\
&-P_s(2\mathcal{A}_1(2^{2R}-1)\alpha_1 P_{r,1}P_{r,2} + 2\mathcal{A}_1(2^{2R}-1)\alpha_2 P_{r,1}^2) - 3P_{r,1}^2 P_{r,2} = 0, \qquad (5.67)\\
&\text{and} \quad \mathcal{A}_1(2^{2R}-1)\left(\alpha_1 P_{r,2}^2 - \alpha_2 P_{r,1}^2\right) = \mathcal{A}_2(2^{2R}-1)\alpha_1\alpha_2 P_s\left(P_{r,1} - P_{r,2}\right). \qquad (5.68)
\end{aligned}$$

On the other hand, when $\alpha_1 = \alpha_2 = \alpha$, similar to (5.58) we have the cubic equation

$$\begin{aligned}
&\epsilon^3 - \epsilon^2\left(1 - \mathcal{A}_1(2^{2R}-1)/(\mathcal{A}_2(2^{2R}-1)\alpha)\right) \\
&-\epsilon\left(4\mathcal{A}_1(2^{2R}-1)/(\mathcal{A}_2(2^{2R}-1)\alpha)\right) - \left(3/(\mathcal{A}_2(2^{2R}-1)\alpha^2)\right) = 0. \qquad (5.69)
\end{aligned}$$

As $\alpha \to \infty$ (5.69) gives us $\epsilon \to 1$, which is not a function of R, thus showing the optimality of equal power allocation. As a quick check, by setting $\mathcal{A}_1(2^{2R}-1) = 1/2$ and $\mathcal{A}_2(2^{2R}-1) = 1/6$, (5.69) reduces to (5.58) of the DF protocol.

Without a direct link, ignoring the constant, the outage probability expression in (5.22) of the DSTC protocol has a form very similar to that of the DF protocol of (5.12). Since the optimum power vector is not a function of the multiplicative constant of the objective function, it then follows that the optimal power vector of the DSTC protocol is exactly the same as that of the DF protocol.

5.5 Coding Gain Considerations

For simplicity, let us define $\Gamma = P_T/\sigma_N^2$, the average SNR. For sufficiently large Γ, the outage probability can be written as $P_{Out} \approx (\mathsf{G}_c\Gamma)^{-\mathsf{G}_d}$ [75], where G_d is the so-called diversity gain, and G_c can be viewed as the asymptotic coding gain. Note that

the use of the term "coding gain" is seemingly a misnomer, since there is no explicit forward error correction in the systems being analyzed. However, the term has been used in the literature, and so we adopt it here. With equal power allocation, [74] studied the coding gain performance of both AF and DF protocols. We now present the coding gain expressions for the AF, DF and DSTC protocols with optimal power allocation. First, upon setting $\underline{P} = [\delta_0, \delta_1, \ldots, \delta_M] \times P_T$ in (5.4), the ACG of the AF protocol with a direct link is

$$\mathsf{G}_{c,AF,DL} = \frac{\delta_0}{2^{(M+1)R} - 1} \left[(M+1)! \Omega_1 \prod_{j=1}^{M} \left(\frac{\Omega_2^j \delta_j}{\delta_j + \delta_0 \alpha_j} \right) \right]^{\frac{1}{M+1}}. \tag{5.70}$$

Upon letting $\underline{P} = [\zeta_0, \zeta_1, \ldots, \zeta_M] \times P_T$ in (5.5), the ACG without a direct link is

$$\mathsf{G}_{c,AF,NDL} = \frac{\zeta_0}{2^{(M+1)R} - 1} \left[M! \prod_{j=1}^{M} \left(\frac{\Omega_2^j \zeta_j}{\zeta_j + \zeta_0 \alpha_j} \right) \right]^{\frac{1}{M}}. \tag{5.71}$$

By setting $\delta_j = P_T/(M+1)$ in (5.70) and $\zeta_j = P_T/(M+1)$ in (5.71), $j = 0, 1, \ldots, M$, we obtain the ACG expressions with an equal power allocation [74]. Similar expressions can easily be found for the DF and DSTC protocols. The coding gain ratio of a protocol with optimal power allocation is defined as

$$\mathsf{CGR} \triangleq \frac{\mathsf{G}_c(\text{Optimal Alloc})}{\mathsf{G}_c(\text{Equal Alloc})}.$$

With the AF protocol, these are

$$\mathsf{CGR}_{AF,DL} = \delta_0 \times (M+1) \times \left(\prod_{j=1}^{M} \frac{\delta_j (1+\alpha_j)}{\delta_j + \delta_0 \alpha_j} \right)^{\frac{1}{M+1}} \tag{5.72}$$

$$\text{and} \quad \mathsf{CGR}_{AF,NDL} = \zeta_0 \times (M+1) \times \left(\prod_{j=1}^{M} \frac{\zeta_j (1+\alpha_j)}{\zeta_j + \zeta_0 \alpha_j} \right)^{\frac{1}{M}}, \tag{5.73}$$

with and without a direct link, respectively. With a single relay, the CGRs of the DF protocol are

$$\mathsf{CGR}_{DF,DL} = 2\tau_0\sqrt{\frac{(1-\tau_0)(2+\alpha_1)}{2(1-\tau_0)+\tau_0\alpha_1}} \tag{5.74}$$

$$\text{and} \quad \mathsf{CGR}_{DF,NDL} = \frac{2(1+\alpha_1)}{(1+\sqrt{\alpha_1})^2}, \tag{5.75}$$

with and without a direct link, respectively. With either $\alpha_1 \to 0$ or $\alpha_1 \to \infty$, (5.75) predicts a 3 dB improvement in ACG with a single relay node and optimal power allocation.

5.6 Results and Discussion

We now present some numerical results illustrating the performance gains of various relaying protocols with optimal transmit power allocation. The relay network topology is the same as that described in Section 5.3.4. The outage performance of the AF protocol is studied in Figs. 5.7 and 5.8 without and with a direct link, respectively. $M = 1, 2,$ and 3 relays are considered. The information rate is $R = 1$ bit/sec/Hz. Without a direct link, Fig. 5.7 shows that a 2 dB improvement can be obtained with optimal power allocation at an outage level of 10^{-2} with a single relay, whereas these gains, at an outage level of 10^{-3}, increase to 3.5 dB with two relays, and 4 dB with three relays. As shown in Fig. 5.8, existence of a direct link boosts the outage performance by providing an additional diversity path. Fig. 5.8 shows that, at an outage of 10^{-3}, optimal allocation with a single relay provides a significant gain of 3 dB. The gains increase to 3.8 and 4 dB with two and three relay nodes, respectively, at an outage level of 10^{-5}. With the same topology as that of the AF protocol, the outage performance of a single relay (location at θ_1) based DF protocol is presented in Fig. 5.9 without and with a direct link. Fig. 5.9 shows that, at an outage probability of 10^{-2}, the SNR gain without a direct link is 5 dB, whereas, at 10^{-3} outage probability, the existence of a direct link provides a gain around 2.0 dB. These gains, by judicious allocation of transmit power across various nodes, and based on the knowledge

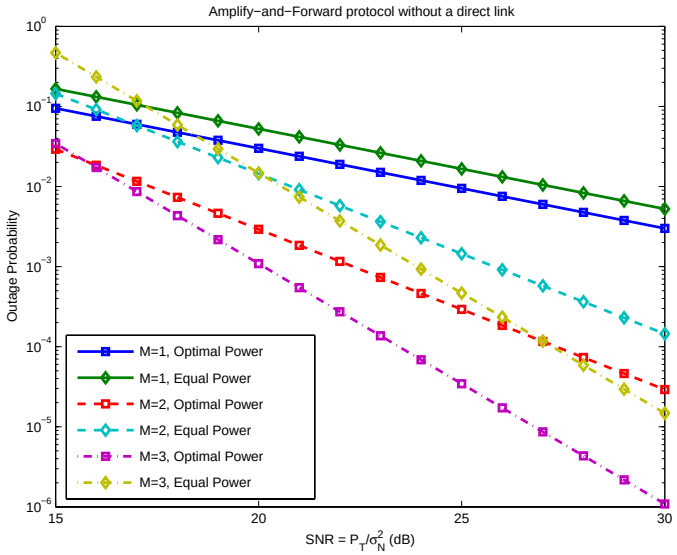

Figure 5.7 *Outage probability of the AF protocol with both equal and optimal power allocation. One, two and three relays are considered without a direct link between the source and the destination.*

of the mean channel power gains alone, directly improve the energy efficiency, and thus lead to a longer network lifetime.

Fig. 5.10 shows the optimal transmit power allocation for the AF protocol under the symmetric relay network assumption. That is, $\alpha_j = \alpha, \forall\, j = 1, \ldots, M$. Due to this symmetry, as shown before, the source transmits at a power level of P_s, and all other relays transmit at an identical power level of P_r such that $P_s + MP_r = P_T$. Fig. 5.10 shows P_s as a function of α, parameterized by the number of relays, M. Both the cases of direct and no direct link between the source and the destination are considered. Two observations are made regarding the behavior of P_s as α is varied: First, when there is no direct link between the source and the destination, a larger value of α implies that the relay is closer to the source than the destination, and it enjoys less path loss from the source. This allows the source to reduce its transmit power, and helps the relay to transmit at a higher power level in order to compensate for the path loss between the relay and the destination. This also explains why the source transmit power decreases gradually with α as the number of relays is increased. However, the situation is quite different when there

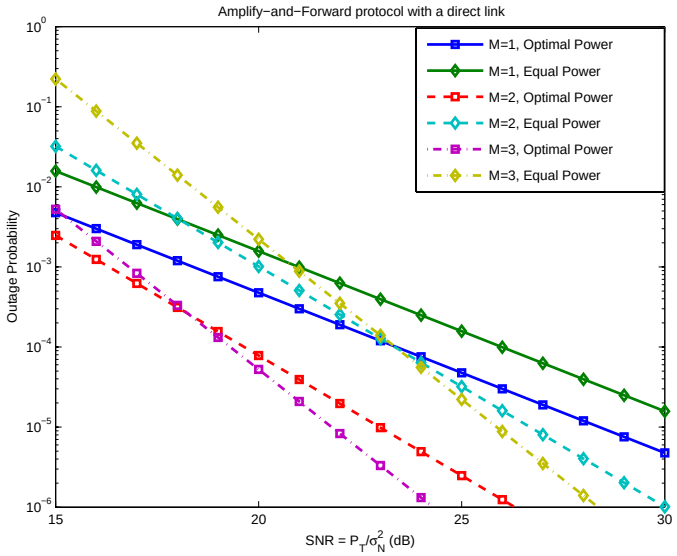

Figure 5.8 *Outage probability of the AF protocol with both equal and optimal power allocation. One, two and three relays are considered with a direct link between the source and the destination.*

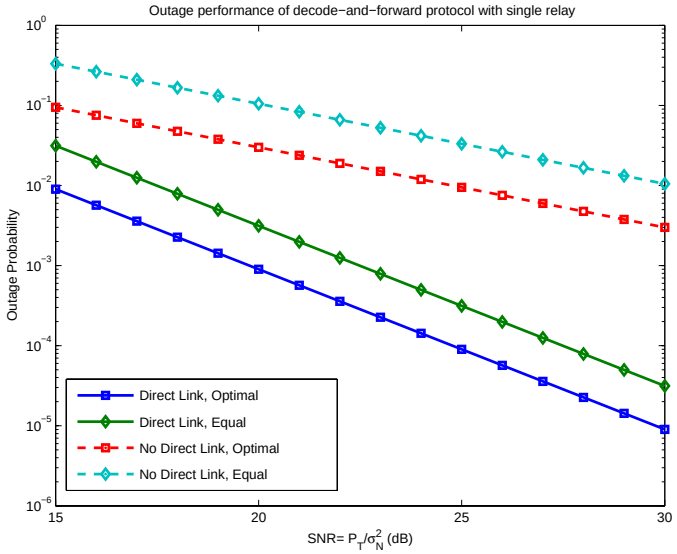

Figure 5.9 *Outage probability of the DF protocol with both equal and optimal power allocation. A single relay is assumed without and with a direct link between the source and the destination.*

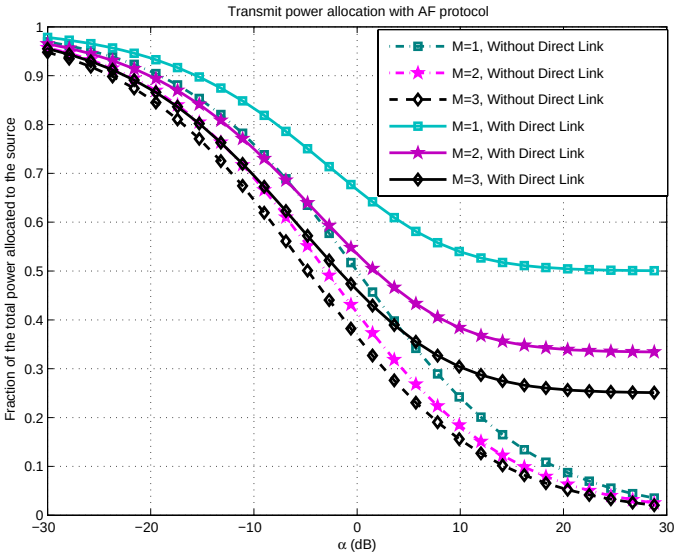

Figure 5.10 *The fraction of the total power allocated to the source with M-relay AF protocol. Both the cases without and with a direct link between the source and the destination are considered.*

exists a direct link between the source and the destination. In this case, irrespective of the value of α, the source has to expend a non-negligible amount of transmit power in order to reach the destination via the direct link. As $\alpha \to \infty$, the existence of a direct link leads to $P_s \to 1/(M+1)$ (i.e., equal power allocation is asymptotically optimum as $\alpha \to \infty$), whereas without the direct link we have $P_s \to 0$ (which is to be interpreted as the negligible transmit power required by the source to reach the relays).

Next, we present the optimal transmit power allocation for the DF and DSTC protocols for a symmetric network topology. With $M = 2$ relays, the fraction of the power utilized by the source is plotted in Fig. 5.11 with $M = 2$ relay nodes, without and with a direct link. Similar to the case of the AF protocol, existence of a direct link requires the source to draw significantly more power than without a direct link. For example, when $\alpha = 10$ dB, the source power with a direct link is twice the power without a direct link, and is approximately three times the power without a direct link when $\alpha = 17$ dB. The results of Fig. 5.11 are also applicable for a DSTC protocol without a direct link. However, with a direct link, the power allocation for a DSTC protocol is dependent on the transmission

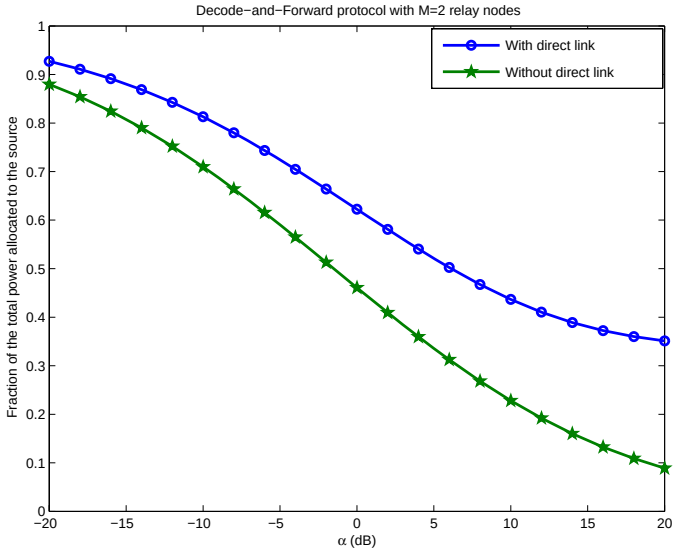

Figure 5.11 *Fraction of the total power expended by the source as a function of* $\alpha = \Omega_2/\Omega_3$. *A DF protocol is assumed with a direct link from the source to the destination with* $M = 2$ *relay nodes in a symmetric relay network (i.e.,* $\alpha_1 = \alpha_2 = \alpha = \Omega_2/\Omega_3$*).*

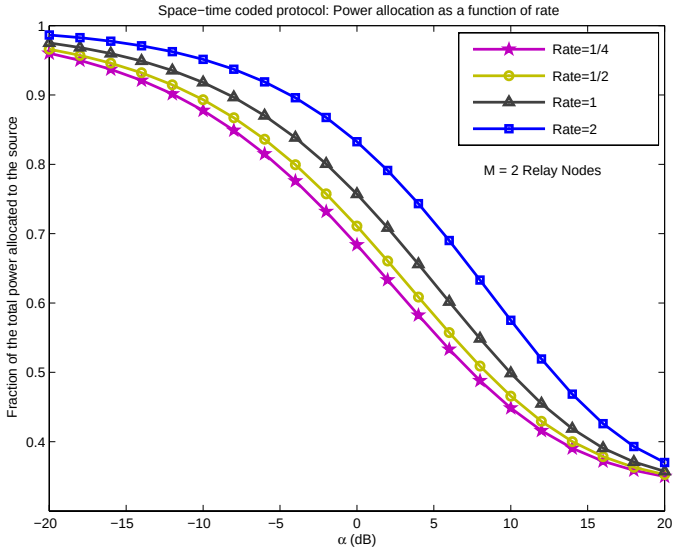

Figure 5.12 *Fraction of the total power expended by the source as a function of* α. *A DSTC protocol is assumed with a direct link from the source to the destination with* $M = 2$ *relay nodes in a symmetric relay network (i.e.,* $\alpha_1 = \alpha_2 = \alpha = \Omega_2/\Omega_3$*).*

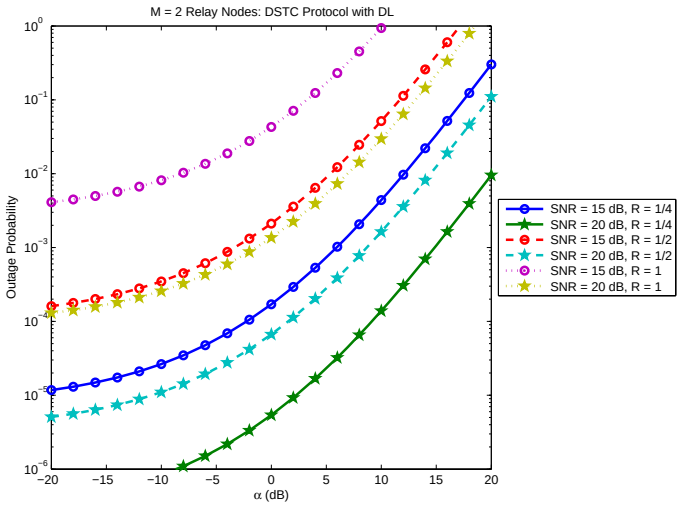

Figure 5.13 *Outage probability of DSTC protocol with $M = 2$ relay nodes and optimum transmission power allocation. A symmetric relay placement is assumed with $\alpha_1 = \alpha_2 = \alpha = \Omega_2/\Omega_3$ and a direct link between the source and the destination. The outage curves are parameterized by the transmission rate R, in bits/sec/Hz, and the SNR P_T/σ_N^2.*

rate. Fig. 5.12 shows this dependency with the transmission rate $R \in \{1/4, 1/2, 1, 2\}$ bits/sec/Hz, and with two relays. From Fig. 5.12, we notice that more power should be invested in the source transmissions for increasing data rates.

Outage performance of the DSTC protocol with two relays is presented, as a function of α, for a symmetric network in Figs. 5.13 and 5.14 for scenarios with and without a direct link, respectively. The outage curves are parameterized by the rate $R \in \{1/4, 1/2, 1\}$ and the average SNR, $P_T/\sigma_N^2 \in \{15, 20\}$ dB. Without loss of generality, we set $\Omega_2^j = 1$ for $j = 1, 2$, and let $\Omega_1 = 1$ with a direct link. In Figs. 5.13 and 5.14, a large value of α implies that the relay nodes are far away from the destination, and their signals are received at the destination with severe attenuation. This leads to a degradation in the outage performance, and is more pronounced at low SNR and when there is no direct link between the source and the destination (i.e., no signal contribution from the source to the destination). Upon comparing Fig. 5.14 with Fig. 5.13 in terms of attempted transmission rate, we observe that an increase in the rate can significantly degrade the outage performance when there is no direct link.

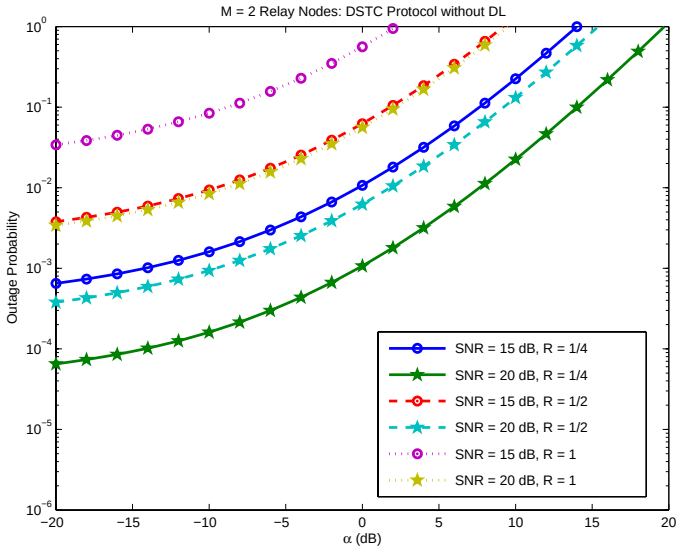

Figure 5.14 *Outage probability of DSTC protocol with $M = 2$ relay nodes and optimum transmission power allocation. A symmetric relay placement is assumed with $\alpha_1 = \alpha_2 = \alpha = \Omega_2/\Omega_3$ without a direct link between the source and the destination. The outage curves are parameterized by the transmission rate R, in bits/sec/Hz, and the SNR P_T/σ_N^2.*

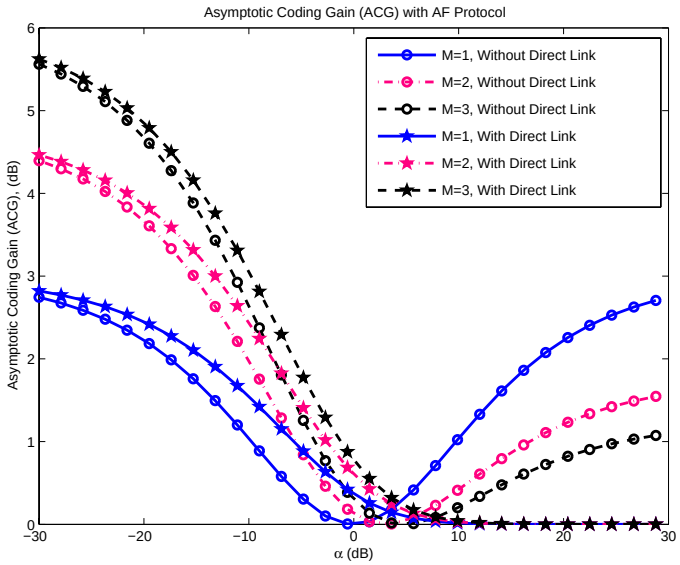

Figure 5.15 *Asymptotic coding gain (ACG) improvement with the AF protocol with optimum power allocation. Both the cases without and with a direct link between the source and the destination are considered.*

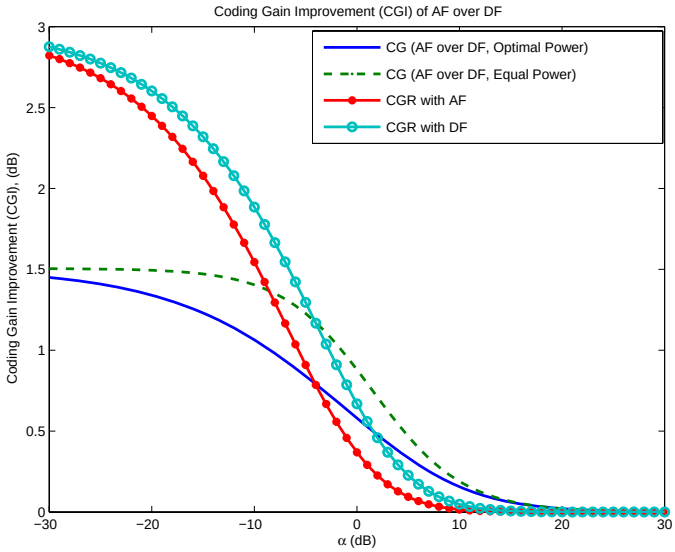

Figure 5.16 *Comparison of coding gain improvements (CGI) for both AF and DF protocols with optimal power allocation. A single relay node is considered. The coding gain gap between AF and DF protocols is also shown. As seen in this figure, this gap is reduced by the use of optimal power allocation.*

The CGR improvement of the AF protocol with optimal power allocation is plotted as a function of α in Fig. 5.15 for both the cases without and with a direct link between the source and the destination. The following conclusions can be drawn from Fig. 5.15: $i)$ In the absence of a direct link, the optimal power allocation provides more coding gain than the equal power allocation for all values of α, except when $\alpha = M$. When $\alpha = M$, from (5.46), we have $P_s = P_r = P_T/(M+1)$, and the resulting ACG over equal power allocation is zero. $ii)$ When a direct link exists, the CGR improvement is significant for smaller values of α (i.e., when the relay is farther away from the source than from the destination); on the other hand, as $\alpha \to \infty$, we have $P_s = P_r = P_T/(M+1)$, leading to no further improvement in CGR. In this regime (i.e., for large values of α) the case without a direct link provides more coding gain than the case with a direct link. $iii)$ Interestingly, without a direct link, a large number of relays is beneficial for smaller values of α, in terms of the CGR benefits, whereas a single relay is good enough for large α.

Fig. 5.16 presents a comparative study of the CGR improvements of the AF and DF protocols with a direct link when a single relay is employed. The ACG of AF over DF,

without and with optimal allocation, and the individual CGRs of AF and DF protocols with optimal power allocation over equal power allocation, are considered. Fig. 5.16 shows that the mean channel gain-based optimal power allocation is more beneficial to the DF protocol than to the AF protocol. We also notice from Fig. 5.16 that, for $-20 \leq \alpha\,(\text{dB}) \leq 0$, the coding gain gap between the AF and DF protocols is reduced by as much as 0.4 dB with optimal power allocation.

5.7 Conclusions

We have presented the optimum transmit power allocation for wireless relaying protocols with mean channel gain information. The results were established, at high SNR, for AF, DF and DSTC protocols operating over a Rayleigh fading network. At high SNR, the optimal power allocation was shown to depend not only on the ratio of mean power gains, but also on whether or not a direct link between the source and the destination exists. Our results showed that, in addition to the improvements in the outage probability, optimal power allocation yields impressive coding gains over equal power allocation. Furthermore, our analysis revealed that the coding gain gap between the AF and DF protocols can be reduced by the optimal power allocation.

CHAPTER 6

Contributions and Future Directions

6.1 Contributions

This dissertation presented a cross-layer study of wideband CDMA systems, and cooperative diversity aspects of wireless ad-hoc networks. The following are the main contributions of this thesis.

In Chapter 2, we looked at the three way tradeoff among source coding, channel coding and spreading for a wideband DS-CDMA system. Our results in Chapter 2 demonstrated that the optimal three-tuple that minimizes the distortion upper bound is quite close to the one based on the lower bound on the average distortion. For small values of spreading factor, our simulations showed that the system performance is hurt by the self-interference of the user of interest, thus cautioning against aggressive channel coding. The optimal bandwidth allocation, in general, is shown to depend on the system and the channel conditions, such as the total number of active users, the average JSR power ratio, and the number of resolved multipath components together with their power delay profile.

To improve the distortion performance on channels with severe NBI, in Chapter 3 we assessed the benefits of using an MC-CDMA system in place of the conventional DS-CDMA system. Our results in Chapter 3 reported an improvement in not only the average distortion performance, but also the three-way tradeoff performance. That is, under various channel conditions, for the same bandwidth constraint with approximately

identical receiver complexities for both DS- and MC-CDMA systems (the DS-CDMA system does not use a notch filter for NBI suppression), our results showed that an MC-CDMA system supports a higher information rate (i.e., a larger source coding rate) than a DS-CDMA system.

Regarding relay-assisted user cooperation diversity, Chapter 4 introduced a parallel relay channel model, and, for both OOK and BFSK modulations, derived optimum noncoherent AF detectors when the receiving nodes have no instantaneous knowledge of CSI. Our upper and lower bounds on the average probability of error showed that the diversity order of a noncoherent AF receiver is twice that of a noncoherent DF receiver. Suboptimum receivers were also proposed along with their performance evaluations.

By constraining the average sum power of the source and all the relay nodes, Chapter 5 considered the problem of optimal transmit power allocation when only the knowledge of average second moments of the channel fading is available at the transmitting nodes. We quantified the improvements in outage probability performance as well as the asymptotic cooperation gain of AF, DF, and DSTC protocols with optimal power allocation.

6.2 Future Directions

We now briefly outline some of the possible extensions to the work presented in this dissertation. For clarity, these extensions are organized chapter-wise.

6.2.1 Chapter 2

In Chapter 2, for tractability reasons, we restricted our analysis to the simplest case of a Gaussian source. It is highly desirable to investigate the tradeoff performance in the presence of a practical source coder, such as an image or a video codec. For example, a progressive image coding scheme such as SPIHT (set-partitioning in hierarchical trees) coding [81] may be a good starting point in this direction. Our analysis is also restricted

in a sense that only a bandwidth constraint is considered. In an energy constrained communication scenario, a system designer is usually faced with both energy and bandwidth constraints. Therefore, it is also of interest to revisit the tradeoff problem with both bandwidth and transceiver energy (i.e., the combined energy required for both sending and receiving the information) constraints.

6.2.2 Chapter 3

We have showed in Chapter 3 that the tradeoff performance in the presence of NBI can be significantly improved by replacing the DS-CDMA system with an MC-CDMA system. However, the performance improvements rely on the assumption that the receiver perfectly knows both the location as well as the power of the jammer. When the jammer is rapidly varying, it may be difficult in practice to identify the location of the jammer, let alone know its power. An evaluation of the degradation in the end-to-end distortion performance due to lack of knowledge of the jammer location and power is very important to assess the true benefits of employing an MC-CDMA system.

In both Chapters 2 and 3, we assumed that the receiver has access to perfect CSI. In practice, power and bandwidth have to be invested to estimate the CSI. Effects of imperfect CSI on the tradeoff among source coding, channel coding and spreading is a promising research area.

6.2.3 Chapter 4

In Chapter 4, we employed the Bhattacharyya upper bound to analyze the asymptotic diversity order of noncoherent OOK and BFSK receivers. Unfortunately, at practical SNR values, the Bhattacharyya bound is not very tight. An immediate extension to the results of Chapter 4 is to tighten the upper bounds. While only binary modulations are considered in Chapter 4, extensions of the receiver structures and error probability performances to M-ary modulations, such as M-ary DPSK and orthogonal modulations, is an impor-

tant research problem. Performance comparison between a coherent AF receiver with imperfect CSI and a noncoherent AF receiver without CSI, as a function of the Doppler spread, is needed to determine the conditions under which a noncoherent receiver is more attractive than a coherent receiver on rapidly varying fading channels.

6.2.4 Chapter 5

In Chapter 5, we assumed equal bandwidth for the source and the M relays. However, it may be possible to improve the outage performance by jointly optimizing the transmission power and the channel time/bandwidth resources [65]. Notice that the presented power allocation approach requires a centralized controller to optimally allocate the transmission powers. In practical systems, due to complexity/implementation concerns, it may be highly useful to have a distributed alternative to the approach presented here. In addition to the Lagrange formulation, ideas such as primal- or dual-decomposition techniques [82] may be starting points to perform power allocation in a distributed manner. Finally, we assume that the mean channel gains are perfectly known, whereas, in practice, they have to be estimated from the received signal [83]. Assessing the effects of noisy estimates of mean channel gains on the outage performance is very important to gain a better understanding of the power allocation policies.

APPENDIX A

A Lower Bound on the Pairwise Error Probability

We start with the conditional PEP of (2.19). With the assumption of $\mathbf{x}$ and $\mathbf{y}$ differing in the first d positions, using (2.21), the conditional PEP of (2.19) can be conveniently written as

$$P_2(d|\underline{\beta}) = Q\left(\sqrt{2\Gamma\sum_{n=1}^{d}\beta_n^2}\right) = \frac{1}{\pi}\int_{\theta=0}^{\frac{\pi}{2}} d\theta \exp\left(-\frac{\Gamma\sum_{l=0}^{L-1}\sum_{n=1}^{d}\alpha_l^2[n]}{\sin^2\theta}\right), \qquad \text{(A.1)}$$

where $Q(x) = 1/\sqrt{2\pi}\int_{x}^{\infty}\exp(-u^2/2)du$ and the second step of (A.1) is due to the alternate representation of $Q(x)$ as $Q(x) = 1/\pi\int_{0}^{\pi/2}\exp(-x^2/(2\sin^2\theta))d\theta$, as presented in [84]. Upon averaging (A.1) over the pdf of $\{\alpha\}$, as given in (2.3), we obtain

$$\overline{P}_2(d) = \frac{1}{\pi}\int_{\theta=0}^{\frac{\pi}{2}} d\theta \prod_{l=0}^{L-1}\left(\frac{\sin^2\theta}{\sin^2\theta + \frac{\Gamma\Omega_l}{m_l}}\right)^{m_l d}. \qquad \text{(A.2)}$$

A lower bound on $\overline{P}_2(d)$ can be obtained by using the inequality $\sin^2\theta + \Gamma\Omega_l/m_l \leq 1 + \Gamma\Omega_l/m_l \leq 1 + 2\Gamma\Omega_l \leq 1 + 2\Gamma\max_l\Omega_l$. By defining $\omega = 2\max_l\Omega_l$, we now lower bound (A.2) as

$$\overline{P}_2(d) \;\geq\; (1+\Gamma\omega)^{-d\sum_{l=0}^{L-1}m_l}\frac{1}{\pi}\int_{\theta=0}^{\frac{\pi}{2}} d\theta\left[\sin^2\theta\right]^{d\sum_{l=0}^{L-1}m_l}$$

$$\triangleq \quad D(m,d)(1+\Gamma\omega)^{-md}, \tag{A.3}$$

where, as previously defined in Chap. 2, $m = \sum_{l=0}^{L-1} m_l$, and

$$\begin{aligned} D(m,d) &= \frac{1}{\pi}\int_{\theta=0}^{\frac{\pi}{2}} d\theta \left[\sin^2\theta\right]^{d\sum_{l=0}^{L-1} m_l} \\ &= \frac{1}{2\pi}\beta\left(md+\frac{1}{2},\frac{1}{2}\right), \end{aligned} \tag{A.4}$$

where $\beta(p,q) = 2\int_0^{\pi/2} d\theta \sin^{2p-1}\theta\cos^{2q-1}\theta$ is the standard beta integral [36].

APPENDIX **B**

Convexity of $D_{lower}(r_s)$

Upon taking the derivative of (2.31), we obtain

$$\begin{aligned}
\frac{d^2}{dr_s^2}D_{lower}(r_s) &= 4\epsilon(\ln 2)^2 2^{-2r_s} + 2t(d_{free})D(m,d_{free})\epsilon(\ln 2)\times \\
&\quad \left(-2^{-2r_s} m d_{free}\omega(1+\Gamma\omega)^{-md_{free}-1}\frac{d\Gamma}{dr_s}\right) \\
&- 4\epsilon t(d_{free})D(m,d_{free})(1+\Gamma\omega)^{-md_{free}}(\ln 2)^2 2^{-2r_s} \\
&+ 2\epsilon t(d_{free})D(m,d_{free})(\ln 2)2^{-2r_s}\times \\
&\quad \left(-md_{free}\omega(1+\Gamma\omega)^{-md_{free}-1}\frac{d\Gamma}{dr_s}\right) \\
&+ t(d_{free})D(m,d_{free})(1-\epsilon 2^{-2r_s})\times \\
&\quad \Big(md_{free}(md_{free}+1)(1+\Gamma\omega)^{-md_{free}-2}\omega^2\left(\frac{d\Gamma}{dr_s}\right)^2 - \\
&\quad md_{free}\omega(1+\Gamma\omega)^{-md_{free}-1}\frac{d^2\Gamma}{dr_s^2}\Big), \qquad \text{(B.1)}
\end{aligned}$$

where $d\Gamma/dr_s$ is given in (2.32), whose derivative, $d^2\Gamma/dr_s^2$, can be calculated as

$$\frac{d^2\Gamma}{dr_s^2} = -\frac{d\Gamma}{dr_s}\left(\frac{\frac{\Delta\gamma_b}{C_0}}{1+r_s\frac{\Delta\gamma_b}{C_0}}\right) + \frac{\Gamma\frac{\Delta\gamma_b}{C_0}}{(1+r_s\frac{\Delta\gamma_b}{C_0})^2}\frac{\Delta\gamma_b}{C_0} = 2\Gamma\left(\frac{\frac{\Delta\gamma_b}{C_0}}{1+r_s\frac{\Delta\gamma_b}{C_0}}\right)^2, \qquad \text{(B.2)}$$

which is always positive. Upon rearranging (B.1), by keeping in mind that

$$t(d_{free})D(m,d_{free})(1+\Gamma\omega)^{-md_{free}} < 1,$$

we arrive at

$$\begin{aligned}
&\frac{d^2}{dr_s^2} D_{lower}(r_s) = -4\epsilon(\ln 2) 2^{-2r_s} t(d_{free}) D(m, d_{free}) \times \\
&m d_{free} \omega (1+\Gamma\omega)^{-m d_{free}-1} \frac{d\Gamma}{dr_s} + \\
&4\epsilon(\ln 2)^2 2^{-2r_s} \left(1 - t(d_{free}) D(m, d_{free}) (1+\Gamma\omega)^{-m d_{free}}\right) + \\
&(1-\epsilon 2^{-2r_s})(1+\Gamma\omega)^{-m d_{free}-2} t(d_{free}) D(m, d_{free}) m d_{free} \omega \times \\
&\left(\frac{\frac{\Delta\gamma_b}{C_0}}{1 + r_s \frac{\Delta\gamma_b}{C_0}}\right)^2 \left(\omega(m d_{free}+1)\Gamma^2 - 2(1+\Gamma\omega)\Gamma\right). \qquad \text{(B.3)}
\end{aligned}$$

Note that the first two terms of (B.3) are always positive. Now consider the expression $\omega(md_{free}+1)\Gamma^2 - 2(1+\Gamma\omega)\Gamma$ in the third term of (B.3), which can be simplified as

$$\begin{aligned}
\omega(m d_{free}+1)\Gamma^2 - 2(1+\Gamma\omega)\Gamma &= (\Gamma\omega(m d_{free}-1) - 2)\,\Gamma \\
&= \left(2\Gamma \max_l\{\Omega_l\}(m d_{free}-1) - 2\right)\Gamma \\
&= 2\left(\Gamma \max_l\{\Omega_l\}(m d_{free}-1) - 1\right)\Gamma. \qquad \text{(B.4)}
\end{aligned}$$

Since $md_{free} > 1$ and $\Gamma \max_l\{\Omega_l\} = \overline{\Gamma}_{\max}$ is the maximum average SINR ratio which we have assumed to be greater than unity (i.e., 0 dB), (B.4) is always positive. Thus, the third term of (B.3) is also positive, which proves that $D_{lower}(r_s)$ is convex.

APPENDIX C

Derivation of Eqn. (4.30)

We need to find the distribution of $U = \sum_{j=1}^{N} U_j$, $N \geq 1$, where the U_js are independent exponential rvs. The mean of U_j is given by $\overline{U}_j$. We consider the case where all $\overline{U}_j$ are distinct. The Laplace transform of the pdf of U_j, $\mathcal{L}_{U_j}(s) = E[\exp(-sU_j)]$, is given by $1/(1 + s\overline{U}_j)$, and the Laplace transform of the pdf of U, $\mathcal{L}_U(s) = E[\exp(-sU)]$, is given by the product of the individual Laplace transforms, $\prod_{j=1}^{N} 1/(1 + s\overline{U}_j)$. Using partial fractions techniques, we can write $\mathcal{L}_U(s) = \sum_{n=1}^{N} \frac{\zeta_j}{(1+s\overline{U}_j)}$, where $\zeta_j = \prod_{i=1, i\neq j}^{N} \frac{\overline{U}_j}{\overline{U}_j - \overline{U}_i}$. Upon inversion, we have the following expression for the pdf of U:

$$f_U\left(x; \overline{U}_1, \ldots, \overline{U}_N\right) = \sum_{j=1}^{N} \frac{\zeta_j}{\overline{U}_j} \exp\left(-\frac{x}{\overline{U}_j}\right) \qquad x \geq 0. \tag{C.1}$$

Integrating (C.1) from 0 to y, the cumulative distribution function of U becomes

$$F_U\left(y; \overline{U}_1, \ldots, \overline{U}_N\right) = \sum_{j=1}^{N} \zeta_j \left(1 - \exp\left(-\frac{y}{\overline{U}_j}\right)\right) \qquad y \geq 0. \tag{C.2}$$

When the signal is not present, from (4.2) and (4.3), we note that $Z_{DS} = |r_{DS}|^2/\sigma_N^2$ and $Z_{DR}^j = |r_{DR}^j|^2/\sigma_N^2$, $j = 1, \ldots, M$, are independent, exponentially distributed r.vs with mean values 1 and $1 + \frac{\overline{\gamma}_3^j}{1+\overline{\gamma}_2^j}$, $j = 1, \ldots, M$, respectively. That is, $c_1 Z_{DS}$ and $c_2^j Z_{DR}^j$ are exponentially distributed with mean values $\overline{X}_0 = \frac{2\overline{\gamma}_1}{1+2\overline{\gamma}_1}$ and $\overline{Y}_0^j = \frac{2\overline{\gamma}_2^j\overline{\gamma}_3^j}{(1+\overline{\gamma}_2^j+\overline{\gamma}_3^j)(1+\lambda(\overline{\gamma}_2^j)\overline{\gamma}_3^j)}$,

respectively. The probability of error is given by

$$\text{Prob}\left(c_1 Z_{DS} + \sum_{j=1}^{M} c_2^j Z_{DR}^j > \text{T}_\text{h}\right),$$

which can be evaluated by applying (C.2) as

$$1 - F_U\left(\text{T}_\text{h}; \overline{X}_0, \overline{Y}_0^1, \ldots, \overline{Y}_0^M\right). \tag{C.3}$$

In the presence of signal, again from (4.2) and (4.3), notice that Z_{DS} and Z_{DR}^j are independent exponentially distributed rvs with mean values $1 + 2\overline{\gamma}_1$ and $1 + \frac{\overline{\gamma}_3^j}{1+\overline{\gamma}_2^j} + \frac{2\overline{\gamma}_2^j\overline{\gamma}_3^j}{1+\overline{\gamma}_2^j} = 1 + \lambda(\overline{\gamma}_2^j)\overline{\gamma}_3^j$, respectively. That is, $c_1 Z_{DS}$ and $c_2^j Z_{DR}^j$ are exponentially distributed with mean values $\overline{X}_1 = 2\overline{\gamma}_1$ and $\overline{Y}_1^j = \frac{2\overline{\gamma}_2^j\overline{\gamma}_3^j}{(1+\overline{\gamma}_2^j+\overline{\gamma}_3^j)}$, respectively. The probability of error is given by

$$\text{Prob}\left(c_1 Z_{DS} + \sum_{j=1}^{M} c_2^j Z_{DR}^j < \text{T}_\text{h}\right),$$

and is simplified by using (C.2) as

$$F_U\left(\text{T}_\text{h}; \overline{X}_1, \overline{Y}_1^1, \ldots, \overline{Y}_1^M\right). \tag{C.4}$$

Finally, upon averaging (C.3) and (C.4), we arrive at (4.30).

APPENDIX **D**

Derivation of Eqn. (4.52)

In this appendix, we derive an expression for the probability that $U = \sum_{j=1}^{N} U_j$ is less than $V = \sum_{j=1}^{N} V_j$, where U_j, V_j, $j = 1, \ldots, N$, are independent exponentially distributed r.vs with U_j having mean $\overline{U}_j$ and V_j having mean $\overline{V}_j$. For simplicity, We assume that all $\overline{U}_j$ and $\overline{V}_j$ are distinct. The case with $\overline{U}_j$ and $\overline{V}_j$ having non-distinct values can be treated in a similar manner. Conditioned on V, we have already obtained an expression for $F_{U|V}(\cdot)$ in (C.2). Upon averaging (C.2) over the pdf of V, as given in (C.1), we obtain

$$\begin{aligned} \text{Prob}\,(U < V) &= \sum_{i=1}^{N} \sum_{j=1}^{N} \frac{\kappa_i \zeta_j}{\overline{V}_i} \int_{x=0}^{\infty} \left\{ e^{-\frac{x}{\overline{V}_i}} - e^{-\frac{x(\overline{V}_i + \overline{U}_j)}{\overline{V}_i \overline{U}_j}} \right\} dx \\ &= \sum_{i=1}^{N} \sum_{j=1}^{N} \kappa_i \zeta_j \left(\frac{\overline{V}_i}{\overline{V}_i + \overline{U}_j} \right), \end{aligned} \tag{D.1}$$

where $\kappa_j = \prod_{i=1, i \neq j}^{N} \frac{\overline{V}_j}{\overline{V}_j - \overline{V}_i}$.

APPENDIX **E**

Performance of Suboptimum OOK Receiver of Eqn. (4.71)

In this appendix, we present an analysis for the performance of the suboptimum OOK receiver of (4.26) with M relay nodes. To start with, when the signal present, we denote $(c_1 Z_{DS} + \sum_{j=1}^{M} c_2^j Z_{DR}^j)/\mathrm{T_h}$ by W_1, whereas the same expression is denoted by W_0 when the signal is absent. With this, the average BER of OOK receiver of (4.26) is given by

$$\begin{aligned}\overline{P}_{e,\text{On-Off,Subopt}} &= \frac{1}{2}\text{Prob}(\mathsf{W}_1 < 1|b=1) + \frac{1}{2}\text{Prob}(\mathsf{W}_0 > 1|b=0) \\ &= \frac{1}{4\pi j}\int_{p_1-j\infty}^{p_1+j\infty} ds\mathcal{L}_{\mathsf{W}_1}(s)\frac{e^s-1}{s} - \frac{1}{4\pi j}\int_{p_2-j\infty}^{p_2+j\infty} ds\mathcal{L}_{\mathsf{W}_0}(s)\frac{e^s}{s}, \quad \text{(E.1)}\end{aligned}$$

where $\mathcal{L}_{\mathsf{W}_0}(s)$ and $\mathcal{L}_{\mathsf{W}_1}(s)$ are the Laplace transforms of the pdf of W_0 and W_1, respectively, $p_1 > 0$, $p_2 < 0$, and the second equality in (E.1) is due to the fact that

$$\begin{aligned}\text{Prob}(w_0 < \mathsf{W} < w_1) &= \int_{w_0}^{w_1} f_{\mathsf{W}}(w)dw = \int_{w_0}^{w_1} dw \int_{p-j\infty}^{p+j\infty} \mathcal{L}_{\mathsf{W}}(s)e^{ws}\frac{ds}{2\pi j} \\ &= \int_{p-j\infty}^{p+j\infty} ds\mathcal{L}_{\mathsf{W}}(s)\frac{e^{sw_1}-e^{sw_0}}{2\pi j s}. \quad \text{(E.2)}\end{aligned}$$

In (E.2), we have used the relationship $f_{\mathsf{W}}(w) = 1/(2\pi j)\int_{p-j\infty}^{p+j\infty} \mathcal{L}_{\mathsf{W}}(s)e^{sw}ds$ between the pdf of W and its Laplace transform $\mathcal{L}_{\mathsf{W}}(s)$. Here, p is chosen to ensure the convergence

of the integral.

Note that, when the signal is present, we see that Z_{DS} is exponentially distributed with mean $1 + 2\overline{\gamma}_1$, whereas Z_{DR}^j, conditioned on γ_3^j, is exponentially distributed with mean $1 + \lambda(\overline{\gamma}_2^j)\gamma_3^j$. Since Z_{DS} and Z_{DR}^j, $j = 1, \ldots, M$, are independent, the conditional Laplace transform of W_1, conditioned on $\{\gamma_3^j\}_{j=1}^M$, is given by

$$\mathcal{L}_{\mathsf{W}|\{\gamma_3^j\}_{j=1}^M}(s) = \frac{1}{1 + s(1 + 2\overline{\gamma}_1)c_1/\mathrm{T_h}} \prod_{j=1}^{M} \frac{1}{1 + s(1 + \lambda(\overline{\gamma}_2^j)\gamma_3^j)c_2^j/\mathrm{T_h}}. \tag{E.3}$$

Upon averaging over $\{\gamma_3^j\}_{j=1}^M$, the Laplace transform $\mathcal{L}_{\mathsf{W}_1}(s)$ is given by

$$\mathcal{L}_{\mathsf{W}_1}(s) = \frac{\mathrm{T_h}}{\mathrm{T_h} + s(1 + 2\overline{\gamma}_1)c_1} \prod_{j=1}^{M} \int_{x=0}^{\infty} \frac{\mathrm{T_h} \exp(-x)dx}{\mathrm{T_h} + s(1 + \lambda(\overline{\gamma}_2^j)\overline{\gamma}_3^j x)c_2^j}. \tag{E.4}$$

Using the result [36]

$$\int_{x=0}^{\infty} \frac{\exp(-x)}{x + c} dx = \exp(c)E_1(c), \tag{E.5}$$

where $E_1(x) = \int_x^{\infty} e^{-u}du/u$ is the exponential integral defined in [36], we can further simplify (E.4) as

$$\begin{aligned} \mathcal{L}_{\mathsf{W}_1}(s) &= \frac{\mathrm{T_h}}{c_1(1 + 2\overline{\gamma}_1)} \times \frac{1}{s + \mathrm{T_h}/(c_1(1 + 2\overline{\gamma}_2))} \times \\ &\quad \prod_{j=1}^{M} \frac{\mathrm{T_h}}{s\lambda(\overline{\gamma}_2^j)\overline{\gamma}_3^j c_2^j} \exp\left(\frac{\mathrm{T_h} + sc_2^j}{s\lambda(\overline{\gamma}_2^j)\overline{\gamma}_3^j c_2^j}\right) E_1\left(\frac{\mathrm{T_h} + sc_2^j}{s\lambda(\overline{\gamma}_2^j)\overline{\gamma}_3^j c_2^j}\right). \end{aligned} \tag{E.6}$$

When $b = 0$, we note that Z_{DS} is exponentially distributed with mean 1, and Z_{DR}^j, conditioned on γ_3^j, is exponentially distributed with mean $1 + \mu(\overline{\gamma}_2^j)\gamma_3^j$. Upon following the steps of (E.3)-(E.6), $\mathcal{L}_{\mathsf{W}_0}(s)$ can be shown to be given by

$$\mathcal{L}_{\mathsf{W}_0}(s) = \frac{1}{1 + sc_1/\mathrm{T_h}} \times$$

$$\prod_{j=1}^{M} \frac{\mathrm{T_h}}{s\mu(\overline{\gamma}_2^j)\overline{\gamma}_3^j c_2^j} \exp\left(\frac{\mathrm{T_h} + sc_2^j}{s\mu(\overline{\gamma}_2^j)\overline{\gamma}_3^j c_2^j}\right) E_1\left(\frac{\mathrm{T_h} + sc_2^j}{s\mu(\overline{\gamma}_2^j)\overline{\gamma}_3^j c_2^j}\right). \qquad \text{(E.7)}$$

Upon substituting (E.6) and (E.7) in (E.1), we obtain an expression for the average BER for the suboptimum OOK receiver which can be evaluated numerically.

APPENDIX **F**

Performance of Suboptimum BFSK Receiver of Eqn. (4.72)

In this appendix, we present an analysis on the performance of the suboptimum BFSK receiver of (4.72) with M relay nodes. Note that, from (4.72), when frequency f_1 is assumed to be transmitted, the r.vs $Z_{DS,1}$ and $Z_{DS,2}$ are independent, exponentially distributed with respective mean values $1+\overline{\gamma}_1$ and 1. For $j=1,\ldots,M$, the r.vs $Z^j_{DR,1}$ and $Z^j_{DR,2}$, conditioned on γ^j_3, are independent and exponentially distributed with respective mean values $1+\gamma^j_3$ and $1+\mu(\overline{\gamma}^j_2)\gamma^j_3$. Let us define the constants $a_0=\overline{\gamma}_1/(1+\overline{\gamma}_1)$ and $a_j=\overline{\gamma}^j_2\overline{\gamma}^j_3/((1+\overline{\gamma}^j_3)(1+\overline{\gamma}^j_2+\overline{\gamma}^j_3))$, $j=1,\ldots,M$. With this, (4.72) can be written as

$$\mathrm{LLR}_{\text{Subopt}}(b)=a_0\left[Z_{DS,1}-Z_{DS,2}\right]+\sum_{j=1}^{M}a_j\left[Z^j_{DR,1}-Z^j_{DR,2}\right]. \tag{F.1}$$

The probability of error is then given by

$$\overline{P}_{e,\mathrm{BFSK}}=\mathrm{Prob}\left(\mathrm{LLR}_{\text{Subopt}}(b)<0\right)=\frac{1}{2\pi j}\int_{p-j\infty}^{p+j\infty}\mathcal{L}_{\mathrm{LLR}_{\text{Subopt}}(b)}(s)\frac{ds}{s}, \tag{F.2}$$

where, in (F.2), $\mathcal{L}_{\mathrm{LLR}_{\text{Subopt}}(b)}(s)$ is the Laplace transform of the pdf of $\mathrm{LLR}_{\text{Subopt}}(b)$, and $p>0$. All we now need is a closed-form expression for $\mathcal{L}_{\mathrm{LLR}_{\text{Subopt}}(b)}(s)$, which can be found as follows: Due to the independence of the r.v pairs $(Z_{DS,1},Z_{DS,2})$, $(Z^1_{DR,1},Z^1_{DR,2})$, $\ldots$, $(Z^M_{DR,1},Z^M_{DR,2})$,

we can write

$$\begin{aligned}
\mathcal{L}_{\mathrm{LLR}_{\mathrm{Subopt}(b)}}(s) &= E\left[\exp\left(-sa_0\left[Z_{DS,1}-Z_{DS,2}\right]\right)\right]\times \\
&\quad \prod_{j=1}^{M} E\left[\exp\left(-sa_j\left[Z^j_{DR,1}-Z^j_{DR,2}\right]\right)\right] \\
&= E\left[\exp\left(-sa_0 Z_{DS,1}\right)\right]\times E\left[\exp\left(sa_0 Z_{DS,2}\right)\right]\times \\
&\quad \prod_{j=1}^{M} E_{\gamma_3^j}\left\{E\left[\exp\left(-sa_j\left[Z^j_{DR,1}-Z^j_{DR,2}\right]\right)\Big|\gamma_3^j\right]\right\} \\
&= \frac{1}{1+s\overline{\gamma}_1}\times\frac{1}{1-\frac{\overline{\gamma}_1}{1+\overline{\gamma}_1}s}\times \\
&\quad \prod_{j=1}^{M} E_{\gamma_3^j}\left\{E\left[\exp\left(-sa_jZ^j_{DR,1}\right)\Big|\gamma_3^j\right]E\left[\exp\left(sa_jZ^j_{DR,2}\right)\Big|\gamma_3^j\right]\right\} \\
&= \frac{1+\overline{\gamma}_1}{1+s\overline{\gamma}_1}\times\frac{1}{1+\overline{\gamma}_1(1-s)}\times \\
&\quad \prod_{j=1}^{M} E_{\gamma_3^j}\left\{\frac{1}{1+sa_j(1+\gamma_3^j)}\times\frac{1}{1-sa_j(1+\mu(\overline{\gamma}_2^j)\gamma_3^j)}\right\} \\
&= \frac{1+\overline{\gamma}_1}{1+s\overline{\gamma}_1}\times\frac{1}{1+\overline{\gamma}_1(1-s)}\times \\
&\quad \prod_{j=1}^{M}\int_{x=0}^{\infty}\frac{\exp(-x)dx}{(1+sa_j(1+\overline{\gamma}_3^j x))\times(1-sa_j(1+\mu(\overline{\gamma}_2^j)\overline{\gamma}_3^j x))}. \qquad \text{(F.3)}
\end{aligned}$$

Each integral in the product of (F.3) can be simplified as follows:

$$\begin{aligned}
&\int_{x=0}^{\infty}\frac{\exp(-x)dx}{(1+sa_j(1+\overline{\gamma}_3^j x))(1-sa_j(1+\mu(\overline{\gamma}_2^j)\overline{\gamma}_3^j x))} = \frac{1}{(1-s^2a_j^2)}\times \\
&\int_{x=0}^{\infty}\frac{\exp(-x)dx}{(1+\frac{sa_j\overline{\gamma}_3^j}{1+sa_j}x)(1+\frac{sa_j\mu(\overline{\gamma}_2^j)\overline{\gamma}_3^j}{sa_j-1}x)} \\
&= \frac{1}{(1-s^2a_j^2)}\times\int_{x=0}^{\infty}\exp(-x)dx\left\{\frac{\mathsf{K}_1(j)}{1+\beta_1(j)x}+\frac{\mathsf{K}_2(j)}{1+\beta_2(j)x}\right\}, \qquad \text{(F.4)}
\end{aligned}$$

where, with the help of partial fractions,

$$\beta_1(j) = \frac{sa_j\overline{\gamma}_3^j}{1+sa_j} \tag{F.5}$$

$$\beta_2(j) = \frac{sa_j\mu(\overline{\gamma}_2^j)\overline{\gamma}_3^j}{sa_j-1} \tag{F.6}$$

$$\mathsf{K}_1(j) = \frac{\beta_1(j)}{\beta_1(j)-\beta_2(j)} \tag{F.7}$$

$$\text{and} \qquad \mathsf{K}_2(j) = \frac{\beta_2(j)}{\beta_2(j)-\beta_1(j)}. \tag{F.8}$$

With the help of (E.5), the integral in (F.4) can be written in closed-form as

$$\int_{x=0}^{\infty} \frac{\exp(-x)dx}{(1+sa_j(1+\overline{\gamma}_3^j x))(1-sa_j(1+\mu(\overline{\gamma}_2^j)\overline{\gamma}_3^j x)} = \frac{1}{(1-s^2a_j^2)} \times$$
$$\Big\{\frac{\mathsf{K}_1(j)}{\beta_1(j)}\exp\left(\frac{1}{\beta_1(j)}\right)E_1\left(\frac{1}{\beta_1(j)}\right) +$$
$$\frac{\mathsf{K}_2(j)}{\beta_2(j)}\exp\left(\frac{1}{\beta_2(j)}\right)E_1\left(\frac{1}{\beta_2(j)}\right)\Big\}. \tag{F.9}$$

Upon using (F.9), (F.4) and (F.3) in (F.2), a single integral-based expression can be obtained for the average BER of the suboptimum BFSK receiver.

We now examine the behavior of (F.2) at high SNR. To be consistent with the approaches taken in Sections 4.3 and 4.4, we use $\overline{\gamma}_1 = \mathsf{t}_1\overline{\gamma}$, and, for $j = 1, \ldots, M$, $\overline{\gamma}_2^j = \mathsf{t}_2^j\overline{\gamma}$, and $\overline{\gamma}_3^j = \mathsf{t}_3^j$, and let $\overline{\gamma} \to \infty$. We first notice that the coefficients a_j, $j = 0, 1, \ldots, M$, in (F.1) are not functions of $\overline{\gamma}$. To analyze (F.2) as $\overline{\gamma} \to \infty$, we need to capture the behavior of $\mathcal{L}_{\mathrm{LLR}_{\text{Subopt}(b)}}(s)$ as $\overline{\gamma} \to \infty$. From (F.3), $\mathcal{L}_{\mathrm{LLR}_{\text{Subopt}(b)}}(s)$ can be approximated as

$$\mathcal{L}_{\mathrm{LLR}_{\text{Subopt}(b)}}(s) = \frac{\frac{1}{\overline{\gamma}}+\mathsf{t}_1}{\frac{1}{\overline{\gamma}}+s\mathsf{t}_1} \times \frac{1}{\overline{\gamma}} \times \frac{1}{\frac{1}{\overline{\gamma}}+\mathsf{t}_1(1-s)} \times$$
$$\prod_{j=1}^{M}\frac{1}{\overline{\gamma}} \times \int_{x=0}^{\infty} \frac{\exp(-x)dx}{(\frac{1}{\overline{\gamma}}+sa_j(\frac{1}{\overline{\gamma}}+\mathsf{t}_3^j x)) \times (1-sa_j(1+\frac{\mathsf{t}_3^j\overline{\gamma}}{1+\overline{\gamma}\mathsf{t}_2^j}x))}$$

$$\approx \left(\frac{1}{\overline{\gamma}}\right)^{M+1} \underbrace{\left[\frac{1}{s} \times \frac{1}{\mathsf{t}_1(1-s)} \prod_{j=1}^{M} \int_{x=0}^{\infty} \frac{\exp(-x)dx}{(sa_j\mathsf{t}_3^j x) \times (1 - sa_j(1 + \frac{\mathsf{t}_3^j}{1+\mathsf{t}_2^j}x))}\right]}_{\triangleq \Lambda(s)}. \quad \text{(F.10)}$$

Note that the term, $\Lambda(s)$, in square brackets of (F.10) is not a function of $\overline{\gamma}$. As a result, the average BER of (F.2), as $\overline{\gamma} \to \infty$, can be expressed as

$$\overline{P}_{e,\mathrm{BFSK}} \approx \left(\frac{1}{\overline{\gamma}}\right)^{M+1} \times \left[\frac{1}{2\pi j} \int_{p-j\infty}^{p+j\infty} \Lambda(s) \frac{ds}{s}\right]. \quad \text{(F.11)}$$

Eqn. (F.11) shows that the proposed suboptimum BFSK detector achieves the full diversity order of $M + 1$ as $\overline{\gamma} \to \infty$.

APPENDIX G

Asymptotic CDF Approximations

In this appendix, we develop an approximation for the cdf of a r.v

$$Z = \sum_{i=1}^{N} X_i^2, \tag{G.1}$$

where the X_is belong to a population of independent Rician or Nakagami r.vs with arbitrary parameters, when the second moments of X_is are large.

G.1 All Xs belong to the Rician Family

Let X_i be a Rician r.v with Rice factor K_i and second moment $E[X_i^2] = \Omega_i$. That is, the pdf of X_i is [57]

$$f_{X_i}(x) = \frac{2x(1+K_i)}{\Omega_i} e^{-K_i - \frac{(1+K_i)}{\Omega_i}x^2} I_0\left(2x\sqrt{\frac{K_i(1+K_i)}{\Omega_i}}\right) \quad x \geq 0, \tag{G.2}$$

where $I_0(\cdot)$ is the zero-order modified Bessel function of first kind [85]. The Laplace transform of the pdf of X_i^2 is [57]

$$\mathcal{L}_{X_i^2}(s) = E[e^{-sX_i^2}] = \frac{\exp\left(-\frac{\frac{sK_i\Omega_i}{1+K_i}}{1+\frac{\Omega_i s}{1+K_i}}\right)}{1+\frac{\Omega_i s}{1+K_i}}. \tag{G.3}$$

The Laplace transform of the pdf of Z in (G.1) is simply

$$\mathcal{L}_Z(s) = \prod_{i=1}^{N} \mathcal{L}_{X_i^2}(s). \tag{G.4}$$

For large Ω_i, we can approximate (G.3) as

$$\mathcal{L}_{X_i^2}(s) \approx \left(\frac{1+K_i}{\Omega_i}\right) \frac{e^{-K_i}}{s}. \tag{G.5}$$

Then, using (G.5), an approximation to (G.4) is

$$\begin{aligned} \mathcal{L}_Z(s) &\approx \prod_{i=1}^{N} \left(\frac{1+K_i}{\Omega_i}\right) \frac{e^{-K_i}}{s} \\ &= \frac{e^{-\sum_{i=1}^{N} K_i}}{s^N} \prod_{i=1}^{N} \left(\frac{1+K_i}{\Omega_i}\right). \end{aligned} \tag{G.6}$$

The inverse Laplace transform of (G.6), using [85], gives us an approximation to the pdf of Z as

$$f_Z(z) \approx \left[\prod_{i=1}^{N} \left(\frac{1+K_i}{\Omega_i}\right)\right] \frac{e^{-\sum_{i=1}^{N} K_i}}{\Gamma(N)} z^{N-1} \quad z \geq 0. \tag{G.7}$$

Therefore, the probability that Z is less than α is

$$\text{Prob}\left(Z < \alpha\right) \approx \left[\prod_{i=1}^{N} \left(\frac{1+K_i}{\Omega_i}\right)\right] \frac{e^{-\sum_{i=1}^{N} K_i}}{\Gamma(N+1)} \alpha^N. \tag{G.8}$$

When the X_is are Rayleigh distributed, we have $K_i = 0, \forall\, i = 1, \ldots, N$. Then (G.8) simplifies to

$$\text{Prob}\left(Z < \alpha\right) \approx \frac{1}{\prod_{i=1}^{N} \Omega_i} \times \frac{\alpha^N}{\Gamma(N+1)}. \tag{G.9}$$

G.2 All Xs belong to the Nakagami Family

When X_i is a Nakagami r.v with Nakagami parameter m_i and second moment $E[X_i^2] = \Omega_i$, then the pdf of X_i is [57]

$$f_{X_i}(x) = \frac{2m_i^{m_i}}{\Omega_i^{m_i}\Gamma(m_i)} \exp\left(-\frac{m_i x^2}{\Omega_i}\right) x^{2m_i-1} \quad x \geq 0, \tag{G.10}$$

The Laplace transform of the pdf of X_i^2 is [86]

$$\mathcal{L}_{X_i^2}(s) = \left(\frac{m_i}{m_i + \Omega_i s}\right)^{m_i}. \tag{G.11}$$

The Laplace transform of the pdf of Z in (G.1) is then

$$\mathcal{L}_Z(s) = \prod_{i=1}^{N} \left(\frac{m_i}{m_i + \Omega_i s}\right)^{m_i}. \tag{G.12}$$

For large Ω_i, we can approximate (G.11) as

$$\mathcal{L}_{X_i^2}(s) \approx \left(\frac{m_i}{\Omega_i}\right)^{m_i} \frac{1}{s^{m_i}}. \tag{G.13}$$

Then, using (G.13), an approximation to (G.12) is

$$\mathcal{L}_Z(s) \approx \left\{\prod_{i=1}^{N} \left(\frac{m_i}{\Omega_i}\right)^{m_i}\right\} \times \frac{1}{s^{\sum_{i=1}^{N} m_i}}. \tag{G.14}$$

The inverse Laplace transform of (G.14), using [85], is

$$f_Z(z) \approx \left\{\prod_{i=1}^{N} \left(\frac{m_i}{\Omega_i}\right)^{m_i}\right\} \times \frac{z^{(\sum_{i=1}^{N} m_i)-1}}{\Gamma\left(\sum_{i=1}^{N} m_i\right)} \quad z \geq 0. \tag{G.15}$$

Therefore, the probability that Z is less than α is

$$\text{Prob}\left(Z<\alpha\right)\approx\left\{\prod_{i=1}^{N}\left(\frac{m_i}{\Omega_i}\right)^{m_i}\right\}\times\frac{\alpha^{\sum_{i=1}^{N}m_i}}{\Gamma\left(1+\sum_{i=1}^{N}m_i\right)}. \tag{G.16}$$

With Rayleigh fading, we have $m_i=1,\forall\, i=1,\ldots,N$, and (G.16) reduces to (G.9).

G.3 The General Case

Let us now assume that out of N X_is N_1 of them come from the Rician distribution, whereas the remaining $N_2=N-N_1$ ones come from the Nakagami distribution. Then, using (G.6) and (G.14), an approximation to the Laplace transform of Z is

$$\mathcal{L}_Z(s)\approx\frac{e^{-\sum_{i=1}^{N_1}K_i}}{s^{N_1+\sum_{j=1}^{N_2}m_j}}\prod_{i=1}^{N_1}\left(\frac{1+K_i}{\Omega_i}\right)\prod_{j=1}^{N_2}\left(\frac{m_j}{\Omega_j}\right)^{m_j}. \tag{G.17}$$

Upon inversion, the pdf of Z is

$$f_Z(z)\approx\frac{e^{-\sum_{i=1}^{N_1}K_i}z^{N_1-1+\sum_{j=1}^{N_2}m_j}}{\Gamma\left(N_1+\sum_{j=1}^{N_2}m_j\right)}\prod_{i=1}^{N_1}\left(\frac{1+K_i}{\Omega_i}\right)\prod_{j=1}^{N_2}\left(\frac{m_j}{\Omega_j}\right)^{m_j}. \tag{G.18}$$

The cdf of Z is then

$$\text{Prob}\left(Z<\alpha\right)\approx\frac{e^{-\sum_{i=1}^{N_1}K_i}\alpha^{N_1+\sum_{j=1}^{N_2}m_j}}{\Gamma\left(N_1+1+\sum_{j=1}^{N_2}m_j\right)}\prod_{i=1}^{N_1}\left(\frac{1+K_i}{\Omega_i}\right)\prod_{j=1}^{N_2}\left(\frac{m_j}{\Omega_j}\right)^{m_j}. \tag{G.19}$$

REFERENCES

[1] Y. K. Kim and R. Prasad, *4G Roadmap and Emerging Communication Technologies,* Artech House, 2006.

[2] S. Shakkottai, T. S. Rappaport, and P. C. Karlsson, "Cross-layer design for wireless networks," *IEEE Commun. Magazine,* vol. 41, no. 10, Oct. 2003, pp. 74-80.

[3] V. Kawadia and P. R. Kumar, "A cautionary perspective on cross-layer design," *IEEE Wireless Commun.,* vol. 12, no. 1, Feb. 2005, pp. 3-11.

[4] M. V. D. Schaar and S. N. Shankar, "Cross-layer wireless multimedia transmission: Challenges, principles, and new paradigms," *IEEE Wireless Commun.,* vol. 12, no. 4, Aug. 2005, pp. 50-58.

[5] V. Srivastava and M. Motani, "Cross-layer design: A survey and the road ahead," *IEEE Commun. Magazine,* vol. 43, no. 12, Dec. 2005, pp. 112-119.

[6] A. S. Tanenbaum, *Computer Networks,* Second Edition, Printice-Hall, Englewood Cliffs, NJ, 1989.

[7] B. Hochwald and K. Zeger, "Tradeoff between source and channel coding," *IEEE Trans. Info. Theory,* vol. 43, September 1997, pp. 1412-24.

[8] B. Hochwald, "Tradeoff between source and channel coding on a Gaussian channel," *IEEE Trans. Info. Theory,* vol. 44, November 1998, pp. 3044-3055.

[9] A. Mehes and K. Zeger, "Source and channel rate allocation for channel codes satisfying the Gilbert-Varshamov or Tsfasman-Vladut-Zink bounds," *IEEE Trans. Info. Theory,* vol. 46, no. 6, September 2000, pp. 2133-2151.

[10] J. Y. N. Hui, "Throughput analysis for code-division multiple accessing of the spread-spectrum channel," *IEEE Journal on Select. Areas Commun.,* vol. 2, July 1984, pp. 482-486.

[11] K. H. Li and L. B. Milstein, "On the optimum processing gain of a block-coded direct-sequence spread-spectrum system," *IEEE Journal on Selected Areas in Communications,* vol. 7, May 1989, pp. 618-626.

[12] J. L. Massey, "Information theory aspects of spread-spectrum communications," *Proc. IEEE International Symposium on Spread Spectrum Techniques and Applications (ISSSTA),* 1994, pp. 16-21.

[13] M. Bickel, W. Granzow, and P. Schramm, "Optimization of code rate and spreading factor for direct-sequence CDMA systems," in *Proc. Int. Symp. Spread-Spectrum Techniques and Applications (ISSSTA),* vol. 2, 1996, pp. 585-589.

[14] N. B. Mandayam and J. M. Holtzman, "Effect of tracking errors on the coding-spreading tradeoff in CDMA systems," in *Proc. IEEE Int. Conf. Universal Personal Commun. (ICUPC),* 1997, pp. 366-370.

[15] M. Motani and V. V. Veeravalli, "The coding-spreading tradeoff in CDMA systems using convolutional codes and direct-sequence spreading," in *Proc. Conf. Information Sciences and Systems (CISS),* Mar. 2000, pp. TP7-5-10.

[16] V. V. Veeravalli and A. Mantravadi, "The coding-spreading tradeoff in CDMA systems," *IEEE Journal on Sel. Areas. Commun.,* vol. 20, no. 2, February 2002, pp. 396-408.

[17] Z. Lian, J. W. Mark, Y. C. Yoon, "Performance of coding-spreading tradeoff in DS-CDMA systems using RCPT and RCPC codes," *IEEE Transactions on Communications,* vol. 52, no. 6, June 2004, pp. 882-886.

[18] Q. Zhao, P. C. Cosman and L. B. Milstein, "Optimal allocation of bandwidth for source coding, channel coding and spreading in CDMA systems," *IEEE Trans. Commun.,* vol. 52, no. 10, Oct. 2004, pp. 1797 - 1808.

[19] H. Wei and R. D. Gitlin, "WWAN/WLAN two-hop-relay architecture for capacity enchancements," in *Proc. IEEE Wireless Commun. and Networking Conf. (WCNC),* 2004, pp. 225-230.

[20] R. Pabst *et al*, "Relay-based deployment concepts for wireless and mobile broadband radio," *IEEE Comm. Magazine,* vol. 42, no. 9, Sept. 2004, pp. 80-90.

[21] H. Yanikomeroglu, "Infrastructure-based wireless multihop, relay, mesh networks," tutorial notes, given at *Proc. IEEE Wireless Commun. and Networking Conf. (WCNC),* 2006.

[22] E. C. van der Meulen, "Transmission of information in a T-terminal discrete memoryless channel," Ph.D. dissertation, Dept. of Statistics, University of California, Berkeley, 1968.

[23] E. C. van der Meulen, "Three-terminal communication channels," *Adv. Appl. Prob.,* vol. 3, 1971, pp. 120-154.

[24] H. Sato, "Information transmission through a channel with relay," The Aloha System, University of Hawaii, Honolulu, Tech. Rep. B76-7, Mar. 1976.

[25] T. Cover and A. El Gamal, "Capacity theorems for the relay channel," *IEEE Trans. Info. Theory,* vol. 25, no. 5, Sept. 1979, pp. 572-584.

[26] R. Saracco, "Fostering the future of information technology: How to make research investiment more cost-effective," *IEEE Comm. Magazine,* vol. 41, no. 12, Dec. 2003, pp. 38-45.

[27] A. Nosratinia, T. E. Hunter, and A. Hedayat, "Cooperative communication in wireless networks," *IEEE Comm. Magazine,* vol. 42, no. 10, Oct. 2004, pp. 74-80.

[28] R. L. Pickholtz, L. B. Milstein and D. L. Schilling, "Spread spectrum for mobile communications," *IEEE Trans. Veh. Technol.,* vol. 40, May 1991, pp. 313-322.

[29] A. J. Viterbi, *CDMA: Principles of Spread Spectrum Communication,* Reading, MA: Addison-Wesley, 1995.

[30] M. K. Simon, J. K. Omura, R. A. Scholtz and B. K. Levitt, *Spread Spectrum Communications Handbook,* Electronic Edition, McGraw-Hill, 2002.

[31] Q. Zhao, P. C. Cosman and L. B. Milstein, "Tradeoffs in source coding, channel coding and spreading in frequency selective Rayleigh fading channels," *Journal of VLSI Signal Processing,* Kluwer Academic Publishers, vol. 30, no. 1-3, February 2002, pp. 7-20.

[32] A. Mehes and K. Zeger, "Binary lattice vector quantization with linear block codes and affine index assignments," *IEEE Trans. Info. Theory,* vol. 44, January 1998, pp. 79-94.

[33] N. Nakagami, "The m-distribution, a general formula for intensity distribution of rapid fading," in *Statistical Methods in Radio Wave Propagation,* W. G. Hoffman, Ed. Oxford, England: Pergamon, 1960, pp. 3-36.

[34] T. Eng and L. B. Milstein, "Coherent DS-CDMA performance in Nakagami multipath fading," *IEEE Trans. Commun.,* vol. 43, nos. 2-4, 1995, pp. 1134-1143.

[35] G. P. Efthymoglou, V. A. Aalo and H. Helmken, "Performance analysis of coherent DS-CDMA systems in a Nakagami multipath fading channel with arbitrary parameters," *IEEE Trans. Veh. Technol.,* vol. 46, no. 2, May 1997, pp. 289-297.

[36] M. Abramowitz and I. A. Stegun Eds., *Handbook of Mathematical Functions,* 9th printing ed. New York: Dover, 1970.

[37] R. Johannesson and K. Sh. Zigangirov, *Fundamentals of Convolutional Codes,* IEEE Press, 1999.

[38] A. Gersho and R. M. Gray, *Vector Quantization and Signal Compression,* Kluwer Academic Publishers, 1992.

[39] E. Erkip, Y. Wang, D. Goodman, Y. Wu, and X. Lu, "Energy efficient coding and transmission," in *Proc. IEEE Veh. Technol. Conf.,* 2001, pp. 1444-1448.

[40] P. Frenger, P. Orten and T. Ottosson, "Convolutional codes with optimum distance spectrum," *IEEE Commun. Letters,* vol. 3, no. 11, November 1999, pp. 317-319.

[41] J. Hagenauer, "Rate-compatible punctured convolutional codes (RCPC codes) and their applications," *IEEE Trans. Commun.,* vol. 36, no. 4, April 1988, pp. 389-400.

[42] S. Kondo and L. B. Milstein, "On the performance of multicarrier DS CDMA systems," *IEEE Trans. Commun.,* vol. 44, Februray 1996, pp. 238-246.

[43] D. N. Rowitch and L. B. Milstein, "Convolutionally coded multicarrier DS-CDMA systems in a multipath fading channel−Part I: Performance analysis," *IEEE Trans. Commun.,* vol. 47, no. 10, October 1999, pp. 1570-1582.

[44] D. N. Rowitch and L. B. Milstein, "Convolutionally coded multicarrier DS-CDMA systems in a multipath fading channel−Part II: Narrow-band interference suppression," *IEEE Trans. Commun.,* vol. 47, no. 11, November 1999, pp. 1729-1736.

[45] M. Dohler, "Virtual antenna arrays," Ph.D. dissertation, King's College, London, U.K, 2003.

[46] A. Sendonaris, E. Erkip and B. Aazhang, "User cooperation diversity-Part I: System description, Part II: Implementation aspects and performance analysis," in *IEEE Transactions on Communications,* vol. 51, no. 11, November 2003, pp. 1927-1948.

[47] J. N. Laneman, "Cooperative diversity in wireless networks: Algorithms and architecture," Ph. D. dissertation, Massachusetts Institute of Technology, August 2002.

[48] J. N. Laneman and G. W. Wornell, "Energy efficient antenna sharing and relaying for wireless networks," in *Proc. IEEE WCNC'00*, October 2000, pp. 7-12.

[49] M. O. Hasna and M. -S. Alouini, "Harmonic mean and end-to-end performance of transmission systems with relays," *IEEE Transactions on Communications,* vol. 52 , no. 1 , Jan. 2004, pp. 130-135.

[50] J. Boyer, D. D. Falconer and H. Yanikomeroglu, "Multihop diversity in wireless relaying channels," *IEEE Trans. Commun.,* vol. 52, no. 10, October 2004, pp. 1820-1830.

[51] J. Ribeiro, X. Cai, and G. B. Giannakis, "Symbol error probabilities for general cooperative links," *IEEE Trans. Wireless Commun.,* vol. 4, no. 3, May 2005, pp. 1264-1273.

[52] D. Chen and J. N. Laneman, "Noncoherent demodulation for cooperative wireless systems," in *IEEE Globecom 2004*, Dallas, November 2004.

[53] D. Chen and J. N. Laneman, "Modulation and demodulation for cooperative diversity in wireless networks," submitted to *IEEE Trans. Wireless Commun.,* in July 2004. Accepted in January 2005.

[54] R. U. Nabar, H. Bolcskei and F. W. Kneubuhler, "Fading relay channels: Performance limits and space-time signal design," *IEEE Jl. Sel. Areas in Commun.,* vol. 22, no. 6, August 2004, pp. 1099-1109.

[55] L. Zheng and D. N. C. Tse, "Diversity and multiplexing: A fundamental tradeoff in multiple antenna channels," *IEEE Trans. Info. Theory,* vol. 49, no. 5, May 2003, pp. 1073-1096.

[56] J. N. Laneman, D. Tse and G. W. Wornell, "Cooperative diversity in wireless networks: Efficient protocols and outage behavior," *IEEE Trans. Info. Theory,*, December 2004.

[57] J. G. Proakis, *Digital Communications,* Fourth Edition, McGraw-Hill, 2001.

[58] W. H. Press, S. A. Teukolsky, W. A. Vetterling, and B. P. Flannery, *Numerical Recipies in C: The Art of Scientific Computing,* Cambridge University Press, 1992.

[59] K. Sha and W. Shi, "Modeling the lifetime of wireless sensor networks," *Sensor Letters,* vol. 3, no. 2, 2005, pp. 1-10.

[60] Special issue on "Energy-aware ad hoc wireless networks," *IEEE Wireless Communications,* vol. 9, no. 4, Aug. 2002.

[61] J. N. Laneman and G. W. Wornell, "Distributed space-time coded protocols for exploiting cooperative diversity in wireless networks," *IEEE Trans. Info. Theory,* vol. 49, no. 10, Oct. 2003, pp. 2415-2425.

[62] A. Host-Madsen and J. Zhang, "Capacity bounds and power allocation for wireless relay channels," *IEEE Trans. Info. Theory,* vol. 51, no. 6, June 2005, pp. 2020-2040.

[63] N. Ahmed, M. Khojastepour, and B. Aazhang, "Outage minimization and optimal power control for the fading relay channel," in *Proc. IEEE Info. Theory Workshop*, San Antonio, Oct. 2004, USA.

[64] Y. Liang and V. V. Veeravalli, "Resource allocation for wireless relay channels," in *Proc. 38th Asilomar Conference on Signals, Systems and Computers,* Nov. 2004, pp. 1902-1906.

[65] E. G. Larsson and Y. Cao, "Collaborative transmit diversity with adaptive radio resource and power allocation," *IEEE Comm. Letters,* vol. 9, no. 6, June 2005, pp. 511-513.

[66] I. Hammerstrom, M. Kuhn, and A. Wittneben, "Impact of relay gain allocation on the performance of cooperative diversity networks," in *Proc. IEEE Veh. Tech. Conf. (VTC),* Sept. 2004, pp. 1815-1819.

[67] Z. Qi, Z. Jingmei, S. Chunju, W. Ying, Z. Ping, and H. Rong, "Power allocation for regenerative relay channel with Rayleigh fading," in *Proc. IEEE Veh. Tech. Conf. (VTC)*, May 2004, pp. 1167-1171.

[68] Z. Jingmei, Z. Qi, S. Chunju, W. Ying, Z. Zhang, and P. Zhang, "Adaptive optimal transmit power allocation for two-hop non-regenerative wireless relaying systems," in *Proc. IEEE Veh. Tech. Conf. (VTC)*, May 2004, pp. 1213-1217.

[69] S. M. Alamouti, "A simple transmit diversity technique for wireless communications," *IEEE Jl. Selected Areas in Commun.,* vol. 16, no. 8, Oct. 1998.

[70] J. Zhang, Y. Wang, and P. Zhang, "STC-based cooperative relaying system with adaptive power allocation," *Lecture Notes in Comp. Science*, vol. 3510, Jan. 2005, pp. 343-353.

[71] M. Hasna and M.-S. Alouini, "Optimum power allocation for relayed transmissions over Rayleigh-fading channels," *IEEE Trans. Wireless Comm.,* vol. 3, no. 6, Nov. 2004, pp. 1999-2004.

[72] J. Luo, R. S. Blum, L. Cimini, L. Greenstein, and A. Haimovich, "Power allocation in a transmit diversity system with mean channel gain information," *IEEE Comm. Lett.,* vol. 9, no. 7, July 2005, pp. 616-618.

[73] X. Deng and A. M. Haimovich, "Power allocation for cooperative relaying in wireless networks," *IEEE Comm. Lett.,* vol. 9, no. 11, Nov. 2005, pp. 994-996.

[74] J. N. Laneman, "Network coding gain of cooperative diversity," in *Proc. IEEE MILCOM'04*, Monterey, CA, USA, Nov. 2004.

[75] Z. Wang and G. B. Giannakis, "A simple and general parameterization quantifying performance in fading channels," *IEEE Trans. Commun.,* vol. 51, no. 8, Aug. 2003, pp. 1389-1398.

[76] L. H. Ozarow, S. Shamai, and A. D. Wyner, "Information theoretic considerations for cellular mobile radio," *IEEE Trans. Veh. Technol.,* vol. 43, no. 5, May 1994, pp. 359-378.

[77] P. Anghel and M. Kaveh, "On the diversity of cooperative systems," in *Proc. IEEE ICASSP'04,* 2004, pp. 557-560.

[78] S. Barbarossa and G. Scutari, "Distributed space-time codes for regenerative relays," *IEEE Trans. Wireless Commun.,* vol. 4, no. 5, Sept. 2005, pp. 2387-2399.

[79] S. Boyd and L. Vandenberghe, *Convex Optimization,* Cambridge University Press, 2004.

[80] *The MOSEK optimization tools manual,* version 4.0. Available at http://www.mosek.com.

[81] A. Said and W. A. Pearlman, "A new, fast, and efficient image codec based on set partitioning in hierarchical trees," *IEEE Trans. Circuits and Systems for Video Technol.,* vol. 6, no. 3, June 1996, pp. 243-250.

[82] D. P. Bertsekas and J. N.Tsitsiklis, *Parallel and Distributed Computation: Numerical Methods,* Athena Scientific, 1999.

[83] M. Peritsky, "Statistical estimation of mean signal strength in a Rayleigh-fading environment," *IEEE Trans. Commun.,* vol. 21, no. 11, Nov. 1973, pp. 1207-1213.

[84] J. W. Craig, "A new simple and exact result for calculating the probability of error for two-dimensional signal constellation," in *IEEE MILCOM'91*, 1991, pp. 571-575.

[85] I. S. Gradshteyn and I. M. Ryzhik, *Table of Integrals, Series, and Products,* Corrected and Enlarged Edition, Academic Press, Inc., 1980.

[86] M. K Simon and M.-S. Alouini, *Digital Communications Over Fading Channels: A Unified Approach to Performance Analysis,* Wiley Series, July 2000.